STRENGTHENING OF RC BEAMS WITH ANCHORED FRP LAMINATE

STRENGTHENING OF RC BEAMS WITH EXTERNALLY BONDED AND ANCHORED FRP LAMINATE

By RYNE CAMERON, B.ENG.

A Thesis Submitted to the School of Graduate Studies in Partial Fulfillment of the Requirements for the Degree Master of Applied Science

McMaster University MASTER OF APPLIED SCIENCE (2012) Hamilton, Ontario

TITLE: Strengthening of RC Beams with Externally Bonded and Anchored FRP Laminate AUTHOR: Ryne Cameron, B.Eng. (McMaster University) SUPERVISOR: Professor A. Ghani Razaqpur NUMBER OF PAGES: xi, 176

ABSTRACT

Premature debonding of externally bonded FRP laminate from retrofitted reinforced concrete (RC) members can lead to inefficient use of FRP and can limit the level of strength increase that can be achieved. In this investigation, novel carbon FRP anchors were used in an attempt to delay the onset of premature debonding and to achieve superior strength. Nine double shear tests were performed on small scale concrete prisms to determine the most suitable epoxy for bonding the anchors to the laminate and the concrete. One type of epoxy increased the ultimate load of the prism retrofitted with two anchors at each end of the laminate 83.7% over the control specimens without anchors. The second phase of the investigation consisted of testing six large scale T-beams with a 4500 mm span, 400 mm height and 500 mm flange width under four point bending. Two beams were tested without FRP reinforcement as control beams, one beam was tested with FRP only epoxy bonded and the remaining three beams were tested with the FRP epoxy bonded and anchored. One of the beams with 30 anchors exhibited a 46% increase in the debonding load over the beam without anchors while the FRP laminate attained a maximum strain equal to 80% of its ultimate strain capacity, a 94% increase over the beam strengthened with only epoxy bonded FRP. The results demonstrate the anchoring system's effectiveness and a feasible way to efficiently utilize the FRP laminate.

ACKNOWLEDGEMENTS

I would like to sincerely thank my supervisor, Dr. A. Ghani Razaqpur, for sharing his knowledge, guidance and patience throughout this process. His continued support led me through this process and I will always be grateful for this wonderful opportunity to work with him.

I would also like to thank all those who helped me complete my experimental work in the Applied Dynamics Laboratory. Most notably, I am very grateful for the help from lab technicians Kent Wheeler and Dave Perrett. Only with their help and patience could my experimental investigation have been completed.

Special thanks to former McMaster student Ahmed Mostafa, PhD and current student Kevin Simonds. I am very grateful for Ahmed's guidance with the manufacturing of the anchors and with FRP application techniques. Thank you also to Kevin who helped with the construction of the concrete prisms.

I would also like to thank my parents for encouraging me to continue my education and showing me the value of hard work through their own example. Finally, I'd like to thank everyone who helped me in any way, big or small, through this process, especially, Zach Cameron, Anneke Cameron, Alec Cameron, Darren Bos, Mark Campbell, Craig Marentette, Matt Bradbury, Eric Durrant, Niel Van Engelen and Sabrina Gismondi.

Ryne Cameron

Department of Civil Engineering

McMaster University

TABLE OF CONTENTS

LIST OF FIGURES

LIST OF TABLES

CHAPTER 1 - INTRODUCTION

1.1 GENERAL

In ordinary reinforced concrete (RC) beams, external load or moment is resisted by the internal couple formed by the concrete in compression and the steel reinforcement in tension. Concrete's inherent strength in compression and the tensile resistance of the steel have been providing RC structures and members with their required strength for over a hundred years. More recently, composite materials with high strength and elastic moduli have been developed, which are ideal for providing tensile reinforcement in RC beams. Specifically, Fibre Reinforced Polymer (FRP) composites have high strength, high elastic modulus, low density and are highly resistant to corrosion, which have led to their use in the rehabilitation of RC structures.

The FRP composite is comprised of high strength fibres within a polymer matrix. The fibres, which can include glass, aramid and carbon fibres, provide the strength of the FRP, while the matrix protects the fibres, providing durability, and under load distributes the load to the fibres. The fibres are oriented in the direction or directions that utilize them most efficiently. Layers of fibres are called laminates or strips, and both terms are used interchangeably within the

present investigation. The FRP laminates are externally bonded to RC members using an adhesive, which is commonly an epoxy resin.

The deterioration of existing RC infrastructure is well documented and has become a crucial problem in today's society. Structural rehabilitation is often a cost effective method for restoring the strength of deteriorating infrastructure. Much of the deterioration is traceable to poor durability of the RC structure leading to corrosion of the steel reinforcement within the concrete. Corrosion of steel reinforcement leads to significant losses in strength, which can, in some cases, initiate failure of the structure. Additionally, change in load levels to be resisted by a structure and construction defects may warrant the use of external FRP for rehabilitation. The external bonding of FRP laminates has emerged as a popular strengthening technique to combat these growing problems. Perhaps the most apt circumstance for the use of external FRP reinforcement is the rehabilitation of bridges. In addition to the strengthening benefit, the fatigue resistance and corrosion resistance are ideal for the moving load and exposure to deicing salts, which apply to bridges in Canada.

Despite the desirable properties of FRP, a structure strengthened with FRP can fail prematurely at the FRP-concrete interface, causing debonding of the FRP. Therefore, the FRP does not reach its full strength and becomes inefficient. Premature debonding in an RC member strengthened flexurally typically initiates

at a flexural or flexural-shear crack which intersects the FRP laminate. Localized debonding at a particular crack can, and usually does, lead to the full debonding of the FRP laminate. As the tensile strength of the adhesive is generally higher than the concrete, the failure plane usually lies a few millimeters into the concrete.

The debonding failure initiated at a major flexural crack is commonly referred to as Intermediate Crack-induced (IC) debonding failure. IC debonding, which is the primary failure mode investigated in this study, is considered particularly significant in relatively slender members with relatively thin FRP reinforcement. As a crack width increases in a beam strengthened with external FRP, the localized strain within the FRP laminate near the crack significantly increases. The linear stress-strain relationship of FRP up to failure does not allow for the redistribution of stresses, like what would be expected of a ductile material. Thus, localized debonding can occur on one side of the crack initiating debonding of the entire FRP laminate.

In an attempt to delay/prevent the onset of premature debonding of the FRP laminate and to promote the efficient use of FRP, various anchoring devices have been developed. Different types of anchoring systems include U-jacketing, mechanical fastening, spike anchors and hybrid anchoring techniques. Depending on the application, each type of anchor has effected some

improvement in delaying premature debonding, but the problem has not been satisfactorily solved yet.

1.2 Problem and Study Motivation

The premature debonding of external FRP reinforcement on RC members limits the strengthening potential of FRP. The anchors, shown in Figure 1.1, have been developed by a research team at McMaster University to delay the onset of debonding and to increase the FRP material efficiency, leading to greater strengthening potential. However, the effectiveness of the anchors to prevent debonding of thick carbon FRP (CFRP) laminates is unknown and will be examined in this investigation. It is important to acknowledge that theoretically, the shear and normal stresses at the concrete-laminate interface are a function of the laminate thickness and elastic modulus; an increase of either quantity will increase the interfacial shear stress and the tendency toward debonding. On the other hand, thick laminates are used in practice for convenience; hence, it is important to investigate whether the new anchor can improve the debonding load of RC beams retrofitted with a 1.2 mm thick CFRP laminate.

Figure 1.1: Anchors for delaying FRP debonding

1.3 RESEARCH METHODOLOGY

A comprehensive literature review was carried out to review the theory behind the FRP-concrete bond, the models and guidelines for predicting FRP debonding and existing anchoring systems for FRP and their effectiveness.

The experimental investigation is divided into two Phases. In Phase One, nine specimens are tested in a near end supported double shear test to investigate the FRP-concrete bond and to determine a suitable epoxy for bonding the anchors to the concrete. Three types of epoxy are used to determine the most suitable one for the present FRP-anchor system. Additionally, control specimens without anchors and with one and two anchors per concrete face are used in an attempt to quantify the effect of doubling the anchor number on the debonding load.

In Phase Two, six large-scale beams are tested in flexure. Two beams without FRP reinforcement are tested as the control beams, one beam with the FRP only

epoxy bonded to the beam and three beams with the FRP bonded and anchored are tested. Among the beams with anchors, two different types of epoxy and two anchor configurations are used.

1.3.1 Objective and Scope

The objective of the present investigation is to experimentally investigate the effectiveness of a new CFRP anchor in delaying/preventing debonding of a 1.2 mm thick CFRP laminate. To achieve the objective, first a number of concrete prisms will be tested in double shear to get a sense of the extent of the improvement in strength that can be achieved through the use of the anchor and to select the most suitable epoxy for bonding the anchor to the concrete and the FRP. Secondly, six large-scale RC T-beams will be tested to determine the effectiveness of the anchors in delaying or preventing premature debonding in retrofit applications involving thick CFRP laminates.

The present investigation will examine the flexural strengthening of RC beams retrofitted with an externally bonded and anchored CFRP laminate. The effects of using different epoxies to bond the anchors to the FRP and the concrete and different anchor configurations will be investigated, and the effectiveness of the present anchor will be compared to those of other anchors reported in the literature.

1.4 THESIS LAYOUT

Following the introduction, the thesis is arranged into five chapters. Chapter 2 is a comprehensive literature review pertaining to key information regarding anchoring FRP to concrete. The FRP-concrete bond, models and guidelines for predicting IC debonding and existing anchoring systems are reviewed.

Chapters 3 and 4 present the experimental program and results. The chapter on the experimental program explains the details of the prism specimens and beams tested, the FRP and concrete material properties and the test methods. Test pictures and schematic diagrams are included to aid the reader. The experimental results chapter presents the results from the experimental program. Results included are load, elongation/deflection, strain within the FRP laminate and visual observations.

Chapter 5 provides an analysis of the test results. The results are compared amongst themselves and with other data found in the literature to determine the effectiveness of the anchoring system in increasing the strengthening potential of externally bonded FRP reinforcement. Finally, Chapter 6 presents a summary of the results, conclusions that can be drawn from the results and recommendations for future work.

CHAPTER 2 - LITERATURE REVIEW

2.1 GENERAL

The use of fiber-reinforced polymer (FRP) to strengthen reinforced concrete (RC) structures has grown in popularity and established itself as an acceptable engineering practice in recent years. In particular, using FRP as external reinforcement is a widely used technique for structural rehabilitation. The properties which make FRP ideal for structural rehabilitation include their ultra-high strength to weight ratio, corrosion resistance and the ease with which they can be applied, especially when the structure is in use.

Due to the desirable properties of FRP, numerous studies have looked at many aspects of using externally applied FRP for structural strengthening. However, one of the key concerns with externally bonded FRP is premature loss of bond between the concrete substrate and the externally bonded FRP laminate. Premature debonding in the present context means loss of bond before the FRP laminate can reach its expected capacity based on a perfect bond. The following literature review will briefly describe the failure modes associated with premature debonding of FRP, provisions of prominent codes and guidelines

which consider premature failure of FRP-concrete bonded systems and existing anchorage systems which purport to prevent/delay premature debonding.

When used for structural rehabilitation, FRP laminates are applied externally to RC structures. The FRP plates are bonded to the tension side of beams, often using an epoxy adhesive. To strengthen the structure, the FRP must transfer its resistance contribution to the concrete section via shear stresses through the epoxy adhesive and the epoxy adhesive-concrete interface. Therefore, a sufficient bond between the epoxy adhesive and the concrete is critical for the strengthening of the structure. If the bond between the concrete and epoxy adhesive remains intact, stress can be transferred from concrete to FRP, and vice versa, and full composite action between the FRP and the unstrengthened RC beam will prevail. If premature debonding occurs, the composite action is lost, thus the RC beam cannot reach the theoretical ultimate capacity of the composite beam.

If an FRP-plated beam retains its composite action, there are two possible failure modes (Saxena et al. 2008): (1) compressive concrete crushing prior to, or after, tensile steel yielding and (2) flexural failure due to rupture of the FRP. When premature debonding occurs between the FRP plate and concrete, the composite action of the beam is lost. The loss of composite action is characterized by the following three failure modes (Liu et al. 2007): (1) plate end

debonding, (2) concrete cover separation and (3) intermediate crack (IC) debonding.

Plate end debonding is caused by high normal and shear stresses developed at the laminate ends during loading. When the stresses exceed the strength of the weakest element, failure occurs. Upon failure, the FRP will debond from the concrete, usually within the concrete, at one end of the beam/slab leading to failure of the specimen.

Concrete cover separation is caused by a crack developing at the laminate end propagating upwards to the level of the steel tensile reinforcement and horizontally along the reinforcement. The extension of the crack along the tensile reinforcement leads to concrete cover separation and the failure of the specimen. This type of failure typically occurs in members with relatively thin cover, large internal reinforcing bars and a strong FRP-concrete interface.

IC debonding occurs when flexural or flexural-shear cracks develop in a RC beam or slab, releasing tensile stress to the adjacent FRP. High strain in the FRP plate is necessary to accommodate the high local interfacial stress across the crack. This high strain causes the propagation of cracks along the FRP-concrete interface. The growth of these cracks toward the region of less moment leads to premature debonding of FRP in the form of IC debonding. The cracks commonly occur in the concrete below the concrete-epoxy interface because the tensile

strength of the epoxy adhesive is much higher than that of the concrete. The vertical displacement on either side of a flexural-shear crack can also cause a peeling force on one side of the crack which also contributes to IC debonding. However, the peeling force is considered less significant than the widening of cracks in causing IC debonding (Chen and Teng 2001). IC debonding is a critical failure mode for relatively slender members with relatively thin FRP strips and is the primary focus of the present investigation (Teng et al. 2003). IC debonding is often studied by testing beams but is also often studied in small scale specimens by a direct shear test (Pan and Leung 2007).

Some disagreement in the literature exists regarding the most prominent failure mode of FRP strengthened concrete beams. Liu et al. (2007) believe the dominant failure mode to be IC debonding. Ceroni and Pecce (2010) claim that failure in many cases is caused by plate end debonding and Saxena et al. (2008) point at concrete cover separation as the most common mode of failure. Nevertheless, IC debonding will be examined in this investigation.

The bond between FRP and concrete is essential when strengthening with external FRP reinforcement. FRP composites have very desirable high strength and high modulus properties, but cannot be utilized properly if there is a poor FRP-concrete bond. Typically, failure of a FRP-concrete bond occurs within the concrete just a few millimeters below the surface (Yuan et al. 2004, Chen and

Teng 2001, Pan and Leung 2007 and Wu et al. 2011). The failure occurs within the concrete because the tensile and shear strength of the concrete are generally lower than that of the adhesive.

Many factors affect the bond strength of an FRP-concrete interface, with the primary factors being the interfacial fracture energy of the FRP/concrete, the bond length and the FRP elastic modulus, thickness and width (Pan and Leung 2007). The bond length is easy to measure and the FRP properties are either given by the manufacture or coupon tests can be performed to determine the actual properties. The interfacial fracture energy is a more difficult parameter to compute. For a FRP-concrete bond, the interfacial fracture energy, G_f, is the area under the shear stress-slip curve, shown in Figure 2.1. In the figure, shear stress is on the y-axis and slip is on the x-axis. As experimental determination of accurate shear-slip curves of FRP-concrete bonds is difficult to perform in the lab, the maximum shear value and slip values are rarely known with certainty. Because the shape of the graph is not known for certain, researchers have tried various ways to predict the interfacial fracture energy. The interfacial fracture energy is often related to a strength parameter of concrete, such as the average surface tensile strength (Neubauer and Rostasy 1997) and the compressive strength of concrete (Wu and Niu 2007). However, Pan and Leung (2007) hypothesized that because failure occurred within the rough concrete surface, the aggregate content would affect the interfacial fracture energy through

aggregate interlock. In their study they conducted shear tests on concrete with ten different material compositions and found that bond capacity had little correlation with the concrete strength parameters of compressive strength and splitting tensile strength. They found bond capacity was correlated with surface tensile strength and the coarse aggregate content.

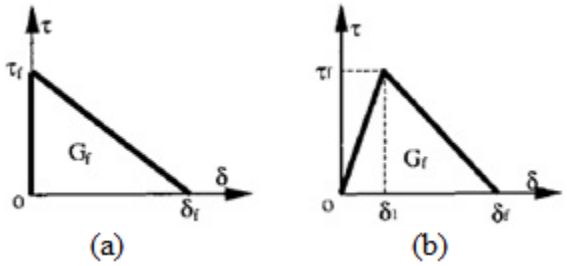

Figure 2.1: Shear-Slip Models for Plate to Concrete Bonds (Chen and Teng 2001, originally from Yuan and Wu 1999)

Another one of the factors which affects bond strength is the length of the bond. Unlike internal steel reinforcement, the ultimate strength of the FRP may not be reached regardless of the length of the bond. This phenomenon is known as the effective bond length. Increasing the length of the FRP-concrete bond beyond the effective bond length will not increase the bond strength. The brittle nature of FRP does not allow for shear stress redistribution along the length of the bond and thus debonding occurs when the maximum bond strength is reached at any local point along the bond.

There exists a closed-form analytical solution for determining the interfacial stresses and the load displacement curve of FRP-concrete bonds which will be described in greater detail later in this chapter (Yuan et al. 2004). However, accurate maximum local shear stress, ultimate slip and interfacial fracture energy values are required for an accurate representation of experimental results.

Consequently, researchers often resort to experimental work when studying anchoring systems or investigating bond strength between FRP and concrete. While notionally the reasons and the types of stresses for the advent of FRP debonding can be explained, practically it is difficult to theoretically determine the precise magnitude and distribution of the interfacial stresses in the concrete; the difficulty exists because the failure begins as a local event and its advent is governed by many parameters that are difficult to characterize, including concrete shear and tensile strength, the magnitude and distribution of stresses in concrete at crack locations, and the role of concrete tension stiffening.

Teng et al. (2002) describe several test methods for determining FRP laminate-concrete bond strength, including single shear tests, double shear tests and modified beam tests. A single shear test consists of one FRP laminate applied to a concrete prism. The prism is held in place and a load is applied to the FRP. A double shear test is similar, except two FRP laminates are bonded to either face

of the concrete prism. The single and double shear tests can be far end supported or near end supported, with the former meaning the concrete prism is supported at the end where the FRP is being loaded and the latter being supported at the opposite end. Modified beam tests have FRP attached to a beam with a pin in the centre. The FRP is applied to the beam and a load is applied at the centre or the ends of the beam, depending on whether the FRP is applied to the top or bottom of the beam. The different tests are shown in Chen and Pan (2006). When determining the effectiveness of an anchoring system, flexural tests are the most popular choice as they incorporate flexural cracking and curvature, which shear tests cannot replicate. However, for small-scale preliminary investigation, shear tests or the modified beam test can be performed. These tests require less work and therefore allow a wider range of variables to be studied more expeditiously.

Flexural tests can be conducted on concrete beams cast for the sole purpose of the experiment or they can be conducted on preloaded beams. Most tests are completed on beams cast specifically for testing, however, occasionally unstrengthened beams are preloaded, followed by FRP strengthening and testing of the strengthened beam. Rahimi and Hutchinson (2001) performed an experimental program on RC beams 2300 mm long of which two beams were preloaded. The two preloaded beams were loaded incrementally to 20 kN prior to FRP strengthening. This load represented 80% of the predicted ultimate load

prior to the application of the FRP and was sufficient to cause cracking and yielding of tensile reinforcement. After the preloading, a 0.8 mm thick carbon FRP (CFRP) laminate was bonded to the beams soffit and the beams were tested along with similar specimens which did not undergo preloading. The preloaded beams had a 3.2% higher ultimate load, 2.5% higher ultimate midspan deflection at the ultimate load over their counterparts which were not preloaded, while experiencing the same type of failure. The similar results highlight that lab tests on beams which do not undergo preloading still give accurate results as to how the repair would work in the field.

The load-deflection curves of FRP strengthened beams follow a trilinear response as observed by many researchers, including Chahrour and Soudki (2005), Wu et al. (2010), Smith et al. (2011) and Wu et al. (2011). The turning points in the load-deflection curves indicate first cracking of the concrete and yielding of tensile reinforcement. Typical load-deflection curves can be seen in Figure 2.2, in which slabs were strengthened in flexure with an anchoring system by Smith et al. (2011). Following debonding of the FRP, the member reverts to its unstrengthened status (Mostafa 2011).

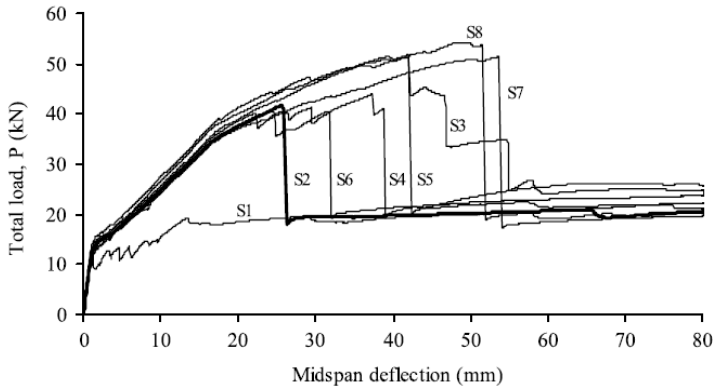

Figure 2.2: Typical tri-linear response of FRP strengthened RC beams/slabs (Smith et al. 2011)

2.2 Predicting Laminate Debonding

When strengthening RC structures with externally bonded reinforcement, there exists a need to be able to predict the failure of the structure. With externally bonded reinforcement, failure is usually caused by debonding at the FRP-concrete interface, thus there is a need to be able to predict this bond strength. By predicting debonding accurately, a designer can ensure a design that is safe and efficient.

Many different models and guidelines have been developed to predict the debonding of FRP and steel plates from RC members. Existing bond strength models can be categorized into empirical models, fracture mechanics models and semi-mechanistic models (Teng et al. 2002). The focus of the research in this study is IC debonding, therefore, literature related to this topic will be reviewed.

When predicting IC debonding, generally, a limitation is placed on the bond shear stress or on the maximum stress or strain allowable in the FRP. The following will review some of the key codes and guidelines with respect to IC debonding.

2.2.1 Closed-Form Analytical Solution

Yuan et al. (2004) provided a closed form analytical solution which was intended to predict the entire FRP debonding process. In the solution, the adhesive is assumed to be subjected to only shear deformations while the concrete and FRP laminate are assumed to be subjected to axial deformation only. Bending effects are neglected. Using equilibrium and the constitutive equations for the adhesive and two adherents, the following governing differential equation can be written

$$\frac{d^2\delta}{dx^2} - \frac{2G_f}{\tau_f^2}\lambda^2 f(\delta) = 0 \tag{2.1}$$

where δ is the interfacial slip between the concrete and FRP, G_f is the interfacial fracture energy, τ_f is the local bond strength and λ is a parameter given as

$$\lambda^2 = \frac{\tau_f^2}{2G_f}\left(\frac{1}{E_f t_f} + \frac{b_f}{b_c E_c t_c}\right) \tag{2.2}$$

where E_f is the FRP laminate elastic modulus, t_f and b_f are its thickness and width, b_c is the width of the concrete prism, E_c is the elastic modulus of the concrete and t_c is the thickness of the concrete prism.

Using a bond-slip model similar to Figure 2.1(b) and solving the differential equation, Yuan et al. (2004) developed a full range theoretical load displacement curve as shown in Figure 2.3. The curve represents a specimen with a bond length substantially longer than the effective bond length.

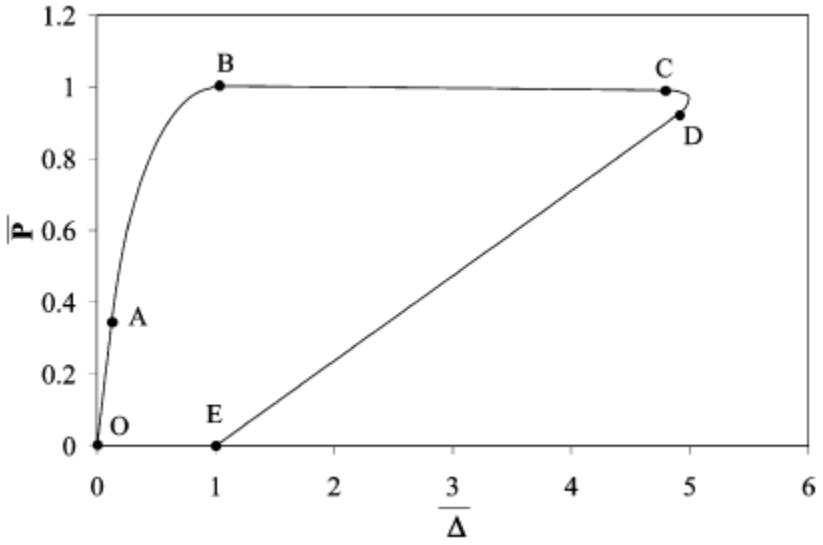

Figure 2.3: Theoretical load-displacement curve (Yuan et al. 2004)

Within the elastic region of the curve, OA, there is no FRP debonding along the interface. The section AB represents the elastic-softening stage of the bond. Within this stage the shear stress at the interface reaches the local bond strength at the loaded end of the FRP laminate, this causes softening to occur and reduces the shear stress at the interface at the bonded end of the FRP. Softening continues to occur until the shear stress at the bonded end becomes zero, leading to the BC stage, called elastic-softening-debonding. Using the shear stress at the interface, the strain within the FRP can be calculated, and this will

be explored further in the analysis of the experimental results of the present investigation.

The ultimate bond strength, P_u, (assuming infinite length bond) can be calculated as

$$P_u = \frac{\tau_f b_f}{\lambda} \tag{2.3}$$

2.2.2 Chen and Teng Model (2001)

An early model describing the anchorage strength of FRP and steel plates bonded to concrete was developed by Chen and Teng (2001). They used a linearly ascending and then descending shear-slip model to describe the plate to concrete bond, as in Figure 2.1(a). They explained that typical values of δ_1 and δ_f are 0.02 and 0.2 mm, respectively, for the shear-slip model in Figure 2.1(b). The slip parameters δ_1 and δ_f represent the bond slip at maximum stress and the ultimate bond slip. Since δ_1 is small compared to δ_f, they argued that the rigid-softening shear-slip model in Figure 2.1(a) adequately represents the actual interface response.

Using a nonlinear fracture mechanics approach in conjunction with the shear-slip model in Figure 2.1(a), they arrived at a practical method for predicting IC debonding (Yuan and Wu 1999). They noted that the interfacial bond strength is proportional to the square root of the concrete strength and based on regression

analysis of the plate-to-concrete shear test data, they gave the following simple bond strength equation

$$P_u = 0.427\beta_p\beta_L\sqrt{f'_c}b_f L_e \tag{2.4}$$

where

$$L_e = \sqrt{\frac{E_f t_f}{\sqrt{f'_c}}} \tag{2.5}$$

$$\beta_L = \begin{cases} 1 & if\ L \geq L_e \\ \sin\dfrac{\pi L}{2L_e} & if\ L < L_e \end{cases} \tag{2.6}$$

$$\beta_p = \sqrt{\frac{2 - b_f/b_c}{1 + b_f/b_c}} \tag{2.7}$$

where f'_c is concrete compressive strength, b_c is the width of the concrete beam web to which the laminate is bonded, L is the length of the laminate and L_e is the effective length of the FRP-concrete bond.

The recommended value of the numerical coefficient in Eq. 2.4 is 0.315 for practical design purposes, which corresponds to the 95% confidence limit. To determine the stress in the bonded FRP laminate at debonding, σ_{deb}, P_u is divided by the cross-sectional area of the FRP or steel plate as in Eq. 2.8. As reported by

Chen and Teng (2001), the model predicted relatively well the failure of 55 specimens tested in single and double shear tests.

$$\sigma_{deb} = 0.427\beta_p\beta_L\sqrt{\frac{E_f\sqrt{f'_c}}{t_f}} \tag{2.8}$$

2.2.3 TENG ET AL. (2003)

Teng et al. (2003) determined that the laminate-concrete bond in a simple shear test simulates the behaviour of the laminate-concrete interface near a flexural crack in an RC beam or slab. With this supposition, Teng et al. (2003) modified the Chen and Teng (2001) model to predict IC debonding. The change was justified by recalibrating the model using experimental data of beams which failed due to IC debonding. They found that changing the coefficient from 0.427 in Eq. 2.8 to 0.48 in Eq. 2.9 provided conservative predictions. The modified limiting stress in the FRP due to IC debonding was given as

$$\sigma_{deb} = 0.48\beta_p\beta_L\sqrt{\frac{E_f\sqrt{f'_c}}{t_f}} \tag{2.9}$$

It should be noted that the data set used to calibrate the design model did not include specimens that failed as a result of IC debonding at flexural-shear cracks. However, the model was used to predict IC debonding at a flexural-shear crack and even with the exclusion of this data the model conservatively predicted IC

debonding. Thus, Teng et al. (2003) recommend using the latter model for all IC debonding.

Said and Wu (2008) evaluated various models to predict IC debonding using a database of 200 beams/slabs which all failed as a result of IC debonding. All specimens within the database were tested with non-prestressed FRP sheets/plates serving as tensile reinforcement. No specimen had anchorage in the midspan, but some had end anchorage. When comparing the Teng et al. (2003) model with the experimental results of the collected database it was found that the model was conservative and had a high level of dispersion compared to other models. It was stated that this is caused by the use of shear test data for to predicting IC debonding. They noted that bending deformations and flexural cracking limit the direct application of shear tests.

2.2.4 American Concrete Institute (ACI) 440.2R-08 Guidelines (2008)

The ACI 440.2R-08 Guidelines (ACI 2008) recommend a strain limit to prevent IC debonding of FRP reinforcement. The formula for the limiting strain is similar in format to the model by Teng et al. (2003) as indicated below

$$\varepsilon_{deb} = 0.41\sqrt{\frac{f'_c}{nE_f t_f}} \leq 0.9\varepsilon_{fu} \qquad (2.10)$$

Where E_f and t_f are the elastic modulus and thickness of a single ply of the FRP laminate and n is the number of plies and ε_{fu} is the ultimate strain capacity of the FRP laminate.

The coefficient of 0.41 was selected after calibration using average FRP strain values at debonding for flexural tests failing as a result of IC debonding.

The ACI 2008 model differs from the 2002 model as it includes the square root of the concrete compressive strength, which represents the role of concrete fracture energy in the model. Moreover, this modification aligns the 2008 ACI guidelines with most other codes and guidelines as almost all include the effect of the square root of f'_c on IC debonding.

2.2.5 Said and Wu (2008)

Said and Wu (2008) proposed an empirical model to predict IC debonding similar to the ACI (2008) model. They gave the FRP strain at debonding as

$$\varepsilon_{deb} = \frac{0.23(f'_c)^{0.2}}{(E_f t_f)^{0.35}} \tag{2.11}$$

The coefficients in this model, i.e. 0.23, 0.2 and 0.35, were calibrated using a database of 200 beams and slabs found in existing literature which were reported to have failed due to IC debonding. Because the model was calibrated using the database, it showed very accurate predictions and a low level of dispersion when predicting failure loads within the database. When formulating

the model, these investigators discovered that concrete strength appears to have an insignificant effect on IC debonding. They postulated that this is because the initiation of IC debonding is due to damage and stress concentration at a flexural crack which is essentially independent of concrete strength.

2.2.6 International Federation for Structural Concrete (fib) Bulletin No.14 (2001)

The fib Bulletin 14 (fib 2001) uses three approaches to design against IC debonding. The first approach is to simply restrict the FRP strain as follows

$$\varepsilon_{f,lim} = \{0.0065 - 0.0085\} \tag{2.12}$$

As reported in the bulletin, using this approach can lead to the uneconomical use of the FRP, especially for use within large spans.

In the second approach, the maximum increase in tensile stress within the FRP that can be transferred through bond between two subsequent flexural cracks is limited. The approach is completed in three steps: (1) First, the most unfavourable subsequent flexural crack spacing is determined. The crack spacing is one to two times the transmission length and can be calculated by assuming constant mean bond stress for FRP and steel reinforcement (2) The tensile stress in the FRP at each crack is calculated using strain compatibility and internal force equilibrium (3) The increase in tensile stress between two subsequent cracks must not exceed the maximum allowable increase in bond stress. To satisfy the

latter condition, one must compute the maximum allowable increase in bond stress three separate ways.

The second approach is very complex, which severely limits its practical application. In addition, the comprehensive comparison of results for beams that failed in IC debonding, carried out by Said and Wu (2008), found the second approach to be conservative with large dispersion within its predictions.

Aram et al. (2008) compared various codes and guidelines with an experimental program of four FRP-strengthened beams as well as finite element analysis. They found the fib second approach to be very conservative in predicting the debonding load.

The third approach of the fib involves verification of the anchorage of the FRP and the force transfer between FRP and concrete. The approach involves two steps. The first is to verify the end anchorage, which is similar to the first approach. The second step is to ensure the shear stress at the FRP-concrete interface is less than the interfacial shear strength of concrete, f_{cbd}, given by

$$f_{cbd} = \frac{V_d}{0.95 d b_f} \leq 1.8 \frac{f_{ctk}}{\gamma_c} \tag{2.13}$$

where V_d is the design shear stress, d is the effective depth of the member, b_f is the width of the FRP laminate, f_{ctk} is the characteristic value of the concrete

tensile strength and γ_c is a material safety factor for concrete. In the above equation, it is assumed that the tensile steel reinforcement yields.

Aram et al. (2008) found that the third fib approach predicts unsafe failure loads when compared with test data.

2.2.7 CNR-DT 200/2004 (2004)

The Italian CNR-DT 200/2004 guideline has a simplified procedure to predict IC debonding. To avoid IC debonding, FRP maximum strain is limited to

$$\varepsilon_{deb} = min\left\{\eta_a \frac{\varepsilon_{fu}}{\gamma_f}, \varepsilon_{fdd}\right\} \tag{2.14}$$

where η_a is an environmental factor, γ_f is a partial resistance (>1.0) factor depending on the type of application and FRP installation process and ε_{fdd} is the maximum strain allowable in the FRP due to IC debonding.

The limiting strain, ε_{fdd}, is calculated using

$$\varepsilon_{fdd} = \frac{k_{cr}}{\gamma_{f,d}\sqrt{\gamma_c}} \sqrt{\frac{2G_f}{E_f t_f}} \tag{2.15}$$

where k_{cr} is a parameter based on calibration of RC beams with FRP laminates which failed by IC debonding, $\gamma_{f,d}$ is partial factor based on the type of application and the FRP installation process and G_f is the fracture energy.

The average value of k_{cr} based on the calibration is 4.289. The fracture energy, G_f, is given as

$$G_f = 0.064 k_b \sqrt{f_{ck} f_{ctm}} \tag{2.16}$$

where k_b is a geometrical factor, f_{ck} is characteristic concrete compressive strength and f_{ctm} is the mean value of the concrete tensile strength.

The fracture energy is the area under the bond slip curve shown in Figure 2.1(b). The geometrical factor, k_b, is defined as

$$k_b = \sqrt{\frac{2 - \frac{b_f}{b_c}}{1 + \frac{b_f}{400}}} \geq 1 \tag{2.17}$$

where b_c and b_f represent the width of the beam and FRP, respectively.

The above equation is only valid if the b_f/b term is greater than or equal to 0.33. If b_f/b is less than 0.33, b_f/b should be replaced by 0.33.

2.2.8 Rosenboom and Rizkalla (2008)

Rosenboom and Rizkalla (2008) noted that many researchers including Chen and Teng (2001) and fib (2001) use a width factor, k_b, term in their expressions for calculating IC debonding stress. All these factors had the form

$$k_b = \alpha_b \sqrt{\frac{X_1 - \frac{b_f}{b_c}}{X_2 + \frac{b_f}{\varphi}}} \tag{2.18}$$

where b_f is the width of the FRP laminate, b_c is the width of the concrete surface to which the FRP laminate is bonded and φ is 400 mm in some models and b_c in others. X_1, X_2 and α_b are empirical constants which vary from 2.0-2.25, 1.0-1.25 and 1.0-1.06 respectively. Rosenboom and Rizkalla (2008) propose a width factor with X_1, X_2, α_b and φ equal to 2.0, 1.0, 1.0 and b_c respectively. Width factors are required as a bonded FRP laminate with a width smaller than the width of concrete to which it is bonded, will induce a non-uniform stress distribution across the surface it is bonded to. If b_f is small relative to b_c, concrete outside the bond area can contribute to the bond strength, leading to higher stresses in the adhesive at debonding (Chen and Teng 2001). Rosenboom and Rizkalla (2008) also note an additional side effect caused by the epoxy adjacent to the edge of the FRP, which can lead to a small increase in strength as a result of the participation of the concrete bonded to this extra epoxy in the overall resistance.

Rosenboom and Rizkalla (2008) also present an analytical model to predict IC debonding. They explained that along a beam, the shear stress at the FRP-concrete interface, τ_i, is due to the applied loading, τ_w, and stress concentrations at flexural cracks, τ_{sc}. The total shear stress at the interface at a distance x from

the support is the summation of the shear stress due to applied loading and stress concentrations, given as

$$\tau_i(x) = \tau_w(x) + \tau_{sc}(x) \tag{2.19}$$

The maximum interface shear stress due to applied loading and stress concentrations are given as

$$\tau_{wmax} = nE_f t_f \frac{\varepsilon_{db} - \varepsilon_{f@y}}{a - x_y}$$
$$\tau_{scmax} = 2.15\left(1.1 - \frac{M_y}{M_{db}}\right)\sqrt{f'_c} \tag{2.20}$$

where nE_ft_f is the FRP axial stiffness per unit width with n being the number of laminate plies, each with thickness, t_f and elastic modulus, E_f, ε_{db} is the strain in the FRP at IC debonding failure at a moment M_{db}, $\varepsilon_{f@y}$ is the tensile strain in the FRP at initial yielding of the tensile reinforcement at a moment M_y, a is the shear span of the beam (for symmetrical loading) and x_y is the distance to first yielding of the tensile reinforcement from the support, which can be calculated (for three and four point bending) as

$$x_y = a\frac{M_y}{M_{db}} \tag{2.21}$$

The failure criterion is when the shear stress at the interface, τ_i, reaches τ_{cmax} which is linked to the tensile strength of concrete and given as

$$\tau_{cmax} = 1.8\left(0.63\sqrt{f'_c}\right) \quad (2.22)$$

The debonding strain is found by iteration, by estimating the debonding strain until the stress at the interface is equal to τ_{cmax}. Because the model was calibrated with a database of 51 beams and slabs which failed due to IC debonding and by FRP rupture, the model predictions gives a mean value of 1.0 of predicted to experimental failure when compared with the database. The standard deviation of the model was 0.181.

2.2.9 ISIS Canada Design Manual

The ISIS Canada research network (ISIS) design manual (ISIS 2001) does not consider failure of externally bonded FRP members at the concrete bond. It is mentioned that the failure at the bond can be avoided by providing sufficient anchorage or by using a sufficient bond length. However, due to the effective bond length phenomenon, increasing the bond length may not allow the ultimate strain capacity to develop within the FRP. Additionally, no anchorage systems are recommended or listed within the manual.

2.2.10 Summary

The above models for predicting IC debonding are not applicable to beams with anchors, as anchors typically increase the debonding strain within the FRP. However, they are intended to give the reader an idea about the difficulty of predicting IC debonding and possible models to predict debonding. Some of the

models will be used later to compare their predictions with the experimental results of the present investigation.

2.3 Anchor Comparison

IC debonding is a premature failure mode leading to inefficient use of FRP reinforcement. Anchoring systems have been shown to aid in delaying debonding and to improve the strengthening of RC members with external FRP reinforcement.

When determining the effectiveness of an anchoring system many variables must be considered. An anchoring system is only useful if it can significantly increase the strength of a structure, compared to a similar beam without anchors, or if it can prevent sudden loss of strength after the commencement of debonding. The ultimate strain achieved in the FRP laminate is a good indicator of the effectiveness of the anchoring system as it shows the efficiency of the strengthening system. To a lesser degree, the mode of failure, ductility, average shear stress, cost to manufacture, difficulty to manufacture and ease of installation all affect the feasibility of an anchoring system. The difficulty in comparing anchoring systems is that within the literature, research groups may only include one, a combination and rarely all the quantitative factors which ultimately determine the effectiveness and feasibility of anchoring systems. In

addition, the qualitative factors, such as difficulty to manufacture and ease of installation, become difficult to compare.

There are many different systems for anchoring FRP to RC for the purpose of strengthening. FRP anchoring systems include, but are not limited to, steel plate anchoring, U-jacketing, fan/spike anchor, mechanical fasteners, ductile anchor system and hybrid bonded anchors. Each anchoring system generally has both strengths and weaknesses as discussed below.

2.3.1 Mechanically-Fastened (MF) Anchors

Mechanically fastening FRP to RC has been studied by a number of researchers (e.g. Bank and Arora 2007 and Lee et al. 2009). Mechanically-fastened (MF) anchors use one or both of steel expansion anchors and steel powder actuated fasteners to anchor the FRP to the concrete. The fasteners are powder actuated and consist of a nail or spike driven through the FRP. The transfer of shear between the RC and the FRP occurs at the bearing face of the fasteners. MF anchors have the advantage of being quick and easy to install. Bank and Arora (2007) explain that the installation requires unskilled labour, minimal surface preparation and the structure can be used immediately after FRP installation. However, a disadvantage of MF anchors is, as Lee et al. (2009) hypothesize, that new cracks initiate at the locations of nails or anchors even if the beam is precracked prior to testing. Additionally, nail rotation can occur at new cracks

leading to slip of the FRP, reducing the effectiveness of the strengthening technique. Single-shear tests have been conducted on MF anchors by Lee et al. (2009), however, due to the nature of the test, they cannot take into account the nail rotation phenomenon observed in flexural tests. Therefore, it may prove problematic to prove the effectiveness of MF anchors through shear tests.

Echoing the work of Lee et al. (2009), shear tests were also conducted by Elsayed et al. (2009), who observed that using shot fasteners created cracks, weakening surrounding concrete. It was found that the fasteners pulled out due to the weakened concrete. On the contrary, screwed fasteners did not damage the concrete and did not pull out.

Bank and Arora (2007) tested one control beam and three beams strengthened with FRP with MF anchors in the form of shot fasteners. The beams were 7320 mm in length with a cross-section of 508 x 508 mm. The beam with the most FRP, with a cross-sectional area of 967 mm^2, experienced the most strengthening over the control with a 58.1% increase and failed due to an expected bearing failure of the fasteners on the FRP. A similar beam with less FRP, 652.8 mm^2, experienced fastener pull out during loading, leading to its failure. It is unclear whether or not the cross-sectional area includes the hole drilled for the fasteners.

Martin and Lamanna (2008) completed experiments using concrete screws to MF FRP to concrete beams with a span of 3353 mm and a cross-section of 304.8 x 304.8 mm. It was found that the flexural capacity increased 12 to 39% over the unstrengthened control beam while experiencing similar ultimate ductility to the unstrengthened control beam. No fastener pull out was reported.

2.3.2 Fan Anchors

Fan anchors act similar to nails by mechanically fastening FRP, except they are made from FRP fabric or tow and their heads are adhesively bonded to the FRP laminate. The anchors consist of two regions: the shaft and splay. The shaft region is inserted into an epoxy filled hole in the concrete acting like the shank of a nail. The splay region extends out of the hole and is splayed onto and bonded with adhesive to the FRP laminate. Fan anchors are manufactured by completing the following steps (Niemitz et al. 2010): (1) Cutting rolled carbon fibre sheets perpendicular to the fibre direction and rolling them, (2) Tying the ends of shaft region of anchor, (3) Cutting transverse stitches in anchor splay region and (4) Inserting the saturated anchor into predrilled holes at the same time as FRP laminate installation. The anchor is installed after the laminate is applied to the concrete. To insert the anchor through the laminate, either a hole must be made in the laminate or its longitudinal fibres must be forced apart at the location of the anchor. The manufacturing process and the details of application strongly

affect the results of FRP fan anchor tests (Ceroni and Pecce 2010, Kim & Smith 2009).

Single shear tests were conducted by Niemitz et al. (2010) and they found that specimens with fan anchors inserted transversely across the laminate and with smaller splay diameters produced better results over larger diameter anchors placed longitudinally along the laminate. They found that two anchors with splay diameters of 13 mm placed across the FRP had the highest ratio of maximum load to ultimate load. Various primary failure modes in the anchored specimens were observed including FRP anchor splay delamination, FRP anchor shear rupture and FRP sheet rupture. Following the primary failure mode, all of the anchored specimens exhibited secondary failure modes, including laminate FRP debonding, laminate splitting or anchor pull out.

A double anchor fan arrangement or bow-tie anchor was used by Smith et al. (2011) to strengthen slabs. The bow-tie anchor consists of one anchor shank with two splayed regions resembling the shape of a bow-tie. Tests were completed on one-way slabs strengthened with external FRP while altering the arrangement of the bow-tie anchors. One significant result found was that the use of small bow-tie anchors enables the laminate to undergo relatively high strain. In particular, two specimens with an arrangement of bow-tie anchors within the shear spans of the slabs reached 78 and 79% of the ultimate strain of

the laminate, compared to 45% of the ultimate strain in the strengthened unanchored control beam. Thus, Smith et al. (2011) found anchors within the shear span of the slabs were most effective and closer spaced anchors enabled larger deflections.

Despite the prevention or delay of FRP debonding, no literature exists regarding the mechanics of the fan anchor. It appears that the anchors effectiveness is dependent on the bearing strength of the laminate at the anchor shank-FRP laminate contact line. Intuitively, unless the laminate is quite thick, this bearing strength does not seem sufficient for transferring large shear forces. Furthermore, no methodology has been developed to aid in the design or placement of fan anchors.

2.3.3 Ductile Anchor System

A steel anchoring system has been developed by Galal and Mofidi (2009) which is proposed to circumvent traditional problems with externally bonded laminate as well as increase the displacement ductility. In the strengthening system, the FRP reinforcement is not bonded to the concrete but rather attached to two anchors at the ends of the beam avoiding the uncertainty within a FRP-concrete bond. The anchoring system consists of steel links connecting the end anchors and FRP. The steel links are designed to yield prior to rupture of the FRP to ensure a ductile failure. Galal and Mofidi (2009) tested four T-beams with their

proposed anchor system and found only modest strength gains over the traditional epoxy bonded system of 8.4 and 10.8%. Despite the modest gain, the deflection at the maximum load of one of the beams with this anchoring system was 96% greater than the maximum deflection of the unstrengthened, traditional RC beam. More results are needed to determine if the strengthening potential of the system can be increased.

2.3.4 Hybrid Bonded FRP

Numerous researchers have conducted experiments on a hybrid bonded (HB) FRP system (Wu and Huang 2008, Wu et al. 2010, Wu et al. 2011). The hybrid bonding technique combines traditional epoxy bonding with mechanical anchors which restrain vertical displacement of the FRP laminate and increase the surface area bonded to the concrete substrate. The mechanical anchors work differently from MF anchors as the legs of mechanical anchors are not installed through the FRP strip, and therefore no damage is caused to the FRP. Instead, shear stress is transferred from the laminate to the anchor head and deep into the concrete substrate through bearing of the anchor legs.

An HB FRP system developed by Wu and Huang (2008) used mechanical fasteners with a metal head with two concrete nails as legs. Slabs 2500 mm long were tested in three-point bending. It was found that the mechanical anchors spaced at 100 mm increased the maximum moment by 79% over the control slab

with identical epoxy bonded laminate without anchors. In addition, when four and six plies of FRP were anchored with the HB FRP system the maximum moment increased 185 and 268% respectively, over the control beam with two plies of FRP. It is important to note that upon failure, the nails of the fasteners were pushed out vertically, unlike the failure of MF anchors which undergo lateral deformation. Wu and Huang (2008) explained that the longitudinal slip of the FRP laminate causes movement of the FRP laminate normal to its plane as in Figure 2.4, which leads to the vertical displacement of the nails.

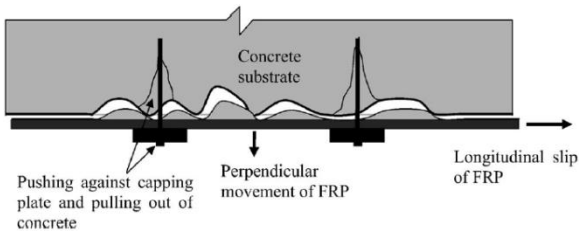

Figure 2.4: Mechanism of HB FRP anchor debonding (Wu and Huang 2008)

In a similar experiment Wu et al. (2010) tested seven beams with a HB FRP system and two control beams which were only epoxy bonded. The mechanical fasteners had a steel head with two 6.35 mm diameter concrete screws as the anchor legs. Of the 2800 mm long beams with a 350 x 180 mm cross-section, the beam with mechanical fasteners spaced at 100 mm intervals had the largest improvement over the epoxy bonded control beam with ultimate moment and strain increasing 53 and 185% respectively. Premature failure modes of IC debonding, concrete cover separation and anchorage failure prevented rupture

the CFRP in all the tests. A model to predict the strength of the HB FRP system is provided by Wu et al. (2010) which estimates the critical bonding strength as either the strength of the anchor system, the strength for concrete cover separation or the material fracture strength of the FRP. The model provided reasonable predictions when comparing the calculated and actual ultimate moments of the tested beams.

A slightly different mechanical fastener was developed by Wu et al. (2011). The fastener developed had a steel head with two bolts inserted into epoxy filled holes for the legs. Nuts were tightened onto the bolts against the steel head to apply a normal force onto the FRP which was also bonded to the concrete. Significant strength increase was reported for beams with a length of 2960 mm and a cross-section of 400 x 200 mm. For beams with six and seven plies of FRP, the ultimate load increased 788 and 967% over the estimated ultimate load of an unstrengthened control beam. However, no beam with only epoxy bonded FRP with the same dimensions was tested for comparison.

Mostafa (2011) developed a lightweight mechanical fastener which is not made of corrosive steel, but rather carbon fibre fabric impregnated with epoxy. The result is a durable, one-piece anchor which needs no additional work completed once it is installed. He tested 21 T-beams with lengths of 4880 mm and depths of 400 mm. With the use of 23 CFRP anchors spaced at 200 mm at midspan and 100

mm at the ends, it was found that eight layers (A_{frp} = 118.8 mm^2) of FRP ruptured after achieving a strain equal to 85% of the ultimate strain capacity of the laminate. Furthermore, in a beam with four layers (A_{frp} = 59.4 mm^2) of FRP sheets, the CFRP anchors allowed the FRP to reach 94% of its ultimate strain capacity prior to debonding. The high ultimate strain values and rupture of the FRP indicate efficient use of the FRP for strengthening.

2.4 SUMMARY

The following conclusions can be drawn from this literature review:

(1) There is no anchor system that can always allow all kinds of FRP laminate-RC beam combinations to reach their full strength based on perfect bond between them.

(2) Prediction of IC debonding load is essentially empirical and the database used for calibration is not comprehensive enough to warrant the acceptability of these methods in all cases, albeit the proposed method of the ACI Committee 440 is in general satisfactory.

(3) The key parameters in nearly all existing models for predicting IC debonding are the axial stiffness of the laminate per unit width, $E_f t_f$, and the concrete strength, f'_c. The additional parameter appears to be the ratio of the width of the laminate to that of the concrete beam web width. However, the inclusion of this

parameter requires careful consideration because in some cases, such as slabs with only a limited number of FRP laminate strips applied to the bottom surface, the role of this parameter is unclear. This may be the reason for its exclusion in the ACI 440.2R-08 Guidelines.

(4) All of these methods indicate that generally as the axial stiffness of the laminate increases, its maximum strain and stress at IC debonding decrease, and this reduction could be substantial compared to the ultimate strain capacity of the laminate. Therefore, the efficiency of the FRP laminate system decreases quite rapidly as the elastic modulus of the laminate or number of laminate plies increase.

(5) Finally, since FRP, particularly CFRP, is an expensive material and since IC debonding is a non-ductile and brittle failure mode, it is advantageous to develop an anchor system that can increase the efficiency of the FRP and, if possible, change the IC debonding from a brittle to a relatively ductile failure mode. Furthermore, the anchor should satisfy durability requirements similar to the FRP laminate.

CHAPTER 3 - EXPERIMENTAL PROGRAM

The objective of the experimental program is to determine the effectiveness of the mechanical anchor system in delaying/preventing premature debonding of FRP. Experimental work is conducted in two phases. Phase One consists of testing the FRP-concrete bond in direct tension in double shear tests, with and without anchors. Phase Two involves strengthening large-scale T-beams with FRP tensile reinforcement, again with and without the aid of anchors.

3.1 PHASE ONE – DOUBLE SHEAR TESTS

3.1.1 GENERAL

It was decided to first complete small scale tests on the FRP and anchoring system to determine the feasibility and effectiveness of the system. A small-scale shear test was chosen for ease of testing and construction. To minimize eccentricity of loading, a double shear test, consisting of two FRP strips on opposite sides of the specimen, was chosen as the test method. The near-end supported double shear test was chosen to ensure the concrete prisms were loaded in compression and to prevent premature failure within the concrete. A typical Phase One specimen is shown in Figure 3.1.

Figure 3.1: Typical Phase One specimen

Schematic drawings of the specimens of Phase One are presented in Figure 3.2, Figure 3.3 and Figure 3.4. The specimens consist of two concrete prisms of dimensions 150 x 250 x 340 mm. The prisms were cast with a pipe of approximately 38.1 mm inside diameter placed at the centre of each prism. Threaded rods were inserted in the pipe and connected to the steel plates of dimension 480 x 146 x 25.4 mm at one end of each prism. A tension force was applied to the threaded rod allowing direct tension to be applied to the FRP strips connecting the concrete prisms. In addition, the tension force applied through the threaded rods to the steel plates ensured the concrete prisms were in compression, since the steel plates transferred the load to the concrete prisms by bearing.

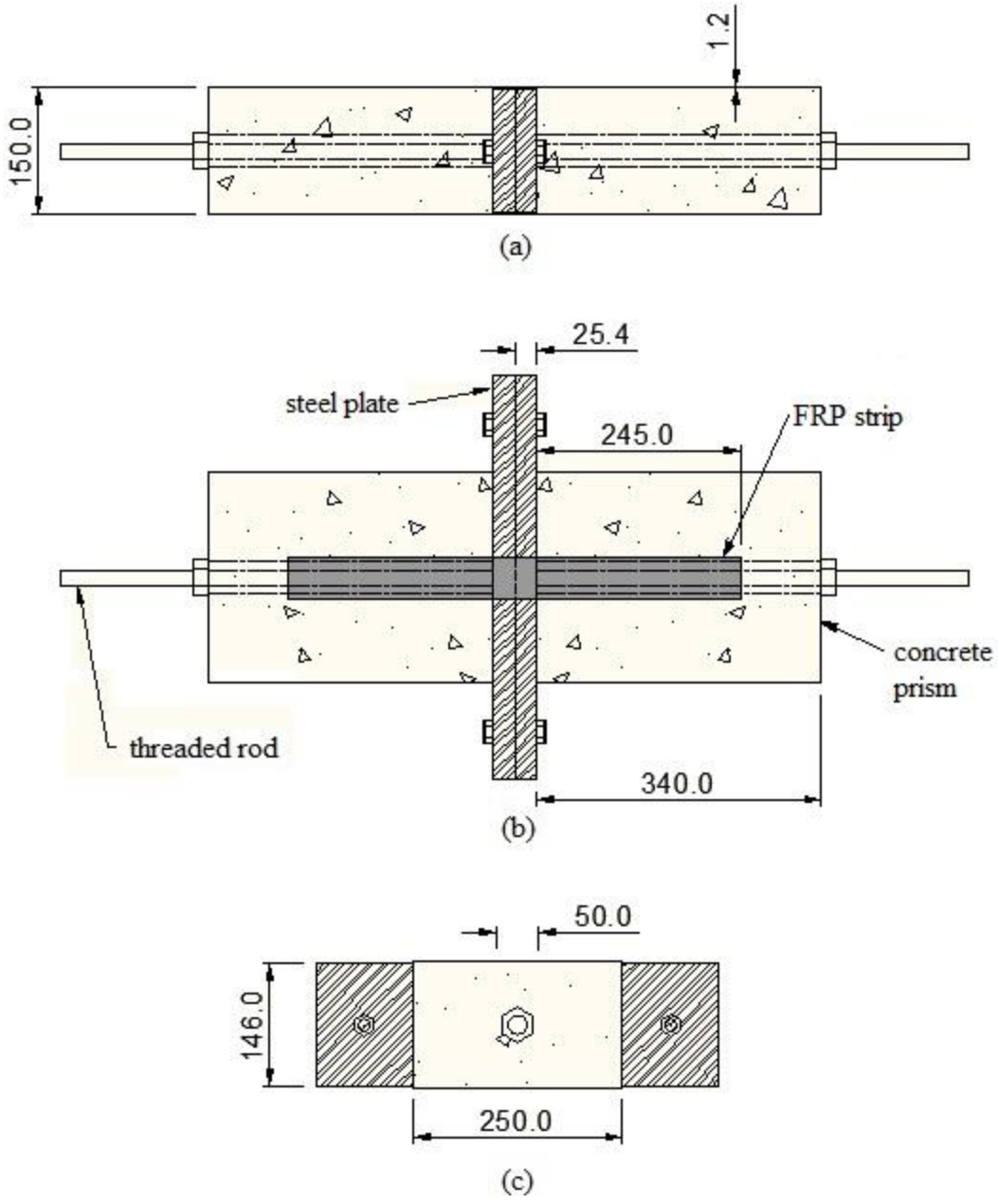

Figure 3.2: Typical specimen without anchors (a) Elevation view, (b) Top view and (c) End view

Note: All dimensions in figures are in units of millimeters

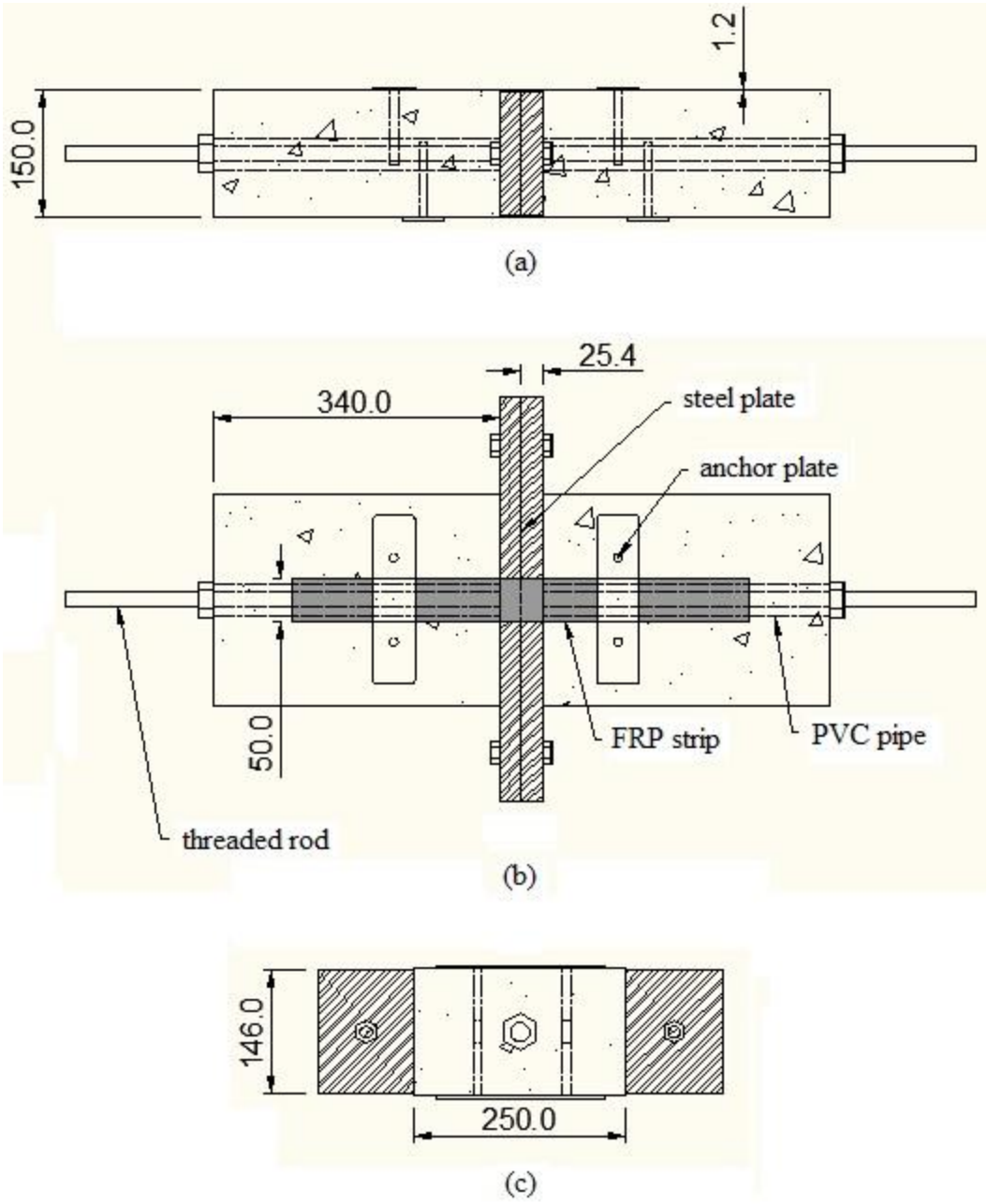

Figure 3.3: Typical specimen with one anchor per face (a) Elevation view, (b) Top view and (c) End view

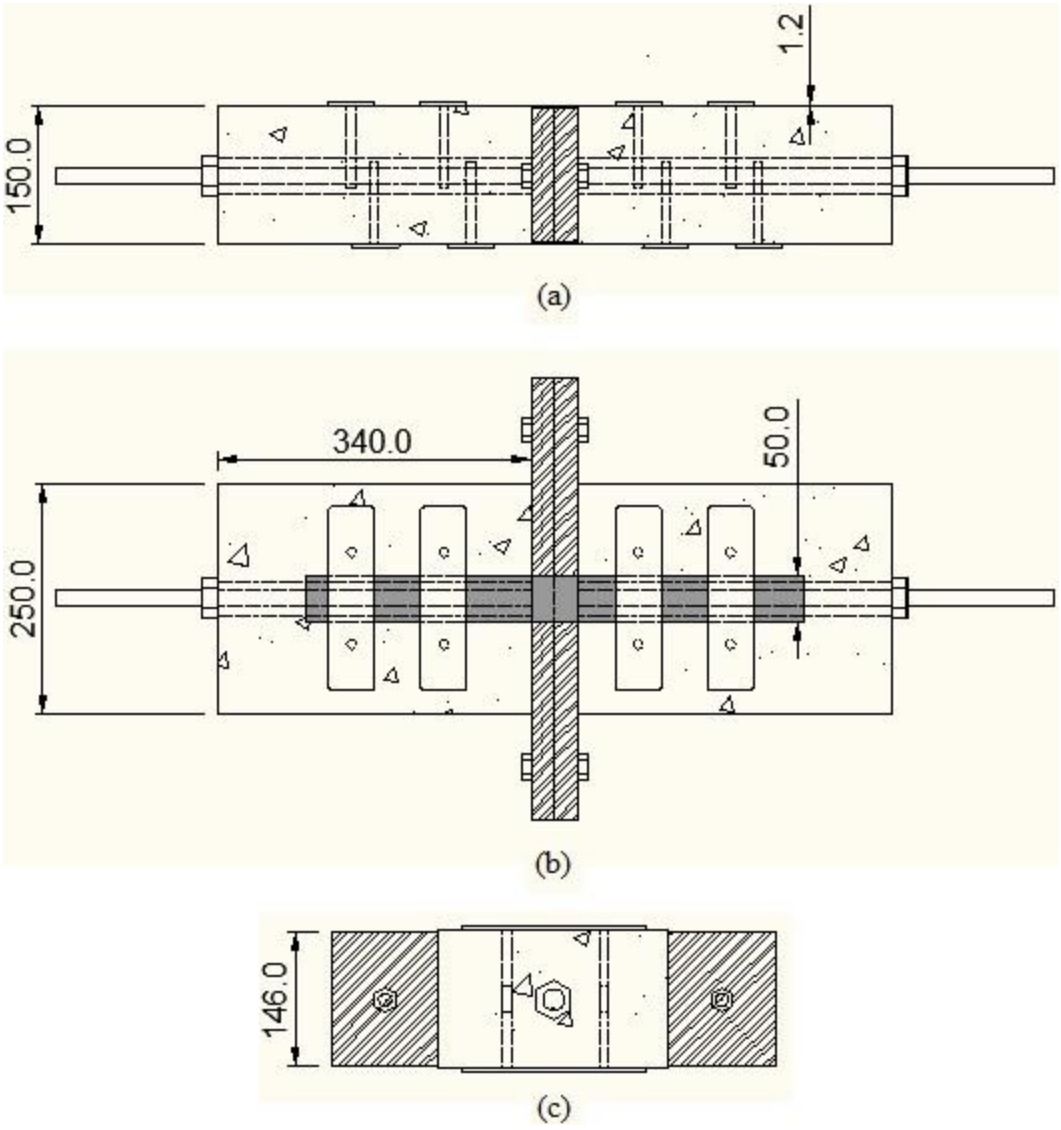

Figure 3.4: Typical specimen with two anchors per face (a) Elevation view, (b) Top view and (c) End view

In all Phase One specimens, the two concrete prisms were joined by two FRP strips 540.8 mm long and 50 mm wide (Sika CarboDur S512 pultruded CFRP laminate strips). The FRP strips were attached to the concrete prism faces of size 250 x 340 mm. The CFRP was bonded with Sikadur 30 structural epoxy paste

adhesive manufactured for use with Sika CarboDur CFRP laminate. Following the application of the CFRP, anchors were installed into predrilled holes in the concrete prisms.

It should be pointed out that the holes were drilled into the concrete adjacent to the CFRP strips, thus the strips were not damaged by the anchor holes, as is the case of spike anchors or metallic fasteners.

Nine specimens were tested in direct tension in a double shear test in Phase One. Specimens are labeled DSx, with DS representing Double Shear test and x representing the test number varying from one to nine. A summary of the specimens tested in Phase One is given in Table 3.1.

Table 3.1: Summary of Phase One specimens

Specimen Name	Number of Anchors	Anchors Per Face	Epoxy Used	Strain Gauges	f'_c (MPa)
DS1	0	0	-	7	39
DS2	0	0	-	7	39
DS3	4	1	MBrace	2	39
DS4	4	1	MBrace	2	35
DS5	4	1	Sikadur 300	2	35
DS6	4	1	Sikadur 30	6	39
DS7	4	1	Sikadur 30	6	35
DS8	8	2	Sikadur 30	5	35
DS9	8	2	Sikadur 30	5	35

3.1.2 Material Properties

Concrete

Concrete prisms were cast in two batches with specified strength of 35 MPa. Two concrete cylinders were cast per batch to determine the ultimate compressive strength of the concrete. Cylinder diameters of 100 mm were used for batch one as there was not enough concrete leftover after casting the prisms to make two 150 mm diameter prisms. The results of the cylinder testing are displayed in Table 3.2.

Table 3.2: Phase One concrete compressive strength

Specimen	Batch	Diameter of Cylinder (mm)	f'_c (MPa)	$f'_{c,avg}$ (MPa)
1	1	100	39.5	39
2	1	100	38.7	
3	2	150	37.5	35
4	2	150	33.2	

The compressive strength of each concrete was taken as the average strength of its two prisms, i.e., 39 and 35 MPa for batch one and two respectively. Note that a few MPa difference in concrete strength has a negligible effect on debonding strength.

CFRP LAMINATE

Commercially available Sika CarboDur S512 CFRP laminate was used as the strengthening material in all specimens. A list of the material properties as given by the manufacturer is given in Table 3.3.

Table 3.3: CFRP laminate properties per manufacturer's specifications

Property	Value
Modulus of Elasticity	165 000 MPa
Tensile Strength	2800 MPa
Elongation at Break	>1.7%
Apparent Density	1.5 g/cm^3
Thickness	1.2 mm
Width	50 mm
Colour	Black

Coupon tests were not conducted on the FRP laminate, as they were deemed unnecessary because rupture of the FRP was not expected in any test. Therefore, the manufacturers' given properties were used for all calculations. Note that this is not a problem because failure was not due to rupture of FRP in any of the tests.

EPOXY

Three different epoxies were used within Phase One: Sikadur 30 epoxy paste, Sikadur 300 impregnating resin and Wabo MBrace primer and saturant. The Sikadur 30 was used to bond the FRP to the prisms for all specimens as well as to bond the anchors to concrete and FRP in specimens DS6, DS7, DS8 and DS9. To

bond the anchors to the concrete and FRP, Sikadur 300 was used for specimen DS5, while the Wabo MBrace primer and saturant were used for specimens DS3 and DS4.

Sikadur 30 is a two-component high-strength epoxy paste adhesive. The two components are white and black, creating a grey colour when mixed. The mixing of the colours makes it easy to tell when the paste has been successfully mixed. The convenient mix ratio of 3:1 by weight and pot life of 90 minutes makes it an ideal choice for work in the field. Moreover, because it is a paste it can be used for overhead applications. The manufactures' specified properties for this epoxy are given in Table 3.4.

Table 3.4: Adhesive properties per manufacturer's specifications

Property	Adhesive			
	Sikadur 30	Sikadur 300	Wabo MBrace Primer	Wabo MBrace Saturant
Mix Ratio (A:B) by volume	3:1	2.38:1	3:1	3:1
Mix Ratio (A:B) by weight	3:1	2.9:1	5:3	2.94:1
Tensile Strength	24.8 MPa	55 MPa	35 MPa	55.2 MPa
Tensile Modulus	4500 MPa	1724 MPa	2097 MPa	3034 MPa
Elongation at Break	1%	3%	1.8%	3.5%
Colour	Light Grey	Clear, Amber	Amber	Blue

Sikadur 300 is a high-strength impregnating resin. It is a clear two component resin. The mix ratio of the two components is 2.38:1 by volume and 2.9:1 by weight. The manufacturers' given material properties are given in Table 3.4.

Wabo MBrace primer and saturant are an epoxy and resin adhesive to be used together to bond FRP to concrete and other surfaces. The primer is a two-component, clear, low viscosity epoxy. The manufacturers' material properties are given in Table 3.4.

The saturant, to be used after the primer, is a low viscosity, blue epoxy encapsulation resin. The manufacturers' given material properties are given in Table 3.4.

CFRP ANCHOR

The anchors used in this study were developed by a research team at McMaster University, led by Professor of Civil Engineering Dr. A. Ghani Razaqpur. They consist of a head plate and two shanks. The shanks are 90 mm long and 10 mm in diameter. The head plate is 200 mm long, 50 mm wide, and 3 mm thick with a 5 mm fillet on the corners. The centre-to-centre spacing between the shanks is 100 mm. The shanks or legs, were fabricated with carbon fibre tow which extends from one shank, through the head and continuously through the other shank. A schematic drawing of the CFRP anchors is shown in Figure 3.5.

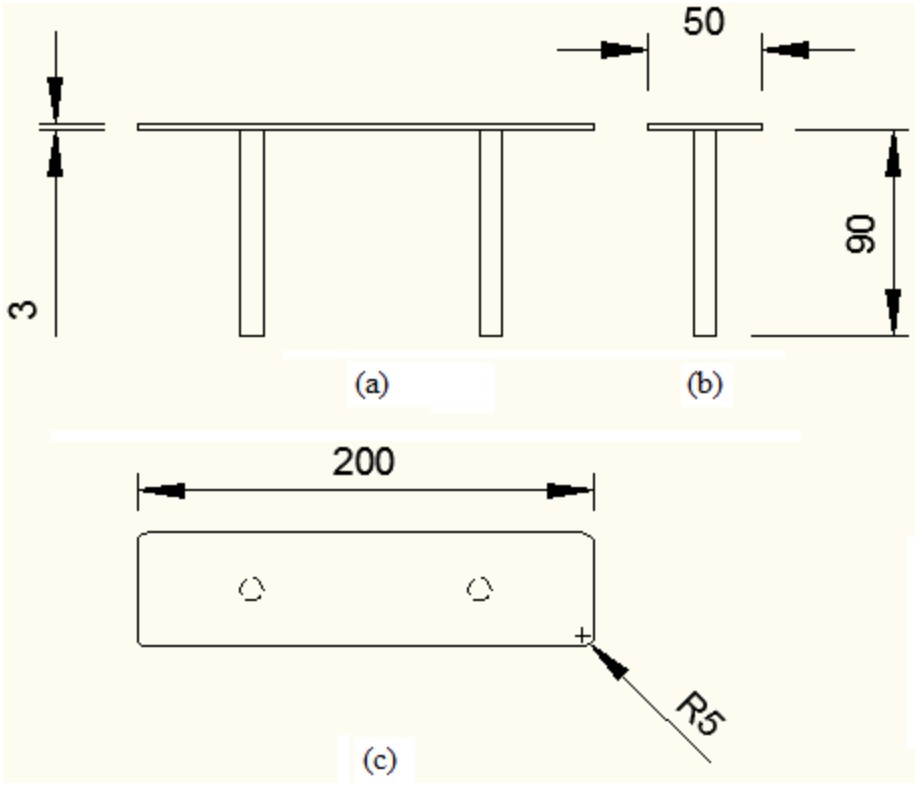

Figure 3.5: Schematic of CFRP anchors (a) Elevation view, (b) Side view and (c) Plan view

The head consists of five layers of WABO MBrace CF 130 Unidirectional High Strength Carbon Fiber Fabric. The bottom two layers of the fabric run longitudinally and have two small holes cut in the transverse fabric at the location of the legs to allow the carbon fibre tow to pass through the layers. The third layer of fabric runs transversely and sits directly on the carbon fibre tow between the legs and on the second layer outside of the legs. The final two layers have the fabric running longitudinally and are positioned on top of the third layer. The properties of the fabric and the carbon fibre tow, as given by the

manufacturer, are shown in Table 3.5. Figure 3.6(a) shows the fabric and carbon fibre tow.

Table 3.5: Carbon fiber fabric and tow properties per manufacturer's specifications

Property	Material	
	Uni-directional Wabo MBrace CF 130 fabric	Grafil 34-700 Carbon Fiber Tow
Nominal Thickness	0.165 mm/ply	-
Tensile Strength	3800 MPa	4890 MPa
Tensile Modulus	227 000 MPa	234 000 MPa
Elongation at Rupture	1.67%	2.0%

The anchors are manufactured by impregnating the carbon fibre tow and fabric with the Wabo MBrace saturant as described above. The anchors are then placed in an aluminum mould which is previously immersed in a polyvinyl alcohol release agent. The aluminum moulds can be seen in Figure 3.6(b). Once the FRP is placed in the moulds, it is left undisturbed for 48 hours to ensure the epoxy is cured prior to removal from the mould. Upon removal of the mould, the excess fabric extending from the legs and head of the anchor is cut to the desired shape with a grinder. Finally, the bottom of the head of the anchor is sand-blasted or sanded to ensure the removal of the release agent and to roughen the surface. The roughened surface will bond better to the adhesive used during the anchor installation into the concrete. Sample anchors are shown in Figure 3.6(c).

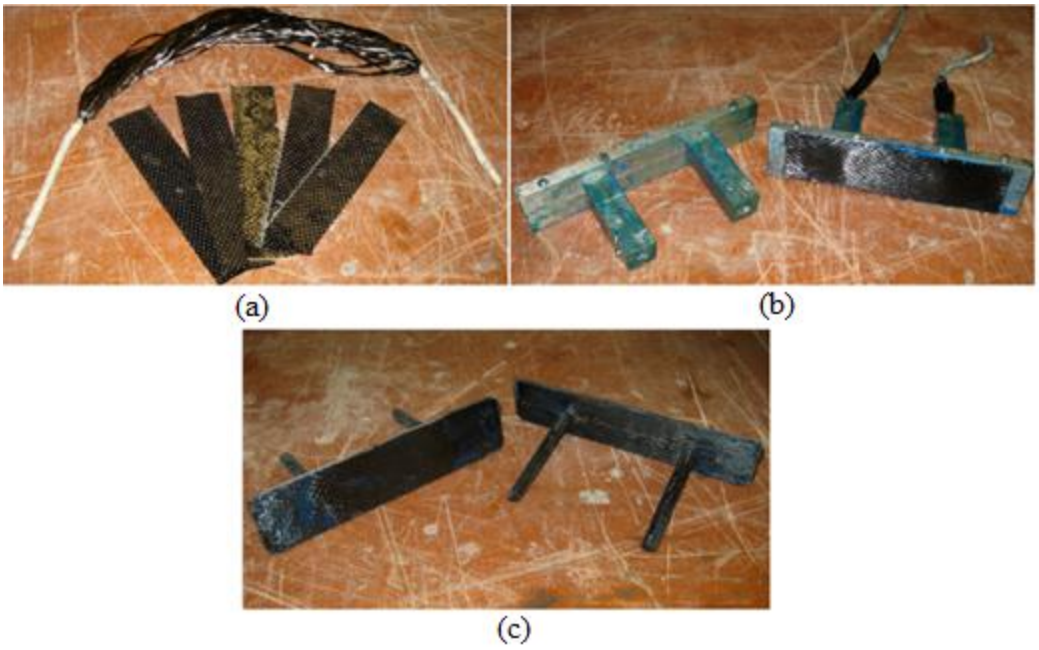

Figure 3.6: CFRP Anchors (a) Carbon fibre fabric and tow for anchor, (b) Aluminum moulds for making anchors and (c) Finished anchors

3.1.3 Fabrication of Specimens

The concrete specimens were cast into wooden moulds with a PVC pipe through the centre to allow for the insertion of the threaded steel rod. The cross-section of one cured concrete specimen is shown in Figure 3.7.

Figure 3.7: Cross-section of Phase One specimens

Following the removal of the wooden mould, holes were drilled into the concrete where the anchor legs were to be inserted. The holes were drilled with a hammer drill with a masonry drill bit. They were drilled to a depth of approximately 100 mm, to ensure the 90 mm long anchor legs could be fully inserted into the concrete.

The surface cement mortar was removed on the bond area with an electrical grinder to expose the aggregate and pore structure of the concrete. Compressed air was used to remove dust from the drilled holes and the bond area. The concrete prisms were placed onto the steel plates with the threaded rod extending through the prism. After testing the first specimen, DS3, hydrostone (gypsum cement) was placed between the steel plate and the concrete prism to eliminate stress concentrations caused by geometric imperfections in the concrete in the remaining specimens. To prevent the two prisms from moving

relative to each other while the epoxy cured, the steel plates were bolted together with 16 mm bolts, but the bolts were removed prior to applying the load during the test.

Sikadur 30 epoxy was mixed according to the manufactures specifications and used to bond the FRP to the concrete. The FRP was cleaned according to the manufacturer's specifications prior to its application. The bonded length of the FRP for all specimens was 220 mm. The first specimen test, i.e., specimen DS3, had no unbonded length while all subsequent tests had an unbonded length of 25 mm. The unbonded length of FRP started from the concrete surface in contact with the steel plate and extended toward its opposite surface. The unbonded length was used to prevent failure at the end of the concrete prism.

In specimens with anchors, the anchors on opposite sides of the concrete prisms had to be staggered because the width of the concrete prisms was less than twice the length of the anchor legs. The length from the termination of the FRP bond to the centre of each anchor present on each specimen is given in Table 3.6.

Table 3.6: Location of anchors on Phase One specimens

Specimen	Length from Termination of FRP Bond to Anchor on Each Face (mm)			
	North Top	North Bottom	South Top	South Bottom
DS3	180	120	120	150
DS4	60	55	90	85
DS5	70	75	105	110
DS6	70	65	105	105
DS7	65	70	100	95
DS8	70, 170	70, 170	40, 140	40,140
DS9	70, 170	70, 170	40, 140	40, 140

Three different types of epoxy were used to bond the anchors to the FRP and concrete. Wabo MBrace primer and saturant were used on two specimens, Sikadur 300 was used on one specimen and Sikadur 30 was used on the remaining four specimens. All specimens were left undisturbed for a minimum of 48 hours after the FRP plate and anchor installation. In addition, all epoxies were left to cure for a minimum of one week prior to testing to ensure a complete cure.

3.1.4 INSTRUMENTATION

Two strain gauges, one on each FRP strip, were installed in the middle of the strip in each specimen. The strain gauges were 30 mm in length and were installed on the unbonded portion of the FRP strip and are subsequently called the north and south strain gauges. In addition, 5 mm strain gauges were placed along the bonded portion of the FRP in an attempt to model the strain profile.

These strain gauges were only placed on one side of one concrete prism per specimen. Depending on whether anchors were used, three to five strain gauges were used to develop the strain profile within the FRP. The location of the strain gauges and the location of any anchors are shown in Figure 3.8 to Figure 3.14.

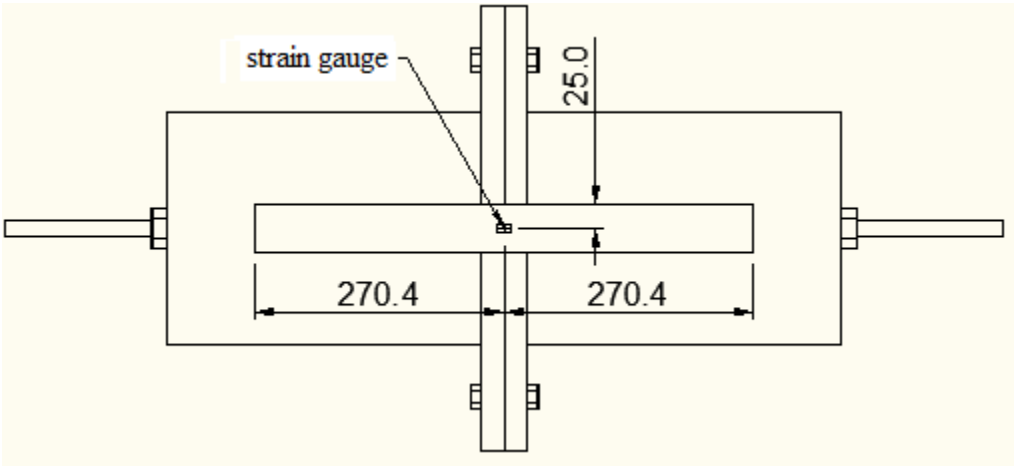

Figure 3.8: Location of centre north and south strain gauges

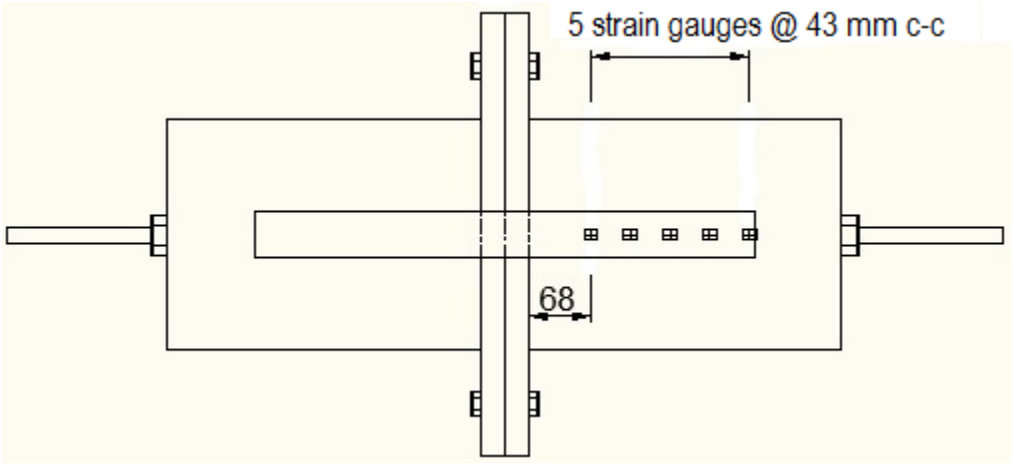

Figure 3.9: Location of strain gauges on specimen DS1 (north side)

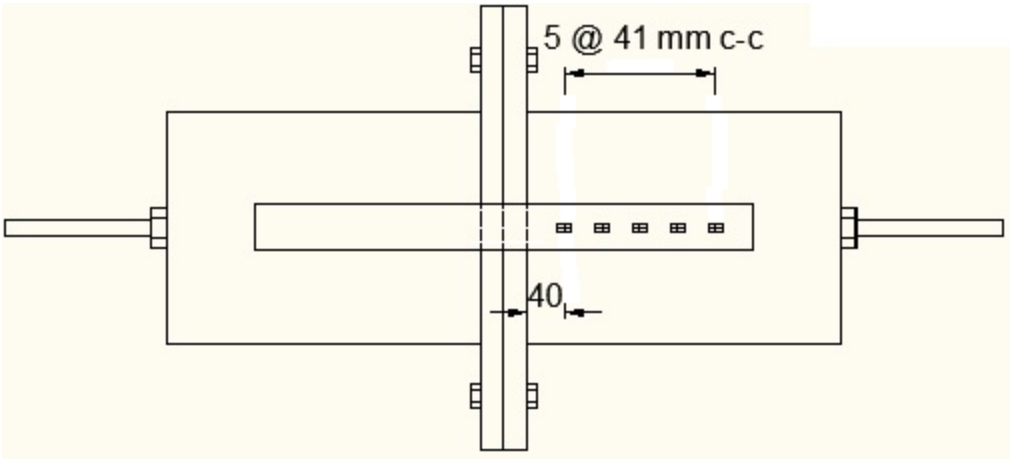

Figure 3.10: Location of strain gauges on specimen DS2 (north side)

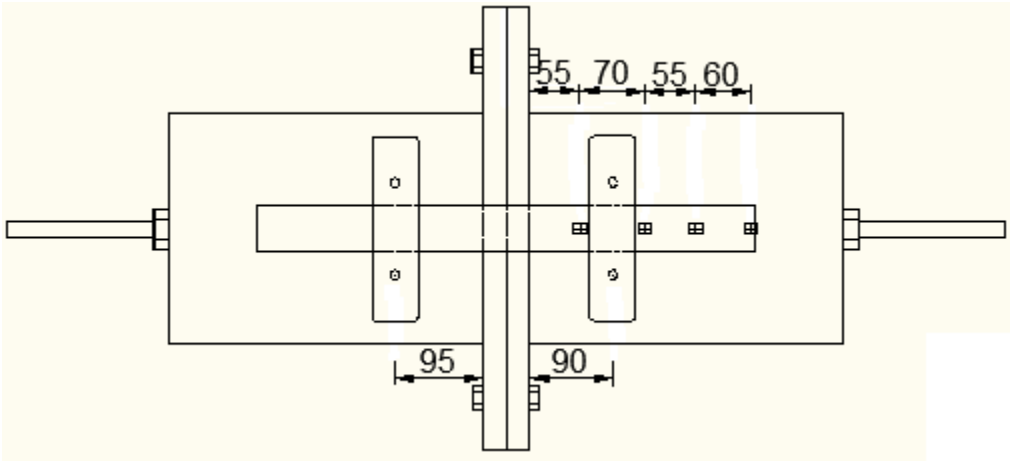

Figure 3.11: Location of strain gauges and anchors on specimen DS6 (north side)

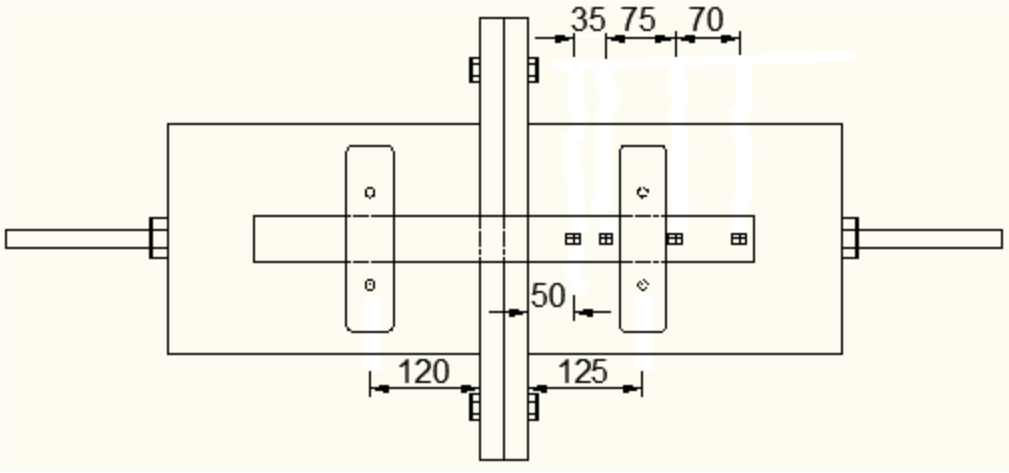

Figure 3.12: Location of strain gauges and anchors on specimen DS7 (north side)

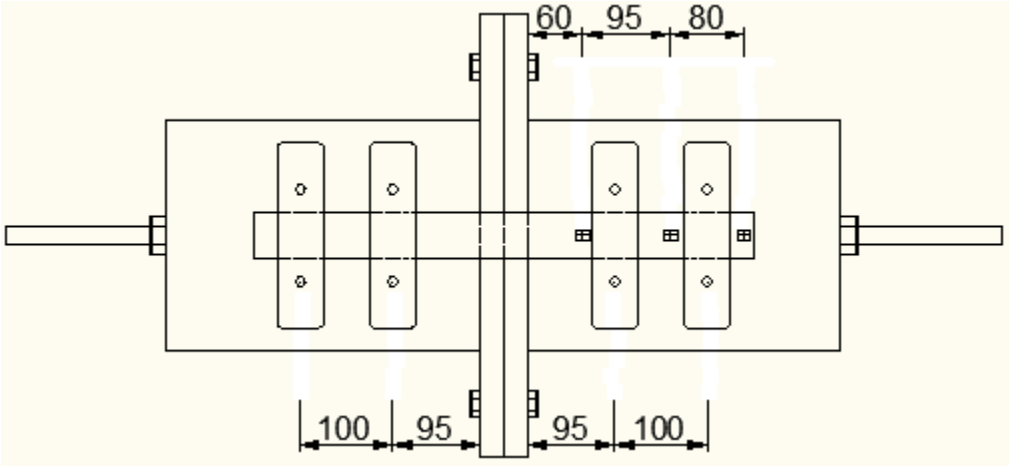

Figure 3.13: Location of strain gauges and anchors on specimen DS8 (north side)

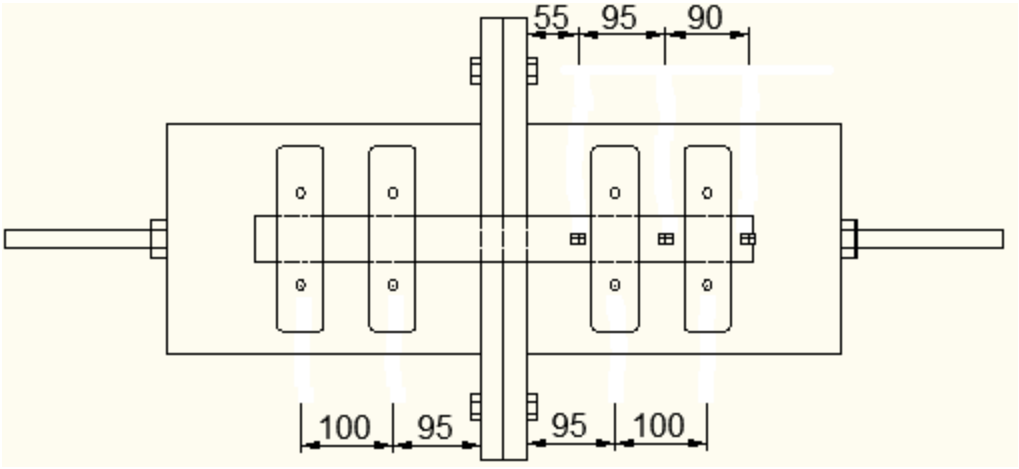

Figure 3.14: Location of strain gauges and anchors on specimen DS9 (north side)

String potentiometers were used to measure the displacement between the concrete prisms for all specimens except specimen DS5, where two dial gauges on each end of the steel plates were used.

A data acquisition system was used to record load, strain and displacement during loading.

3.1.5 TEST SETUP

Specimens were tested in the Applied Dynamics Laboratory at McMaster University in the Tinius Olsen hydraulic universal materials testing machine. A typical specimen within the testing machine is shown in Figure 3.15. The displacement was applied monotonically and the strain and load were continuously measured until the FRP debonded from the concrete or other causes that led to failure.

Figure 3.15: Typical specimen within testing device

3.1.6 Summary of Test Specimens

As seen in Table 3.1, nine specimens were tested in Phase One: two control specimens without anchors, five tests with one anchor on each prism face and two tests done with two anchors on each concrete prism face.

3.2 Phase Two – Large-Scale T-Beams

3.2.1 General

Phase Two was completed to determine the effectiveness of the proposed anchoring system when applied to full-scale RC beams. Six specimens were tested within Phase Two. Five RC beams were used, with one beam being tested twice as two different specimens. Bearing this in mind, all Phase Two specimens will be referred to as beams, henceforth, in the investigation. Of the six beams,

two were control beams with no FRP strengthening, one beam had FRP strengthening without anchors and the remaining three beams had FRP strengthening with different anchoring configurations. In all tests the FRP used for strengthening was the CFRP laminate described in Section 3.1.2.

T-beams were used to provide a large area of concrete resisting compression to ensure yielding of longitudinal steel, even with the addition of FRP tensile reinforcement. The beams were 4880 mm in length and had a span of 4500 mm. The depth of each beam was 400 mm with 100 mm being the flange depth. The width of the flange was 500 mm and the width of the web was 250 mm. Three 15M bars were used as tensile reinforcement and two 10M bars as hanger bars for the stirrups. The u-stirrups used were 10M bars spaced 150 mm centre-to-centre. The beams, designed according to CSA Standard A23.3-04 (CSA 2004) were designed to fail in flexure prior to shear failure. Details of the beam dimensions and reinforcement are provided in Figure 3.16 and Figure 3.17.

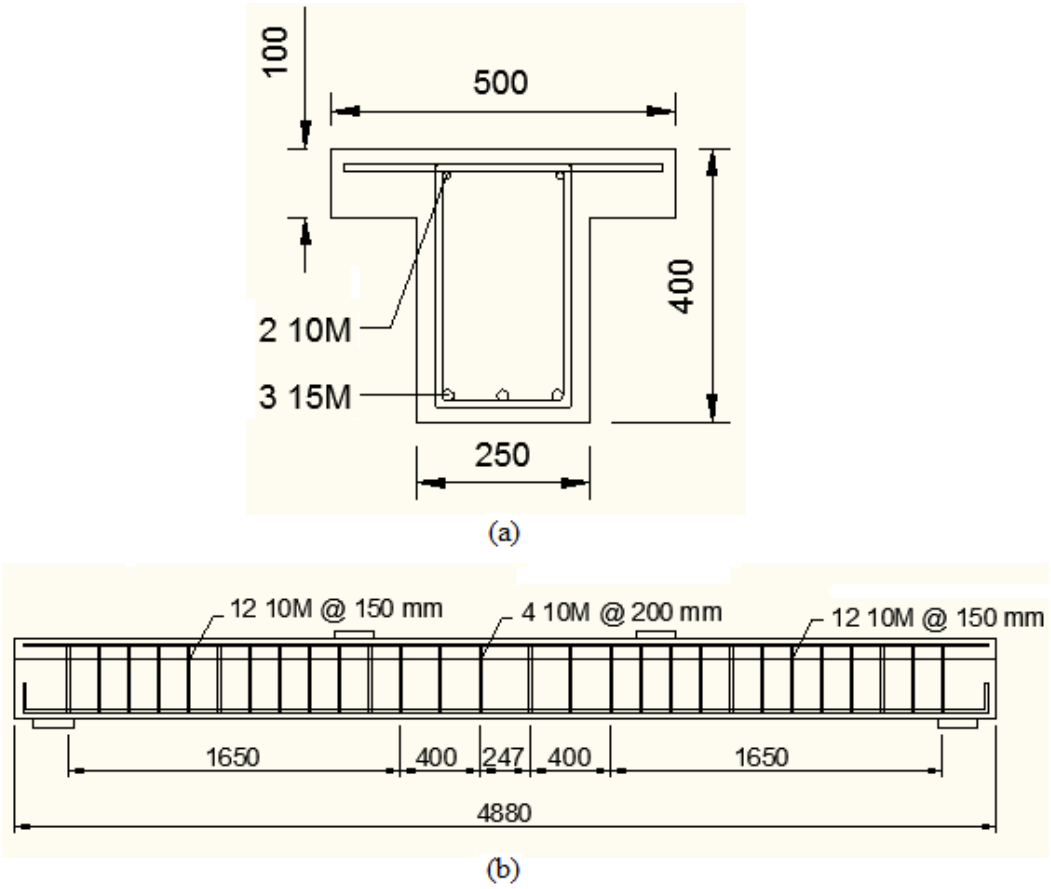

Figure 3.16: Phase Two beam (a) Cross-section and (b) Elevation view

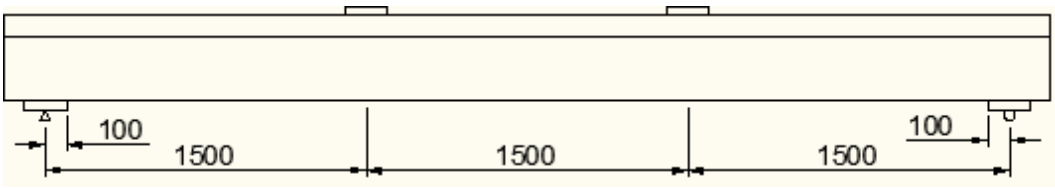

Figure 3.17: Loading and support dimensions

The tested beams were labeled with prefixes, CB, EB or EBA. The prefixes represent Control Beam, Epoxy Bonded FRP strip without anchors and Epoxy Bonded FRP strip with Anchors, respectively. Two control beams were tested and

therefore CB was followed by numbers one or two, similar to the EBA, as three beams were tested and were labeled one through three. Only one EB beam was tested and thus the beam was labeled EB1.

3.2.2 Material Properties

Concrete

The concrete beams were cast with ready mixed concrete ordered from a plant. Concrete with a specified strength of 40 MPa was ordered with maximum aggregate size of 12.5 mm. A super-plasticizer was added to the concrete to achieve the desired slump of 100 mm. The results of compressive and splitting tests from both batches of concrete are presented in Table 3.7, where f'_c is the concrete compressive strength and f'_t is its tensile strength. The compressive strength was calculated by completing a standard compression test on a cylinder with dimensions 300 x 150 x 150 mm. The tensile strength was obtained from completing splitting tests on cylinders of the same dimensions. Batch one and two refer to concrete delivered from two different trucks.

Table 3.7: Concrete cylinder test results after 46 days

Cylinder	Batch One		Batch Two	
	f'_c (MPa)	f'_t (MPa)	f'_c (MPa)	f'_t (MPa)
1	59.9	3.0	61.9	4.6
2	58.8	1.7*	56.8	3.6
3	58.6	3.4	61.0	4.4
4	57.3	3.4	59.1	4.7
5	62.1	-	58.3	-
6	60.1	-	52.2*	-
Average	59.5	3.3	59.4	4.6

Note that the values with an asterisk differed greatly from the strength values of the other cylinders. It was thought that these values were caused by inadequate preparation or testing and thus were omitted from the calculated averages. The average compressive strength for to the total amount of concrete delivered was approximately 59.4 MPa.

LONGITUDINAL STEEL REINFORCEMENT

In all beams, three 15M bars were used as tensile reinforcement and two 10M bars as hanger bars. Four samples were tested from the 15M longitudinal steel reinforcement and the results are presented in Table 3.8. The yield stress, f_y, yield strain, ε_y, ultimate strain, ε_u, modulus of elasticity, E_s, and ultimate strength, f_u, are given in the table.

Table 3.8: Longitudinal steel reinforcement properties (Mostafa 2011)

Sample	f_y (MPa)	ε_y	ε_u	E_s (MPa)	f_u (MPa)
1	505	0.0025	0.0078	202 000	637
2	465	0.0023	0.005	202 000	660
3	408	0.002	0.0071	203 900	656
4	428	0.0028	0.0066	152 900	691
Average	451	0.0024	0.0066	190 200	661

TRANSVERSE STEEL REINFORCEMENT

10M bars were used as shear reinforcement in the concrete beams. As previously mentioned, the beams were designed to fail in flexure well before shear failure due to the nature of the flexural strengthening investigation. In light of the expected flexural failure, samples of the transverse steel reinforcement were not tested. Instead, the yield strength was assumed as 400 MPa and the modulus of elasticity as 200 000 MPa for all design calculations.

CFRP LAMINATE

The FRP tensile reinforcement used in Phase Two was the same FRP laminate used in Phase One and was described in Section 3.1.2 (See Table 3.3 for material properties). All beams, except the two control beams, had one ply of CFRP laminate applied to the beam soffit.

EPOXY

In all the beams strengthened with the FRP strip, the Sikadur 30 epoxy paste described in Section 3.1.2 was used to bond the FRP to the beam. In addition,

Sikadur 30 epoxy was also used to bond the anchors to the FRP laminate and the concrete in two out of the three beams in which anchors were installed. In the remaining beam, the anchors were bonded to the FRP laminate and concrete using the two-component Wabo MBrace primer and saturant also described in Section 3.1.2. Upon review of the Phase One results it was decided not to use Sikadur 300 in Phase Two.

CFRP Anchor

The anchors used in Phase Two were the same as the anchors used in Phase One and described in Section 3.1.2.

3.2.3 Fabrication of Specimens

Concrete Casting

Wooden forms were constructed in order to cast the beams. Reinforcement cages were placed into the forms with high accuracy prior to the pouring of concrete. Plastic chairs were used under the cages to ensure 40 mm of cover. Oil was applied to the inside of the wooden forms to ease form removal following curing of the concrete. Strain gauges were applied to the longitudinal steel prior to casting. The strain gauges were coated with a layer of silicon for protection during the casting process and will be described further in Section 3.2.4.

Details regarding the concrete specifications and properties can be found in Section 3.2.2. The concrete was poured in two batches and was vibrated to

remove any large voids. Once pouring was complete, the exposed concrete was finished. Upon completion, the beams were covered with a plastic tarp to prevent moisture evaporation for seven days. The forms were removed one week after casting and the beams were air cured for their remaining life.

FRP Application

Two control beams were tested without FRP reinforcement, while the remaining beams were tested with bonded FRP laminate. Prior to the bonding of FRP to the beams, the surface concrete on the beam soffit was removed with an electric grinder with a sanding head. The result of grinding the surface was a smooth bonding surface with the aggregate and the internal pore structure exposed. Compressed air was used to clean the bond surface following grinding and immediately preceding installation of FRP. For ease of application, the FRP was applied with the beam inverted, using the Sikadur 30 epoxy described in Section 3.1.2. The size and location of the FRP strip are shown in Figure 3.18.

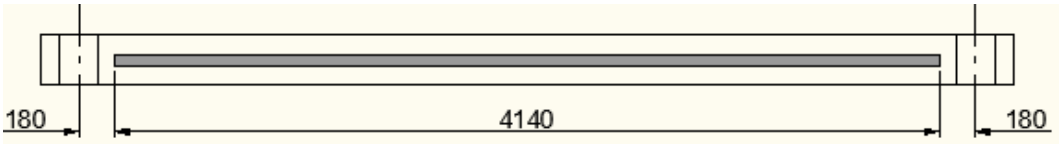

Figure 3.18: Layout of FRP reinforcement

In the case of beam EBA2, the beam tested was the same beam as EB1 tested prior. Therefore, large flexural cracks were present prior to the application of

FRP. Prior to the application of the FRP, most of the epoxy from the previous test, EB1, was removed from the beam with a hammer and chisel. The remaining epoxy was removed using a grinder with a sanding head. Compressed air was used to remove any loose pieces of concrete from the large flexural cracks. Following the process stated above, the FRP was applied similarly to applying it to the other beams.

Beams were inverted and undisturbed for a minimum of one week following the installation of FRP before being transported into place and tested.

Anchor Installation

Before the grinding of the soffit of the beams and the application of the FRP plate, holes were drilled in the soffit for the anchor legs to be inserted into. The holes were drilled using an electric hammer drill with masonry drill bits. The 12.7 mm holes were drilled to an approximate depth of 100 mm to ensure the anchors full insertion into the holes.

The anchor spacing in beams EBA1 and EBA2 was 200 mm for the length of the FRP strip. A total of 21 anchors were used in each beam. A schematic view of beams' EBA1 and EBA2 soffits with anchor locations is shown in is given in Figure 3.19.

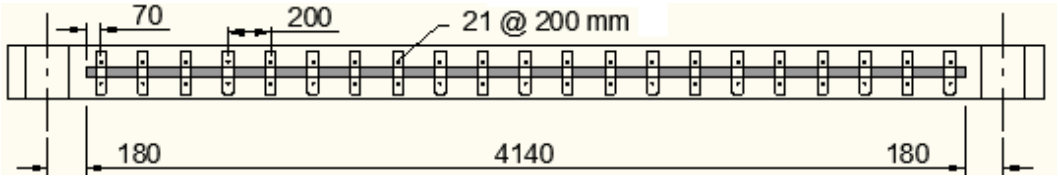

Figure 3.19: Soffit of beams EBA1 and EBA2

Anchor spacing for beam EBA3 was 100 mm for 300 mm at both ends of the laminate for a total of four anchors at each end. In the middle portion, 22 anchors were spaced 150 mm apart as shown in Figure 3.20. A total of 30 anchors were used in specimen EBA3.

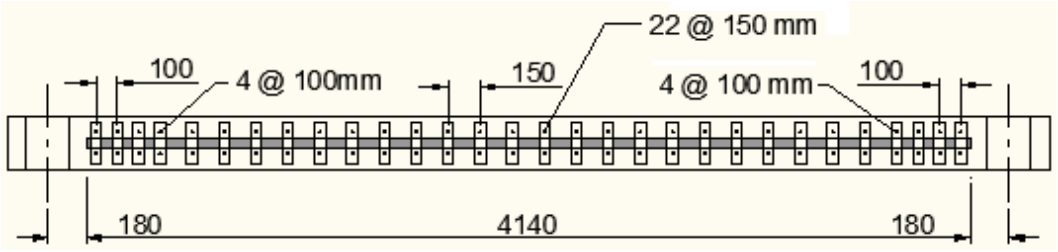

Figure 3.20: Soffit of beam EBA3

Some holes for anchor legs had to be moved to avoid drilling through the internal steel reinforcement cage. Thus, some anchors could not be placed perpendicular to the FRP strip, as shown in Figure 3.20. However, no anchor hole was displaced more than 20 mm from its originally planned location.

3.2.4 INSTRUMENTATION

INTERNAL REINFORCEMENT STRAIN GAUGES

Seven strain gauges were installed on the tensile reinforcing steel. The location of the strain gauges is shown in Figure 3.21. The strain gauges were installed prior to casting and a layer of silicon was applied over them for protection during casting of the beams.

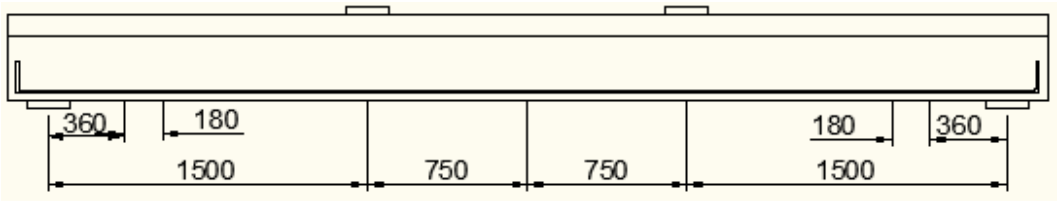

Figure 3.21: Location of strain gauges on tensile steel reinforcement

Due to damage during casting and the corrosion of wires as a result of storage of the beams outside, many strain gauges malfunctioned. Because the strain gauges were inside the beam, they could not be repaired or replaced, thus making them unusable. However, all functioning strain gauges were used. In addition, beam EBA2 was the same beam originally tested as EB1 and subsequently strengthened again and retrofitted with anchors, therefore, the tensile steel was assumed to have yielded. Therefore, the strain gauges on the tensile steel were disregarded during the testing of EBA2. Knowing the exact value of steel strain in the current tests is not necessary, but is desirable and may assist the analysis.

STRING POTENTIOMETERS

String potentiometers were used to measure displacement during Phase Two testing. As shown in Figure 3.22, the string potentiometers were placed at midspan and under one of the loading points. The string potentiometers were attached to a small wire circling the beam at the correct location to ensure cracking would not alter displacement measurements.

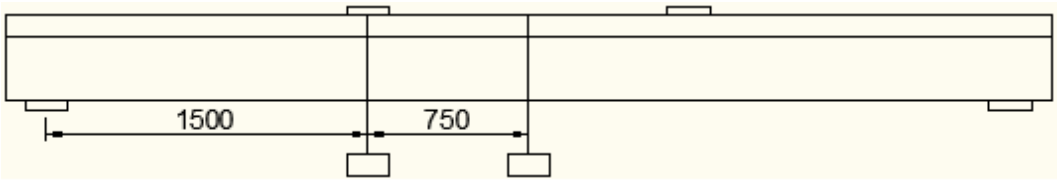

Figure 3.22: Location of string potentiometers

FRP STRAIN GAUGES

After the application of the FRP to the beams, strain gauges were installed on the FRP laminate surface. The strain gauges were installed to develop the strain profile within the FRP during testing and to compare measured strain values with values calculated by sectional analysis. The strain gauges used had a length of 30 mm. Five or six strain gauges were applied to the FRP. In all beams either one or two strain gauges were applied in the centre of the FRP strip, the location where the maximum strain is expected. Two strain gauges were also positioned at approximately distance, d, from the strip end where d is the effective depth of the beam. The other two strain gauges were placed midway between the centre

and end strain gauges. The strain gauges were placed between anchors and therefore their locations are not symmetrical in all tests due to anchor locations. The exact locations of the strain gauges are shown in Figure 3.23 to Figure 3.26, with the northeast end of the beam displayed on the left in all the figures.

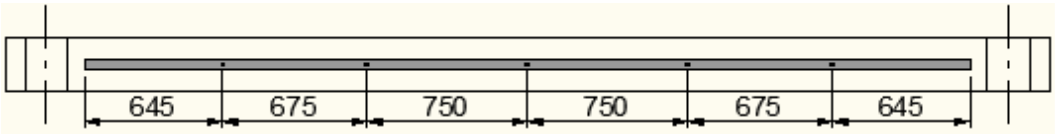

Figure 3.23: FRP strain gauge locations of EB1

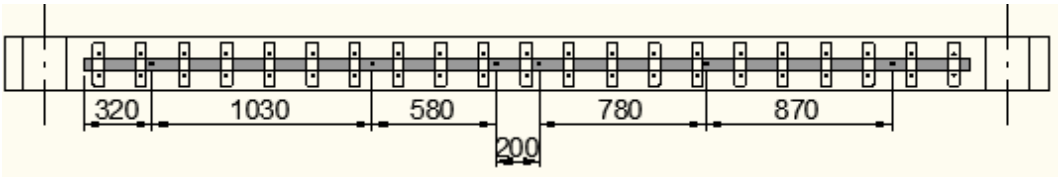

Figure 3.24: FRP strain gauge locations of EBA1

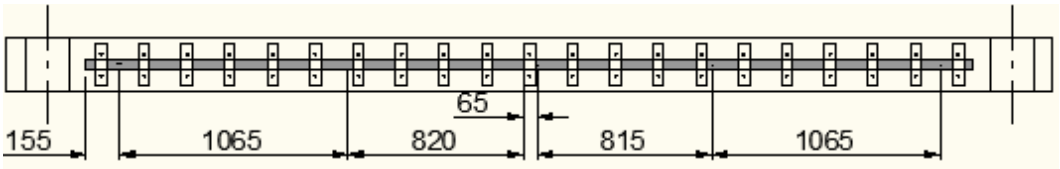

Figure 3.25: FRP strain gauge locations of EBA2

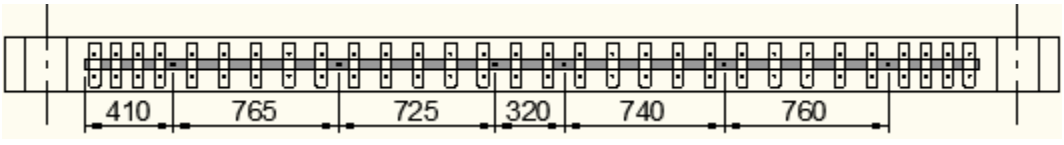

Figure 3.26: FRP strain gauge locations of EBA3

Load Cell

A load cell with a capacity of 890 kN and attached to a hydraulic actuator was used to measure the load during testing.

3.2.5 Test Setup

The Phase Two beams were tested in the Applied Dynamics Laboratory at McMaster University. The beams were simply supported on a 4500 mm span, with a roller at one support and a pin at the other. Hydrostone was placed between the supports and the beam to eliminate any stress concentrations due to irregular beam geometry. The load was applied by a jack supported by a steel frame fixed to the strong floor of the laboratory. The jack had a capacity of 890 kN and a stroke of 500 mm. The beams were tested in four-point bending. A spreader beam was used to apply the load at two points 1500 mm apart. The spreader beam was mounted on a pin and a roller support which were also placed on hydrostone to prevent stress concentrations. A typical setup is shown in Figure 3.27.

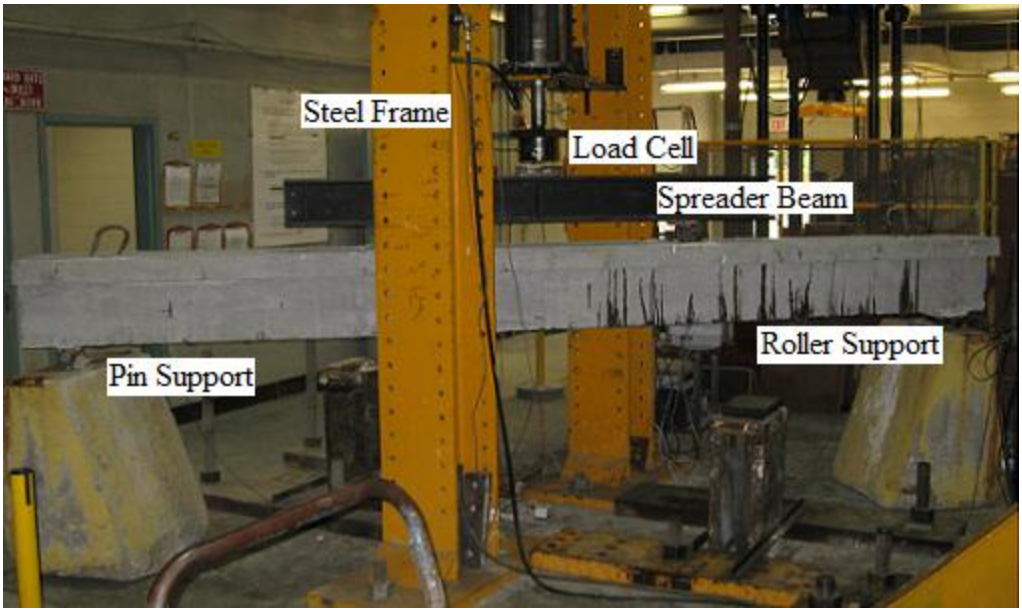

Figure 3.27: Typical setup of Phase Two beams

3.2.6 SUMMARY

As displayed in Table 3.9, seven beams were tested in Phase Two of this experimental investigation. Three control beams were tested, one beam with only epoxy bonded FRP and three beams were tested with epoxy bonded FRP with anchors.

Table 3.9: Summary of Phase Two specimens

Beam	f'_c (MPa)	Number of Anchors	Number of FRP Strain Gauges	Epoxy Used To Bond Anchors
CB1	59.4	-	-	-
CB2	59.4	-	-	-
EB1	59.4	0	5	-
EBA1	59.4	22	6	MBrace
EBA2	59.4	22	6	Sikadur 30
EBA3	59.4	30	6	Sikadur 30

CHAPTER 4 - EXPERIMENTAL RESULTS

4.1 PHASE ONE

Nine specimens were tested in direct tension in a double shear test in Phase One. Schematic drawings of all the specimens are shown in Section 3.1. The parameters investigated were the presence/absence of anchors, different epoxy types and the number of anchors. Specimens are labeled DSx, with DS representing Double Shear test and x representing the test number, varying from one to nine.

4.1.1 CONTROL SPECIMENS

Two control specimens with FRP reinforcement, but no anchors, were tested to determine the strength of epoxy bonding the FRP to the concrete prisms. Like all specimens, the FRP was applied using Sikadur 30 paste epoxy. During testing of the first control specimen, DS1, the first cracking sounds could be heard at 17 kN. However, cracks were not visible until 67 kN, when a crack became visible in the epoxy on the bottom south side at the loaded end of the FRP. Debonding of the FRP occurred at the latter location suddenly, with little warning, at a load of 72.5 kN. The failure plane was primarily at the adhesive-concrete interface, but also partially within the concrete as shown in Figure 4.1. At debonding the

corresponding elongation was 4.0 mm. The three faces not experiencing debonding did not exhibit cracking or damage.

Initial cracking during the testing of the second control specimen, DS2, was heard at 52 kN. At a load of 61 kN, cracks could be seen propagating through the epoxy and concrete on the bottom south side of the loaded end of the FRP. Debonding of FRP on the bottom of the north and the top of the south side occurred at a load of 64.8 kN. Upon observing the test, it is believed that the south side debonded prior to the north side with the dynamic effects resulting from the sudden release of energy instigating debonding on the north side. The failure plane on the south side was once again at the concrete-adhesive interface, except for 75 mm at the free end of the FRP, which failed at the FRP-adhesive interface as shown in Figure 4.1. The elongation at debonding was 2.8 mm. The faces in which debonding did not occur showed no cracking or debonding.

Figure 4.1: Failure plane of (a) Bottom south side of DS1 and (b) Top south side of DS2

The load-elongation curves for the control specimens are presented in Figure 4.2. The initial portion of the curves indicated the presence of some slack in the beginning of the test inherent within the testing device, and was not reflective of the actual behaviour of the FRP laminate. Therefore, the data indicating the slack was omitted from all Phase One load-elongation curves. Elongation was measured by a string potentiometer fixed to the moving head on the universal testing machine. The curves seem to be in agreement, however, the DS1 curve which failed partially within the concrete, achieved higher load and elongation.

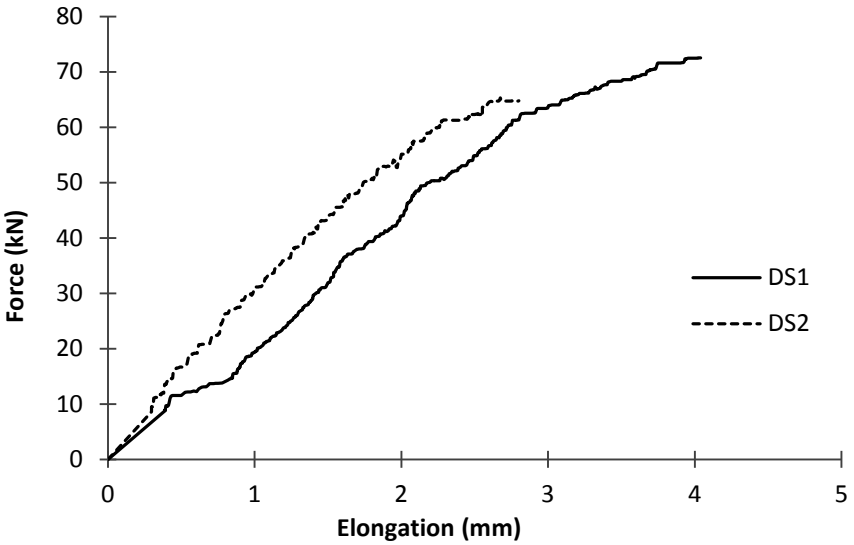

Figure 4.2: Load-elongation curve for control specimens DS1 and DS2

For specimen DS1, the peak strain values were 3539 and 3549 με for the north and south side, respectively. For specimen DS2, the peak strain for the north and south side were 2872 and 2950 με, respectively. The larger peak strain value for each specimen was 20.9 and 17.4% of the ultimate strain capacity of the FRP laminate (17 000 με) for specimens DS1 and DS2, respectively. The full load-strain curves for specimen DS1 and DS2 are shown in Figure 4.3 and Figure 4.4, along with the approximate locations of the strain gauges. The precise locations of the strain gauges are given in Section 3.1.4.

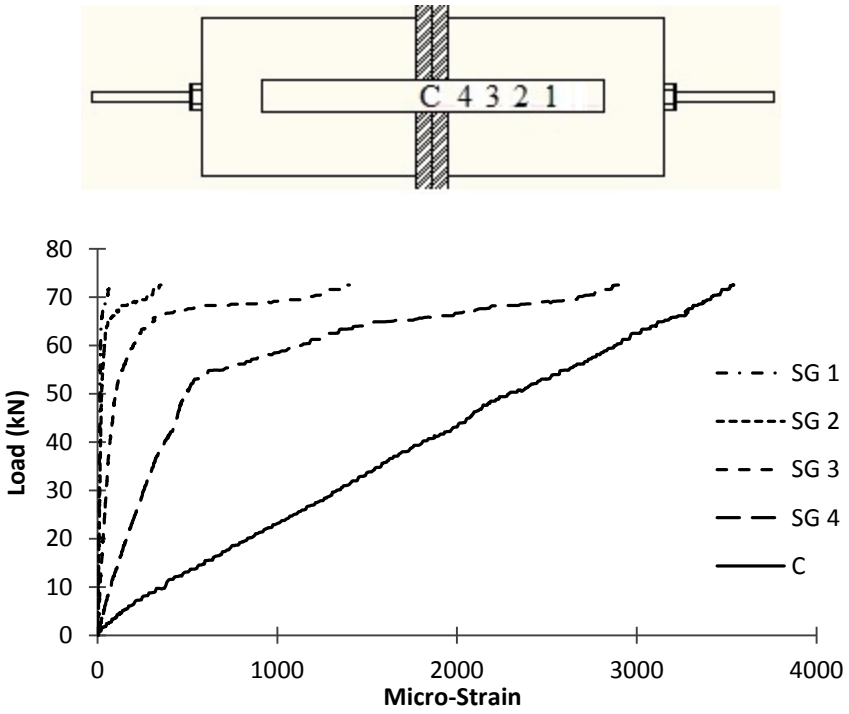

Figure 4.3: DS1 load-strain curves

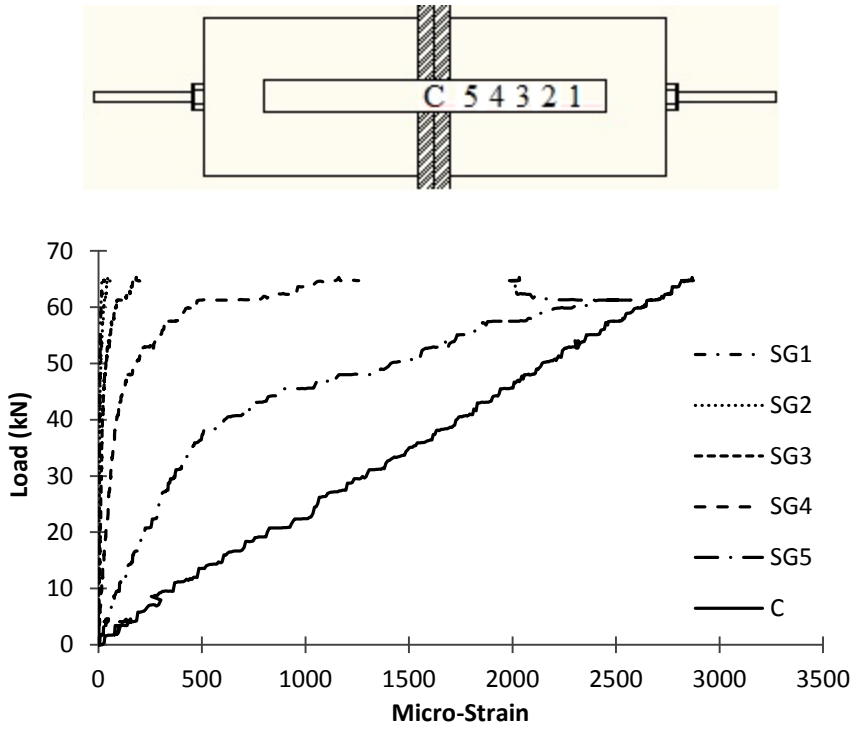

Figure 4.4: DS2 Load-strain curves

The strain profile of the bonded FRP was measured on one face of each of the control specimens. Both specimen had five strain gauges to capture the strain profile, however, one strain gauge malfunctioned during the DS1 test resulting in the use of data from only four gauges. The strain profiles at debonding and half the debonding load in both control specimens, DS1 and DS2, are shown in Figure 4.5. The strain gauges were placed on the top north face on both specimens, and were not at the location where debonding occurred in either test.

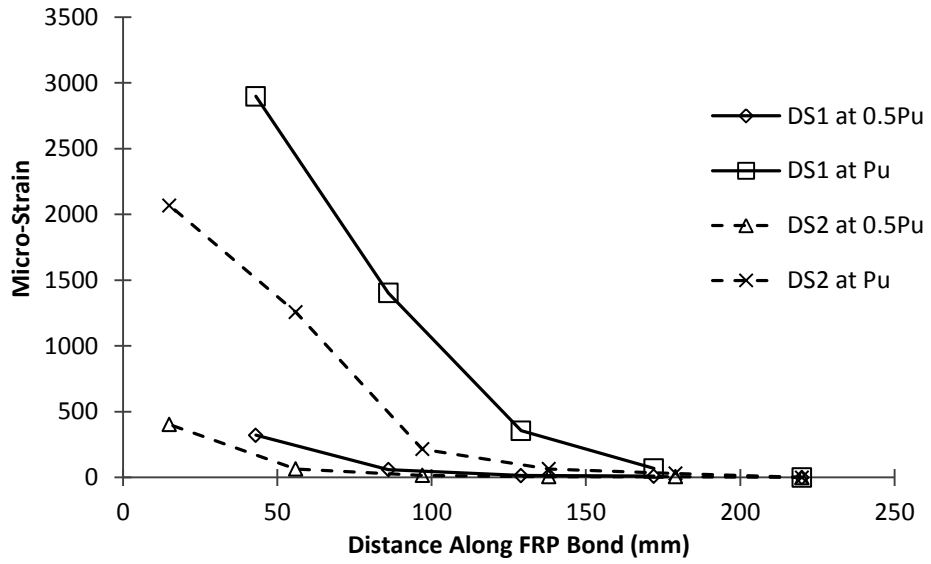

Figure 4.5: Strain profile in FRP at half and full debonding load of specimen DS1 and DS2

4.1.2 Specimens with One Anchor on Each Face

Five specimens were tested with one anchor on each face with three different types of epoxy to bond the anchors to the FRP and concrete. Since the 90 mm height of the anchor legs was more than half the 150 mm depth of the concrete

prisms, anchors could not be positioned in the same location on opposing faces. Therefore, the position of the anchor on the FRP is different on different concrete faces. However, the bonded length of FRP was kept at 220 mm for all the specimens. The material properties of the epoxies used can be found in Section 3.1.2.

SPECIMEN DS3, DS4 AND DS5

Specimen DS3, DS4 and DS5 were part of the preliminary tests in Phase One, which were conducted to assess the effectiveness of the anchor in terms of the maximum load that the laminate could resist prior to debonding and were not designed to study the strain distribution at the FRP-concrete interface. Therefore, no strain gauges were installed on the bonded portion of the FRP laminate. In addition, DS3 was tested without hydrostone or gypsum cement between the concrete prisms and the steel plates. In all subsequent tests, gypsum cement was placed between the prisms and steel plates to minimize any stress concentrations. Specimen DS3 and DS4 were tested with Wabo MBrace primer and saturant and both only had two strain gauges, one on each laminate strip placed in the centre of the unbonded segment of the FRP strip.

During the testing of DS3, cracking sounds were first audible at a load of 50 kN. The FRP debonded from the concrete prism on the bottom south face at a load of 65.8 kN as shown in Figure 4.6(a). The FRP plate slipped under the anchor,

leaving the anchor unmoved and undamaged. Failure occurred at the adhesive-concrete interface above the anchor and at the FRP-adhesive interface below the anchor. However, a small volume of concrete from the end of the concrete prism was attached to the FRP. As a result of the volume of concrete attached to the FRP, it was decided to include a 25 mm unbonded length at the end of the concrete prisms to prevent concrete block failure in the following tests. The faces on the north side displayed no signs of debonding or damage. At debonding of the FRP, the corresponding elongation was 4.0 mm.

Figure 4.6: (a) Failed specimen DS3, (b) Initial debonding of specimen DS4 and (c) Failure of specimen DS4

With a similar failure load to that of the control specimens, it was decided that insufficient epoxy was used on the south side of the specimen, possibly leading to a premature failure. Therefore, it was decided to repeat the test using more epoxy on specimen DS4. A comparison of the amount of epoxy used on DS3 and

DS4 is shown in Figure 4.7. Upon testing specimen DS4, the first crack was heard at 69 kN. At a load of 91.3 kN the anchor and the FRP in front of the anchor appeared to debond from the concrete as shown in Figure 4.6(b). However, the FRP plate behind the anchor did not debond and thus the load-elongation curve peaked again at 59.9 kN when the FRP fully debonded from the concrete and the anchor as shown in Figure 4.6(c). At the debonding load of 59.9 kN, the corresponding elongation was 4.0 mm. It should be noted that following the initial debonding some bending was induced in the specimen due to the elongation of its side.

Figure 4.7: Comparison of amount of epoxy used on (a) South side of DS3 and (b) North side of DS4

The load-elongation curves for DS3 and DS4 are shown in Figure 4.8. Specimen DS4, in which more epoxy was used, achieved a higher load at a similar deflection as specimen DS3, as the stiffness was greater than that of specimen DS3.

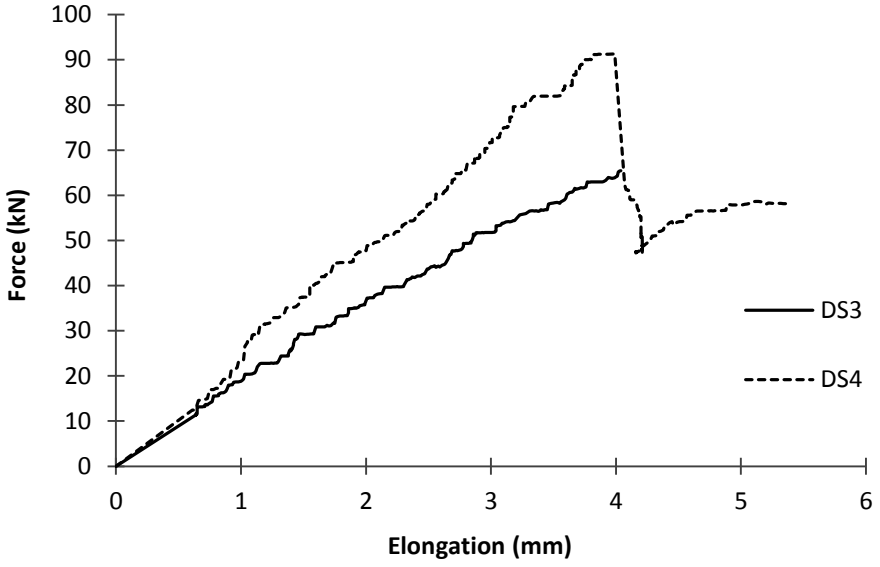

Figure 4.8: Load-elongation curves for DS3 and DS4

For specimen DS3, the peak strain measured in the centre of the FRP plates was 3003 and 3014 με on the north and south side, respectively. In specimen DS4, the peak strain measured was 4343 and 4482 με on the north and south side, respectively. The larger peak strain value in specimen DS3 and DS4 represents 17.7 and 26.4% of the ultimate strain of the FRP laminate, respectively. The load-strain curves for specimen DS3 and DS4 are shown in Figure 4.9. The load-strain curve of specimen DS4 is only shown up to the peak load of 91.3 kN, thus, the

second peak phenomenon observed in the load-deflection curve is not included. In addition, the north and south strain gauges on each specimen were in good agreement with each other so only one curve is included for each specimen.

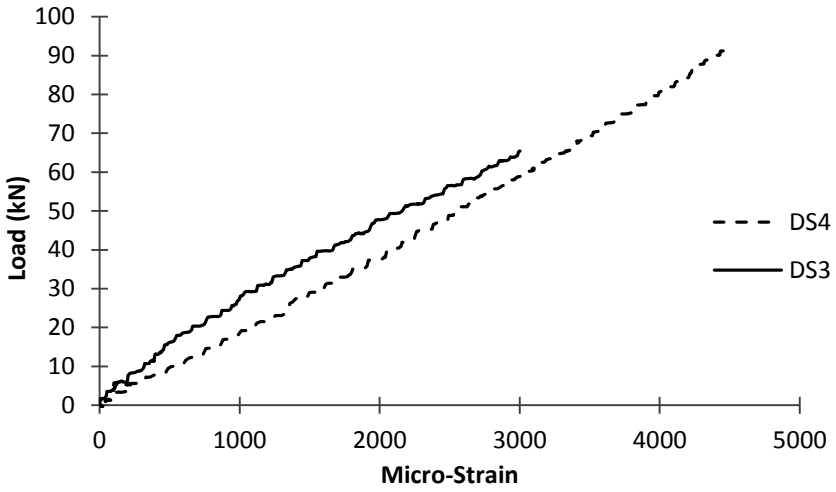

Figure 4.9: Load-strain curve for specimen DS3 and DS4

Specimen DS5 was similar to specimens DS3 and DS4, except that Sikadur 300 epoxy was used to bond the anchors to the FRP and concrete. It was decided to use the Sikadur 300 epoxy because of ease of installation and the lack of need for a primer. It was believed that the elimination of primer would make Sikadur 300 epoxy a more desirable choice for field applications. The material properties of Sikadur 300 are given in Section 3.1.2. When using the low viscosity Sikadur 300, voids with no epoxy were discovered between the anchor head and concrete. To eliminate the voids, epoxy was injected into the cavities with a

plastic syringe. After one round of epoxy injections, the anchor head was deemed to be fully bonded with the concrete surface.

The behaviour of DS5 was similar to those observed in the previous tests. No indication of any damage occurred until a cracking sound was heard at a load of 50 kN. At a load of 80 kN, cracks began to form in the Sikadur 30 epoxy used to bond the FRP to the concrete. The cracks appeared in the epoxy on the bottom south face at the loaded end of the FRP. At a load of 96 kN the FRP on the bottom north face debonded, as shown in Figure 4.10(a). The failure was a few millimeters below the concrete surface and is also shown in Figure 4.10(b).

Figure 4.10: Failure of DS5 (a) Bottom north face and (b) Failure plane

The load-elongation curve for DS5 is shown in Figure 4.11. The elongation of specimen was measured with two Linear Variable Differential Transformers

(LVDTs), in an attempt to measure the elongation more accurately. The LVDTs were placed on the east and west side of the top steel plate and measured the separation between the plates. The displacement from the LVDTs was averaged to get the displacement at the centre of the specimen. However, small eccentricities inherent within the specimen during loading were thought to limit the accuracy of measuring elongation with LVDTs and it was decided to use string potentiometers for all subsequent tests. Because of the small flexural effects present during loading, the elongation values measured with the LVDTs are questionable. Bearing that in mind, the averaged elongation at the time of FRP debonding was calculated as 2.6 mm.

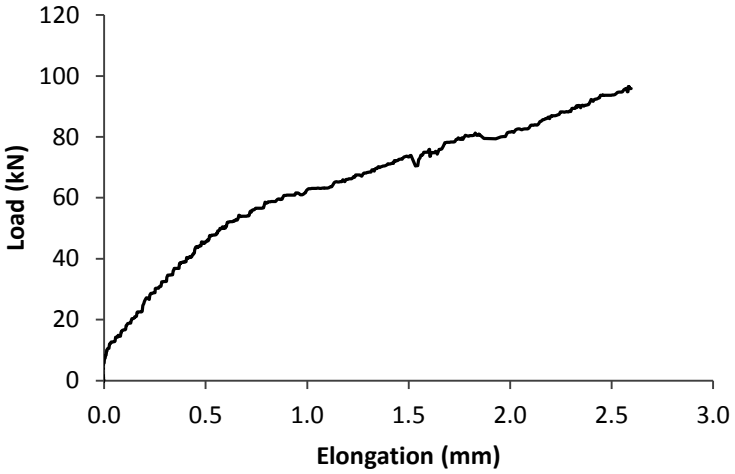

Figure 4.11: Load-elongation curve for DS5

Strain gauges placed in the centre of the FRP plates on the north and south side measured strains of 4647 and 4728 με, respectively, at debonding, the larger of

which represents 27.8% of the ultimate strain of the FRP laminate. The full load-strain curve for specimen DS5 is shown in Figure 4.12.

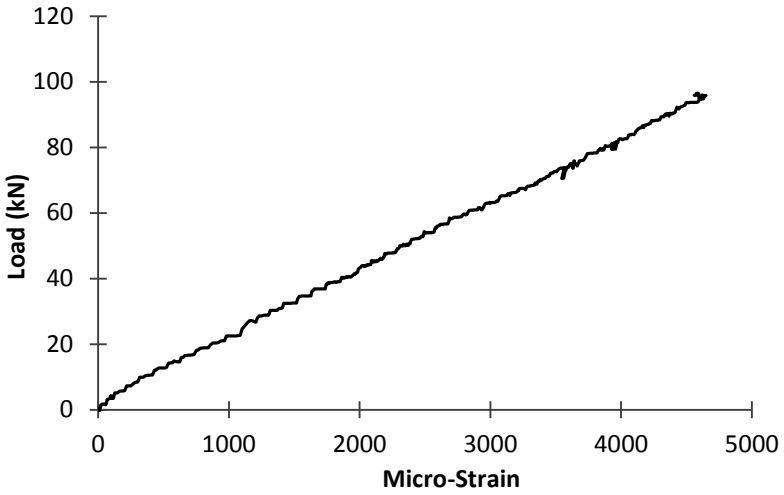

Figure 4.12: Load-strain curve for specimen DS5

SPECIMEN DS6 AND DS7

Specimens DS6 and DS7 were constructed with Sikadur 30 epoxy paste (see Section 3.1.2 for details) which was used to bond the FRP to the concrete prisms as well as the anchors to the FPR and prisms. In addition, four strain gauges were placed on the bonded portion of the top north face to determine the strain profile within the FRP. Similar to all Phase One specimens, an additional two strain gauges were placed in the centre of both FRP strips to measure the strain within the FRP strips.

During the testing of DS6 it could be seen that the load was being applied at an eccentricity due to inequalities in the measured strain on the north and south

sides. Therefore, in an attempt to minimize any bending effects, the load was reduced to zero and the specimen was repositioned after previously reaching a load of 65 kN. When the positioning of the specimen was deemed to be reasonable, the specimen was loaded again. Upon loading again, it was noticed that the strain gauges in the centre of each FRP plate were significantly different again. It was decided to again reposition the specimen to minimize any eccentricity and loading was resumed.

Once the load reached 66 kN, a loud cracking sound was heard, indicating damage somewhere within the specimen. However, upon visual inspection, no damage could be seen at a load of 66 kN. At a load of 96 N, it could be seen that the FRP on the bottom south face had debonded in front of the anchor. It is believed that faces of the concrete prisms, and thus the FRP, were not parallel or in proper alignment possibly causing premature debonding. If the concrete faces were not parallel or if they were not in proper alignment, it may have caused eccentricity in the loading, leading to the discrepancy between the measured north and south strains. At a load of 111 kN, both the north and south FRP debonded on the top and bottom face respectively. Because of the initial debonding in front of the anchor on the south face, it is believed that the south side debonded first, with the dynamics effects causing the top north face to debond shortly after as shown in Figure 4.13. The elongation corresponding to the failure load was 8.4 mm.

Figure 4.13: Debonding of DS6 (a) Top north face and (b) Bottom south face

DS7 was the companion specimen of DS6 and thus was similar to DS6 in the type of epoxy used and the number of anchors. Unlike DS6, the north and south strain in DS7 were in agreement with each other and there was no need to reposition the specimen during loading. Upon loading the first crack was heard at 55 kN. At a load of 110 kN, it appeared as though the FRP in front of the anchor on the bottom south face had debonded from the concrete. It is speculated that debonding had indeed occurred because of the presence of many cracks in the epoxy in front of the anchor. Debonding of the FRP on the top north and bottom south face occurred at a load of 118 kN. It is believed that the debonding first occurred on the top north face with the dynamic effects causing the bottom south face to debond. The elongation at the failure load of 118 kN was 8.4 mm.

Following the debonding, the specimen was still loaded to remove the FRP strips from under the anchors to determine where the failure planes occurred. On the

south side, the failure plane occurred at the adhesive-concrete interface in front of the anchor and at the FRP-adhesive interface behind the anchor as shown in Figure 4.14(a). On the top north face the failure plane was almost entirely within a few millimeters into the concrete, but some failure could also be seen at the FRP-adhesive interface immediately following the anchor as shown in Figure 4.14(b). Since the specimens with Sikadur 30 epoxy used to bond the anchors to the concrete and the FRP outperformed the other epoxies, it was decided to complete all subsequent tests with Sikadur 30 epoxy.

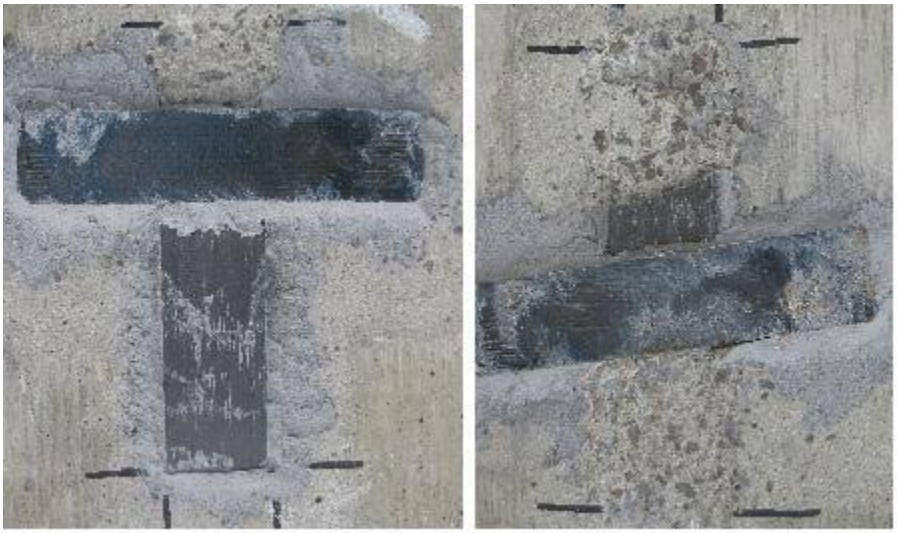

Figure 4.14: Failure planes of DS7 (a) Bottom south face and (b) top north face

The load-elongation curves for specimens DS6 and DS7 are shown in Figure 4.15. Both specimens exhibited a similar linear relationship between load and elongation. The termination point of both curves is also very similar at

approximately 115 kN and an elongation of approximately 8.6 mm. The loading and unloading as a result of apparent eccentricities in specimen DS6 are displayed as loops on the load-elongation curve. It is interesting to observe how the loading and unloading did not affect the specimen behaviour because after reloading the specimen followed its original load-elongation path.

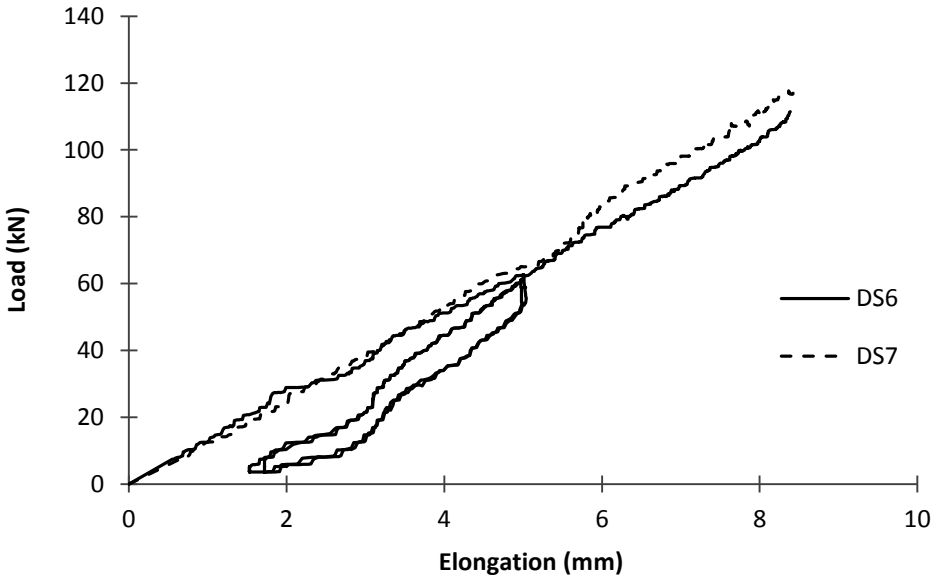

Figure 4.15: Load-elongation curves of DS6 and DS7

The peak strain in the north and south strips was 5289 and 5451 με, respectively, for specimen DS6. Similarly, the peak strain for specimen DS7 was 5260 and 5520 με, for the north and south side, respectively. The larger of the peak values for DS6 and DS7 represent 32.1 and 32.5% of the ultimate strain of the FRP laminate. The full load-strain curves for specimen DS6 and DS7 are shown in Figure 4.16 and Figure 4.17, respectively. The load-strain curve for specimen DS6

only represents the load and strain values after the specimen was positioned correctly.

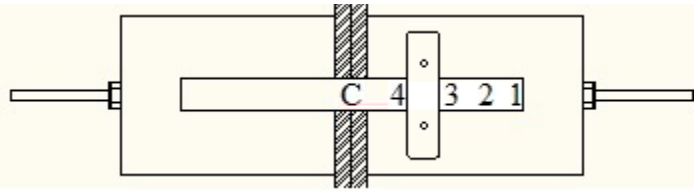

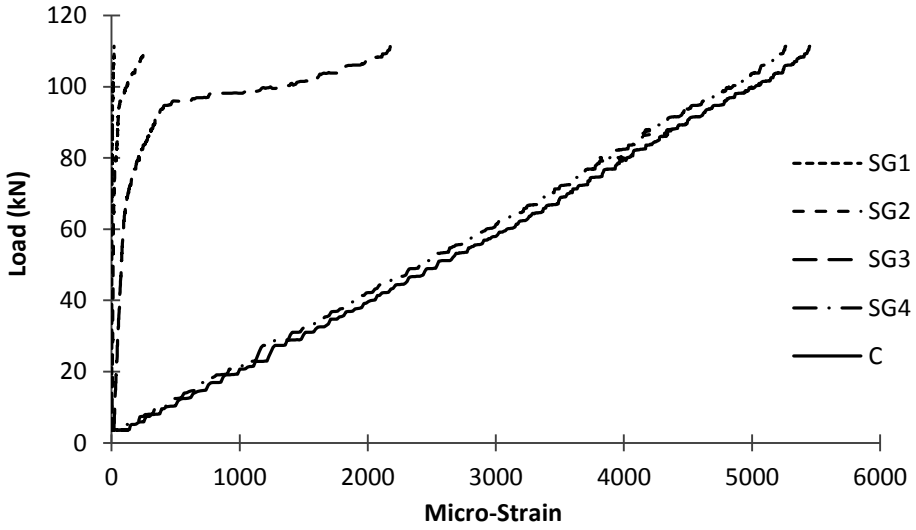

Figure 4.16: DS6 load-strain curves

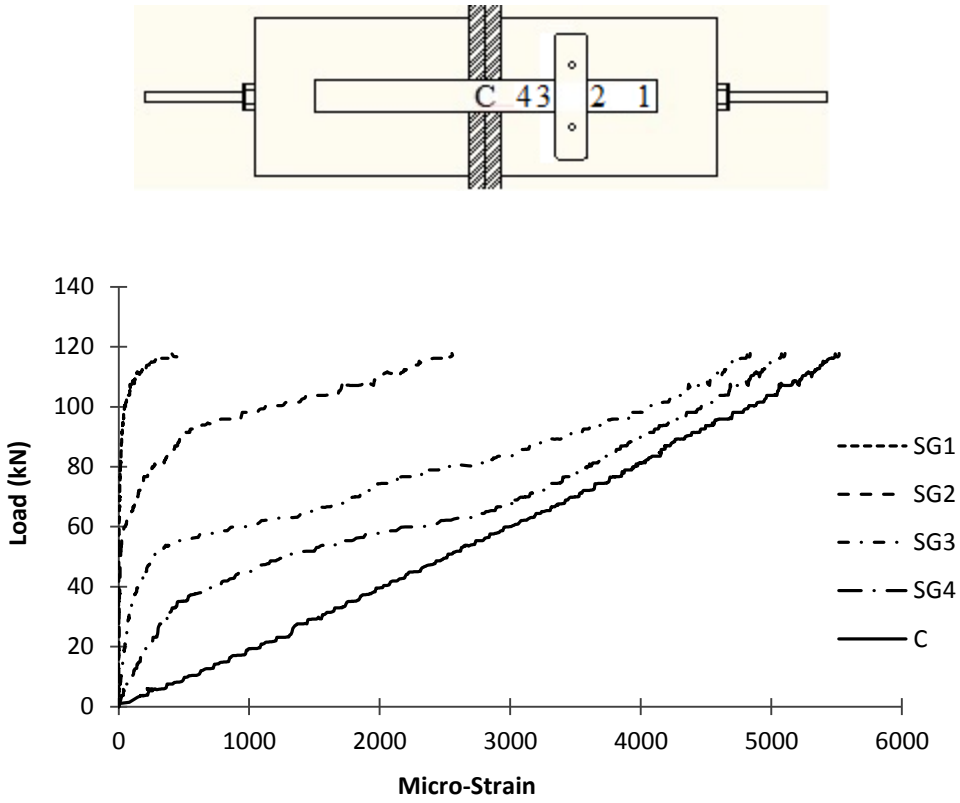

Figure 4.17: DS7 load-strain curves

Four strain gauges were placed on the bonded portion of the FRP on one face of the DS6 and DS7 specimens to determine the strain profile along their bonded length. The strain gauges were placed on the bottom north face of specimens DS6 and the top north face of DS7. The strain profiles corresponding to the half and the full debonding load of each specimen are shown in Figure 4.18. The centre of the 50 mm wide anchor was 65 mm in DS6 and 100 mm in DS7 from the point where the strip was initially bonded to the concrete. Consequently, the strain gauges were not placed at the same position in the two specimens.

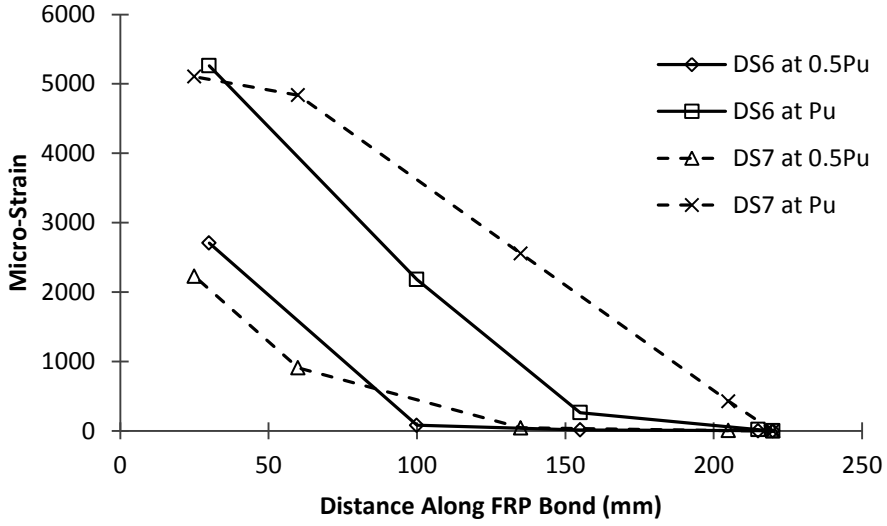

Figure 4.18: Strain profile within FRP at half and full debonding load of specimen DS6 and DS7

4.1.3 Specimens with Two Anchors on Each Face

Two tests were completed with two anchors on each face, DS8 and DS9. It was believed that the additional anchor would further increase the bond strength between the FRP and the concrete. As mentioned earlier, Sikadur 30 epoxy was used to bond the anchors to the concrete and FRP for the tests with two anchors. In addition, three strain gauges were installed on one face to determine the strain profile in these specimens.

During the testing of DS8 the first cracking sound was heard at 53 kN, however no visible damage could be seen. At a load of 105 kN, debonding of the FRP occurred on the top north face. Both faces on the south face showed no signs of

debonding or damage. The failure plane of the debonded FRP was primarily at the adhesive-concrete interface. This indicates an irregularity as the failure plane is expected to be within the relatively weak concrete. The failed specimen and failure plane of DS8 are shown in Figure 4.19(a). The elongation corresponding to the debonding load was measured to be 6.3 mm. Some doubt exits regarding the validity of this test as the failure plane was not at all within the concrete, and the dynamic effect of debonding did not debond the opposite face. It is possible that the specimen experienced premature debonding as a result of a manufacturing defect.

Specimen DS9 was the companion specimen to DS8 and thus both had the same epoxy type and number of anchors. During loading of DS9, the first cracking sounds were heard at a load of 51 kN. At a load of 125 kN, cracks were visible in the epoxy in front of the top anchor on the south bottom face. At a load of 121.1 kN, the FRP debonded from the south bottom face, leaving the anchors on that face intact. The elongation at debonding was 8.1 mm. However, prior to debonding, a load of 127 kN was resisted, with a corresponding elongation of 8.0 mm. There was no sign of damage on the north faces, nor the south top face. After the initial debonding the FRP was pulled out from under the anchors to inspect the failure plane. The failure plane was located a few millimeters within the concrete as shown in Figure 4.19(b).

Figure 4.19: Failure plane of (a) DS8 and (b) DS9

The load-elongation curves of companion specimens DS8 and DS9 are shown in Figure 4.20. One can see that the stiffnesses of the two specimens were very similar as their curves are almost on top of each other. Despite the similarity of their stiffnesses, it can be seen that DS8 failed at a load significantly less than the maximum load resisted by DS9.

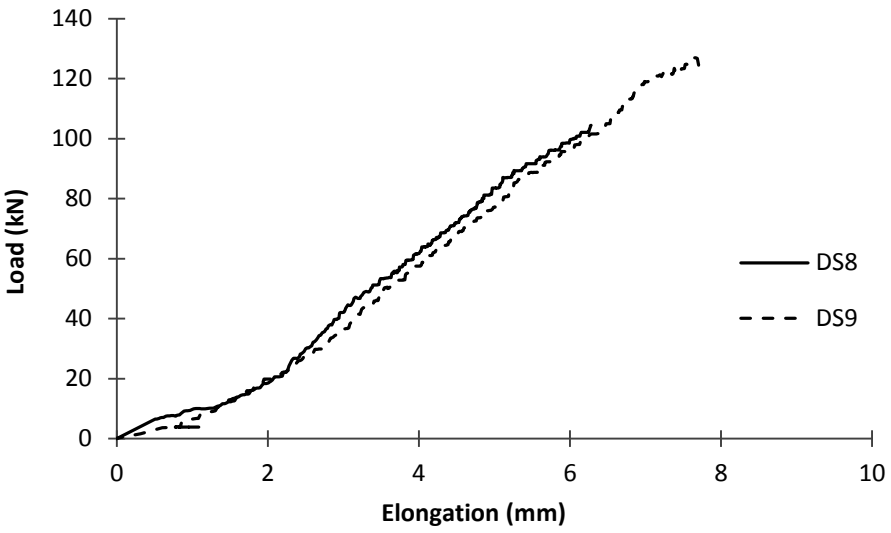

Figure 4.20: Load-elongation curve for DS8 and DS9

The peak strain measured in the FRP strips in specimen DS8 were 4656 and 4596 με on the north and south sides, respectively. At debonding in specimen DS9, the strain in the north and south face was 5691 and 5522 με, respectively. The larger peak strain value for specimens DS8 and DS9 represent 27.4 and 33.5%, respectively, of the ultimate strain of the FRP laminate. The load-strain curves for specimen DS8 and DS9 are shown in Figure 4.21 and Figure 4.22.

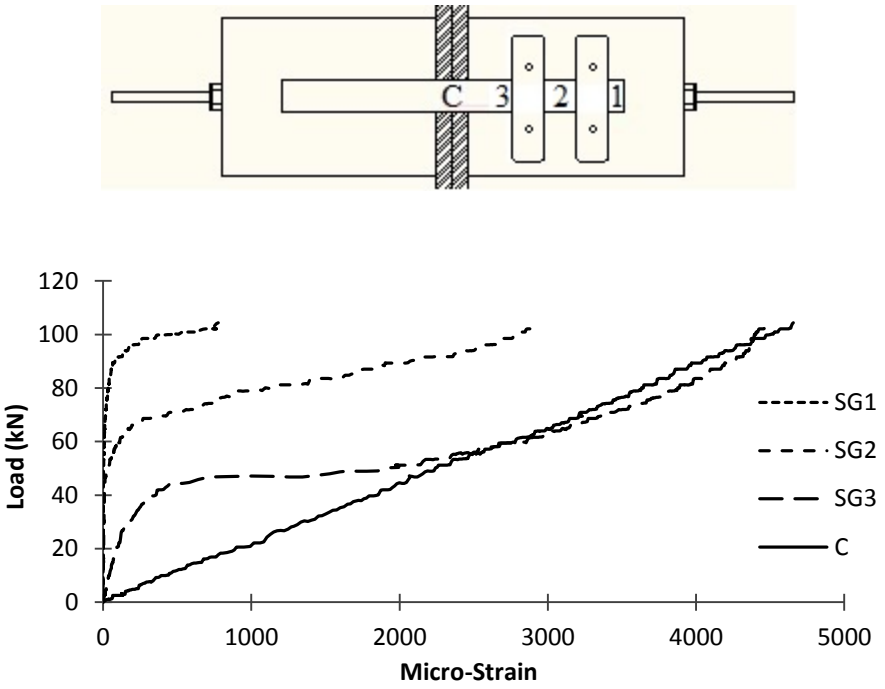

Figure 4.21: DS8 load-strain curves

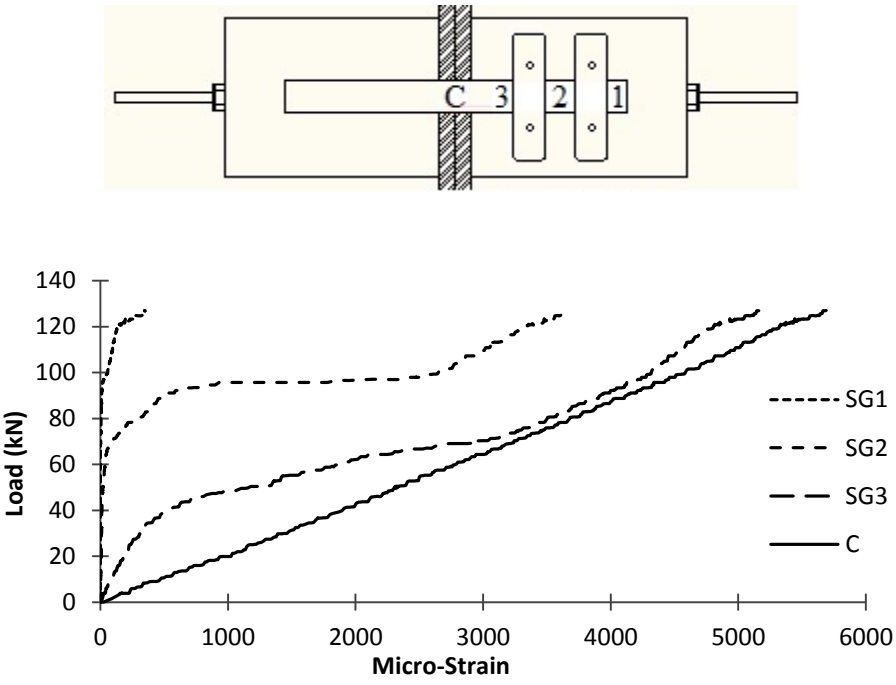

Figure 4.22: DS9 load-strain curves

The strain profiles in Figure 4.23 display the strain at debonding and half the debonding load in the bonded portion of the FRP in specimens' DS8 and DS9. The strains were measured on the top north face of both specimens, where the centres of the two 50 mm wide anchors were located 70 and 170 mm from the beginning of the bonded length of FRP in both specimens. In specimen DS8, debonding occurred at the face containing strain gauges i.e., the top north face. However, for specimen DS9, debonding occurred on the bottom south face. Nevertheless, the strain profiles seem very similar. It is important to point out that the convex form of the strain profiles at failure in Figure 4.23 noticeably differ from the concave shape of the ones in Figure 4.5 and Figure 4.18. It would appear that at ultimate load, the full bonded length is mobilized to resist the load.

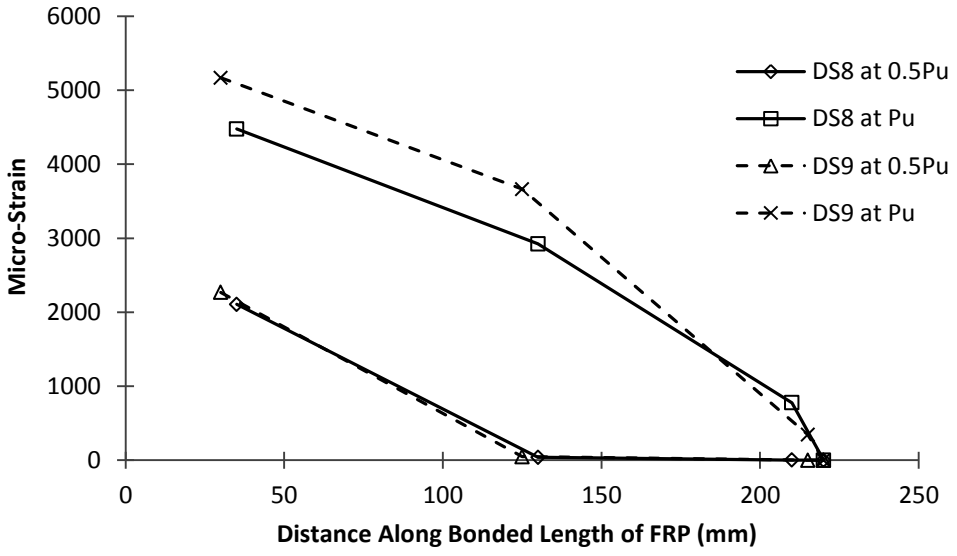

Figure 4.23: Strain profile within FRP at half and full debonding load for DS8 and DS9

4.1.4 SUMMARY OF PHASE ONE RESULTS

Phase One consisted of testing nine small-scale specimens in double shear tests. Two tests were conducted without anchors, with the FRP only epoxy bonded to the concrete, five tests were conducted with one anchor at each end of the FRP strips and two tests were conducted with two anchors at each end. Three types of epoxy were used to determine the most suitable epoxy for bonding the anchors to the FRP and the concrete. Six of the specimens also had a number of strain gauges applied to one face to determine the strain profile within the FRP along its bonded length. The results and some properties of Phase One specimens are summarized in Table 4.1, which will be further discussed in the following chapter, which provides an analysis of the test results.

Table 4.1: Summary of Phase One results

Specimen	Anchors Per Face	Epoxy to Bond Anchors	f'_c (MPa)	Ultimate		Peak Strain	
				Load (kN)	Elongation (mm)	North (με)	South (με)
DS1	0	-	39.1	73.4	4.04	3539	3549
DS2	0	-	39.1	64.8	2.80	2872	2950
DS3	1	MBrace	39.1	65.5	4.24	3150	3230
DS4	1	MBrace	35.4	91.3	4.49	4437	4585
DS5	1	Sikadur 300	35.4	96.5	2.60	4647	4728
DS6	1	Sikadur 30	39.1	111.4	8.69	5289	5451
DS7	1	Sikadur 30	35.4	117.8	8.53	5260	5520
DS8	2	Sikadur 30	35.4	104.5	6.68	4656	4596
DS9	2	Sikadur 30	35.4	127.0	8.06	5691	5522

With the significant increase in ultimate load and corresponding strain within the bonded FRP caused by the anchors, it was decided to expand the experimental investigation to large-scale beams.

4.2 Phase Two

Phase Two was the principal focus of this experimental investigation. It consisted of testing the anchor system on large-scale beams, as it would be utilized in real-world applications. A total of six RC T-beams were tested in flexure to investigate the effectiveness of the anchoring system. The parameters investigated were the type of epoxy used to bond the anchors, the presence/absence of mechanical anchors and the number of anchors. Schematic drawings and material properties can be found in Section 3.2.

As previously mentioned, the beams of Phase Two are labeled with the prefixes CB, EB and EBA representing Control Beam, Epoxy Bonded FRP strip and Epoxy Bonded FRP strip with Anchors, respectively. The prefixes CB, EB and EBA are followed by a number signifying the test number of the particular beam. Two control beams were tested, one beam was tested with the FRP strip only epoxy bonded to the beam and the remaining three beams were tested with the FRP strip epoxy bonded and anchored.

4.2.1 CONTROL BEAMS

Two control beams with no external FRP strengthening were tested to determine the strength of the RC beams. Note that the control beams were tested by Ahmed Mostafa as part of a previous investigation (Mostafa 2011).

CB1 was the first control beam tested. During testing, strain gauges on the tensile reinforcement in this beam indicated that the steel yielded at a load of 97 kN. The maximum load reached was 193 kN, with a corresponding deflection of 205 mm. The full load-midspan deflection curve is shown in Figure 4.25.

Figure 4.24: Typical concrete compression failure of control beams (Mostafa 2011)

The second control beam tested was CB2. Beam CB2 reached a maximum load of 180 kN at a deflection of 273 mm. Failure was initiated by yielding of the tension reinforcement followed by crushing of the compression flange as shown in Figure 4.24. It was determined that yielding in the tension reinforcement at

midspan occurred at a load of 127 kN, which is consistent with the change in stiffness observed in the load-deflection curve. The maximum load of CB2 was 93.5% of that of, CB1, which could be due to the difference in strength of the tensile steel in the two beams. The lower strength compared to the previous control beam is noticeable in Figure 4.25. From the figure, one can also see the load-deflection curve of this beam is similar to that of the other control beam.

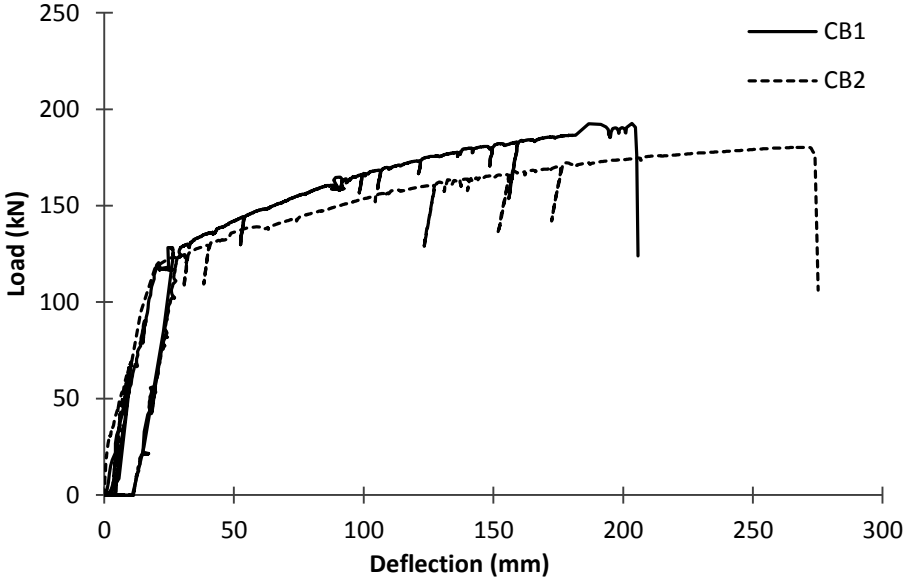

Figure 4.25: Load-deflection curves of control beams

4.2.2 Epoxy Bonded Beam

Beam EB1 had an epoxy bonded FRP strip on the beams soffit with no anchoring system. Prior to testing this beam, small flexural cracks were observed in the constant moment region of the beam. Upon loading, the first signs of debonding occurred at a load of 123 kN, when cracking noises could be heard. Cracking

noises continued until the load reached 156 kN, when a 3270 mm long piece of the FRP strip debonded from the east side of the beam, however, just prior to debonding the load peaked at 159 kN. The corresponding midspan deflection at the debonding load was 43.0 mm. It is believed that the debonding initiated near two large flexural cracks near the east loading point. The area of initiation was guessed through visual observation. The failure plane was found to be in large part at the concrete-adhesive interface. However, small areas also failed within the concrete and at the FRP-adhesive interface, as shown in Figure 4.26.

Figure 4.26: Failure plane of east side EB1

After debonding of the FRP, the beam was not tested to ultimate failure as it was assumed it would behave as a regular RC beam, failing due to concrete crushing at the top flange. In addition, not testing the beam to failure presented the opportunity to test the beam later by retrofitting it with an identical FRP strip as in EB1, but also applying anchors to it.

The load-deflection curve of EB1 exhibits a trilinear response, shown in Figure 4.27, which is typical of beams with epoxy bonded FRP tensile reinforcement. The transition points on the curve represent cracking of the beam and yielding of the reinforcement. An example of a trilinear load-displacement curve with the transition points labeled is shown in Figure 4.31. Since the strain in the tensile reinforcement was not measured, it can be estimated that the steel yielded at a load of 121 kN based on the load-displacement curve. The corresponding deflection at the yield transition point was 16.6 mm.

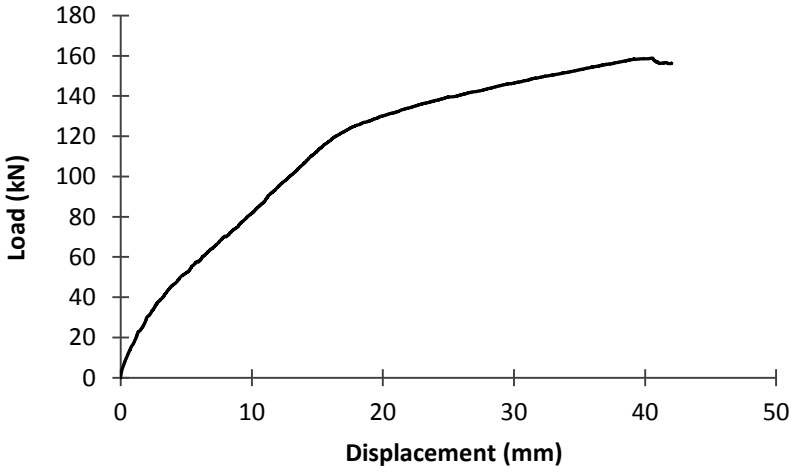

Figure 4.27: Load-displacement curve of EB1

The strain in the FRP was measured with five strain gauges spaced over the length of the FRP. The strain at the laminate ends was not measured but is assumed to be zero because it is a free end, and is displayed as such in this and subsequent strain profiles. Strain gauge one, or the strain gauge located 645 mm

from the east end of the FRP strip, experienced a significant, approximately 3000 με, increase in strain within the application of the last millimeter of displacement at the debonding load of 156 kN as shown in Figure 4.28. It is believed that this was caused either by a strain gauge malfunction or the opening of a large flexural-shear crack in close proximity of the strain gauge. The maximum strain measured in the FRP at debonding was 7051 με, corresponding to 41.5% of the ultimate strain of the FRP. The strain profiles along the laminate at the debonding load and half the debonding load are shown in Figure 4.29.

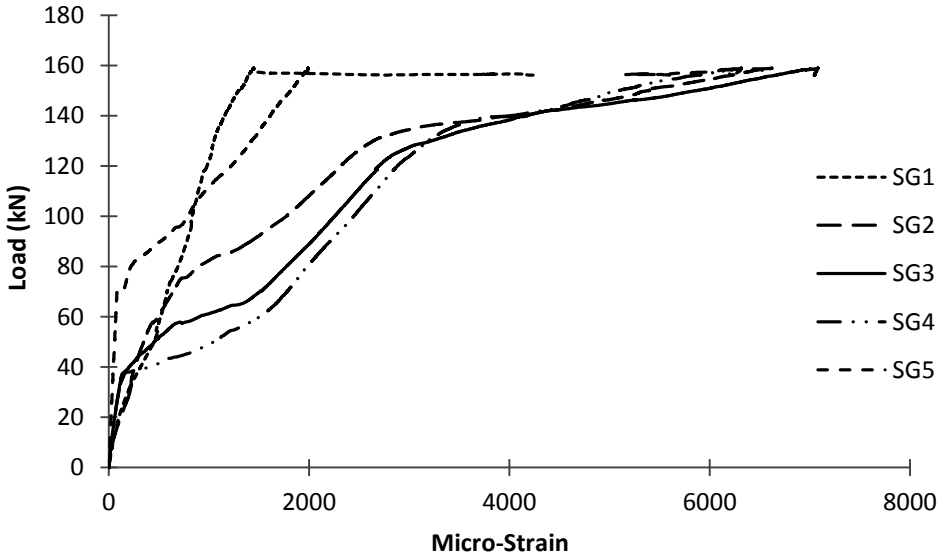

Figure 4.28: EB1 load-strain curves

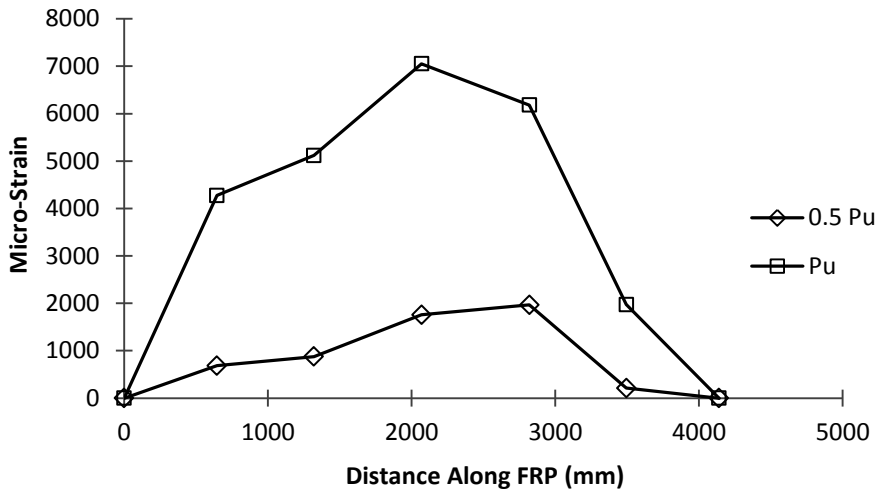

Figure 4.29: Strain profile within FRP for EB1

4.2.3 Beams with Epoxy Bonded FRP with Anchors

Three beams were tested with epoxy bonded FRP with anchors, EBA1, EBA2 and EBA3. The beams were tested with differing epoxies and anchor spacing. The results from these tests can be compared with those from beam EB1 to determine the effectiveness of the anchoring system.

EBA1

Beam EBA1 was tested with epoxy bonded FRP as well as 21 anchors spaced at 200 mm centre-to-centre over the length of the FRP. The anchors were bonded to the concrete and FRP with Wabo MBrace primer and saturant. It was decided to use Wabo MBrace primer and saturant because that was the epoxy specially manufactured for the carbon fibre fabric used in the manufacturing of the anchors. At the time of testing, a significant time after casting, only two strain

gauges on the internal steel were functional, but during testing even the functioning strain gauges were giving measurements which did not seem logical and were therefore discarded. Before testing, small cracks, with lengths less than 40 mm, were observed in the central region of the beam.

During the testing of EBA1 the first crack was heard at 158 kN. Loud cracking sounds were heard periodically until 191.8 kN, when the FRP debonded from the beam and the anchors on the east side of the beam. The corresponding displacement at debonding was 71.4 mm. At debonding, the FRP slipped underneath the anchors as shown in Figure 4.30. The FRP on the west side of the beam remained bonded to the concrete and anchors. No anchor was damaged during the debonding, nor were any pulled out. After visual inspection the failure plane was deemed to be mainly at the concrete-adhesive interface and within the concrete, although inspection was difficult as the FRP could not be fully stripped from the beam.

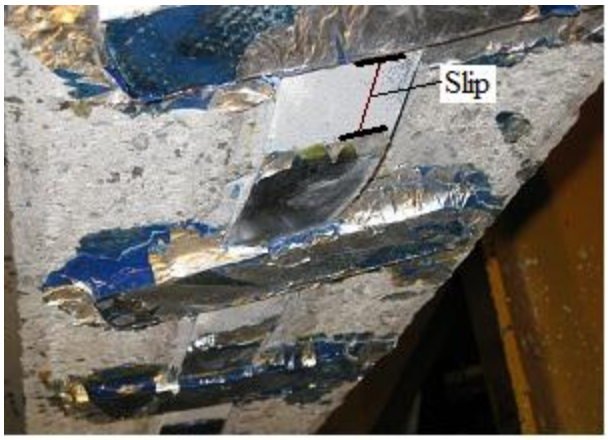

Figure 4.30: Debonding of FRP on east side of EBA1

After debonding, the beam reverted to the original unstrengthened RC beam and testing was continued until the beam failed. The beam failed due to compression failure of concrete in the top flange at a load of 150.8 kN with a corresponding midspan deflection of 102.6 mm.

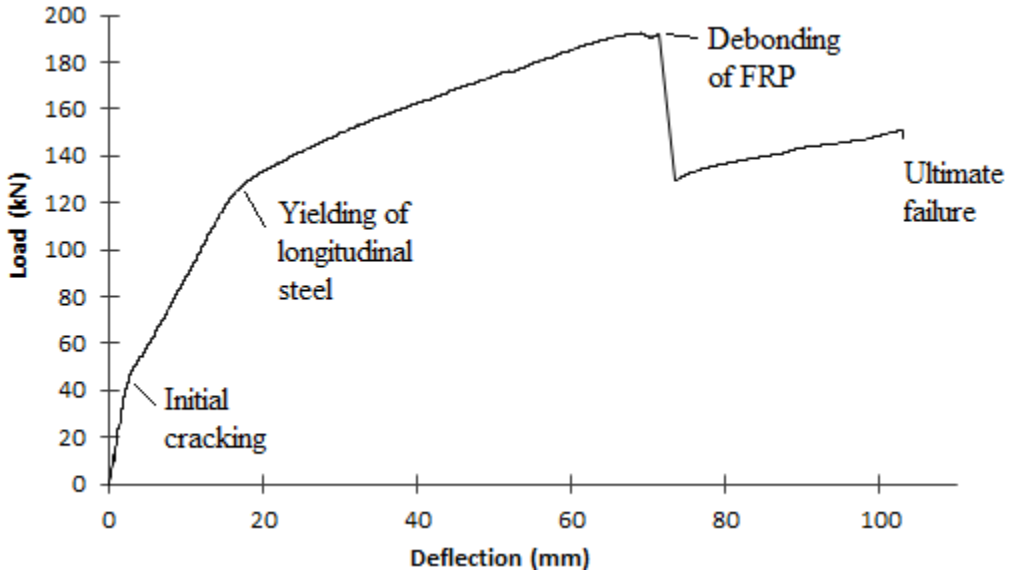

Figure 4.31: Load-displacement curve of EBA1

Figure 4.31 shows the load-midspan deflection of beam EBA1, where, for the sake of convenience, the key events during the loading process are marked. Once again, the load at which the tensile reinforcement yielded can be found by inspection of the practically trilinear load-midspan displacement curve before debonding. The yield load is estimated to be 124 kN at a corresponding deflection of 16.2 mm.

The maximum strain measured in the FRP was just prior to debonding at the centre of the beam. The maximum strain measured was 11 616 με, which is 68.3% of the ultimate strain of the FRP. The full load-strain curves of beam EBA1 are shown in Figure 4.32. The strain profiles along the FRP laminate at debonding and half the debonding load, measured with six strain gauges, are shown in Figure 4.33.

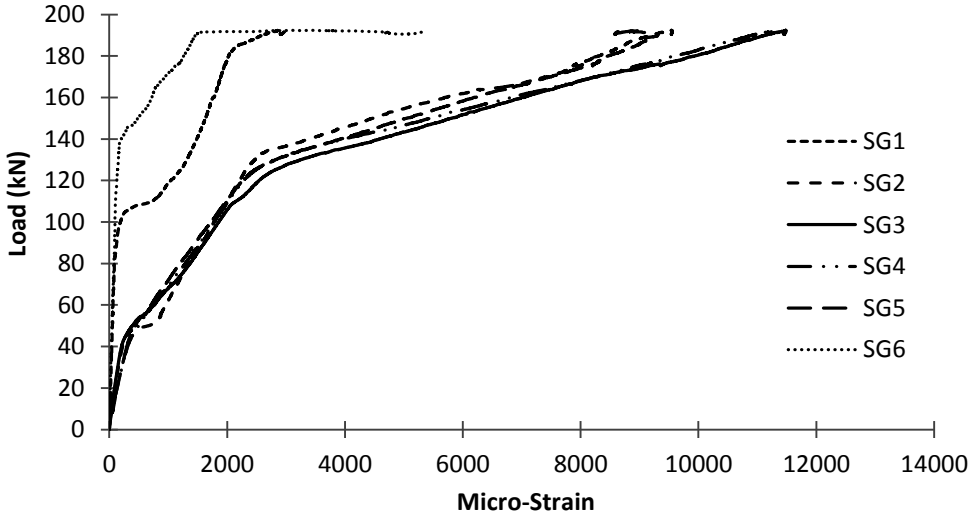

Figure 4.32: EBA1 load-strain curves

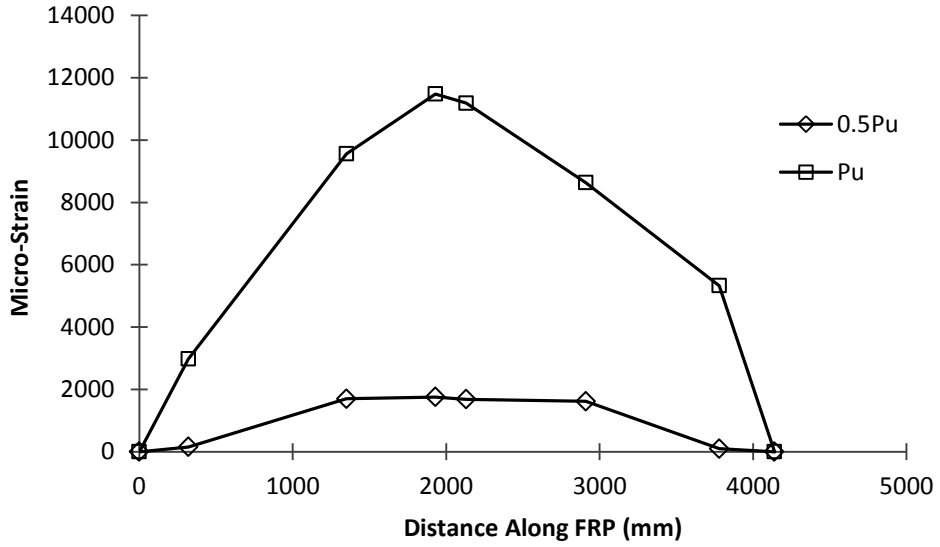

Figure 4.33: Strain profile within FRP for EBA1

EBA2

Specimen EBA2 had the same anchor spacing as EBA1, 200 mm, and the same amount of anchors, 21. However, there were two differences between EBA2 and EBA1; Sikadur 30 epoxy was used to bond the anchors to the FRP and concrete in EBA2 and this beam had been tested prior to the installation of the FRP laminate and was designated before as EB1. The Sikadur 30 epoxy was used because it was the most successful epoxy in the small-scale testing, and it was anticipated this would also apply to the large-scale beams under bending. Also, it may be recalled that the EB1 testing was terminated after the FRP debonded, prior to the failure of the beam. This allowed the remaining FRP to be peeled off and the associated epoxy to be removed. A portion of the beam with epoxy chipped off, but prior to mechanical grinding, is shown in Figure 4.34(a). The procedure for

the application of the new FRP reinforcement on the beam is described in greater detail in Section 3.2.3. The re-strengthening was performed to imitate a beam which has experienced damage and yielding of tensile steel as in a real world application. The beam contained a significant number of flexural cracks after being tested earlier as shown in Figure 4.34(b), which also shows the holes drilled for anchors.

Figure 4.34: EBA2 (a) After the chiseling away of excess epoxy and (b) With significant cracks from previous testing

The completed beam with the FRP and anchors installed is shown in the inverted position in Figure 4.35. From the figure, one can notice three anchors near the end of the beam which could not be placed exactly perpendicular to the FRP strip. These anchors were positioned this way as they were the first anchors installed and upon drilling of the holes for the anchor legs, the tensile steel was hit. After drilling the holes for three anchors, it was decided to shift the holes to

miss the tensile steel and to ensure the anchor lengths were perpendicular to the length of the beam.

Figure 4.35: EBA2 prior to testing

Because the beam had been tested before, the tensile steel reinforcement can be assumed to have yielded, and therefore, the strain on the steel could not be measured, as the initial strain was unknown.

During loading of EBA2, cracking was first heard at a load of 155 kN. Upon further loading the west end of the FRP debonded at a load of 225.1 kN, at a displacement of 77.7 mm. The slip and the debonded FRP are shown in Figure 4.36. The east side of the FRP did not experience debonding.

Figure 4.36: Slip in debonded FRP in EBA2

Upon inspection of the beam after the test was complete, it appeared that debonding occurred at the concrete-adhesive interface between points located at 1200 and 3550 mm from the east end of the beam. Beyond 3550 mm from the east end, failure occurred at the FRP-adhesive interface. Within the 1200 mm distance from the east end, the adhesive and anchor system remained intact. The bond between the anchors and the concrete appeared intact for all anchors, except for some large flexural cracks extending through the adhesive as shown in the failed specimen in Figure 4.37.

Figure 4.37: Inverted failed EBA2 specimen

Upon further loading, the FRP began to slip under the anchors on the west end. The beam was tested to failure until the concrete in the flange began to crush under the west loading plate. The failure load of the beam was 204.1 kN with a centre deflection of 195.3 mm. Upon completion of the test, the total FRP slip at the east end was measured as 70 mm. The load deflection curve for EBA2 is shown in Figure 4.38. It should be noted that the load deflection curve may not represent a typical curve due to the tensile steel reinforcement having yielded in the previous test.

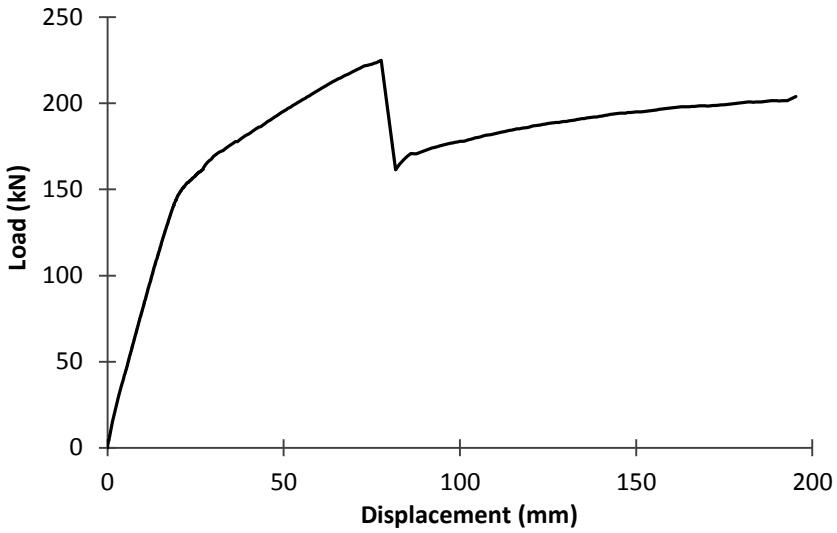

Figure 4.38: Load-displacement curve for EBA2

The maximum strain measured at the time of debonding within the FRP strip was 12 338 με, or 72.6% of the ultimate strain of the FRP. The full load-strain curves for beam EBA2 are shown in Figure 4.39. The strain profiles along the FRP laminate at the debonding and half the debonding load are shown in Figure 4.40. Following debonding, the release of energy caused five out of the six strain gauges installed on the laminate to malfunction. However, the strain gauge closest to the east end remained functioning for the remainder of the test. The functioning gauge measured a strain of approximately 2300 με for the remainder of the test. This indicates the east end of the FRP, the still bonded end, was engaged in tension for the remainder of the test.

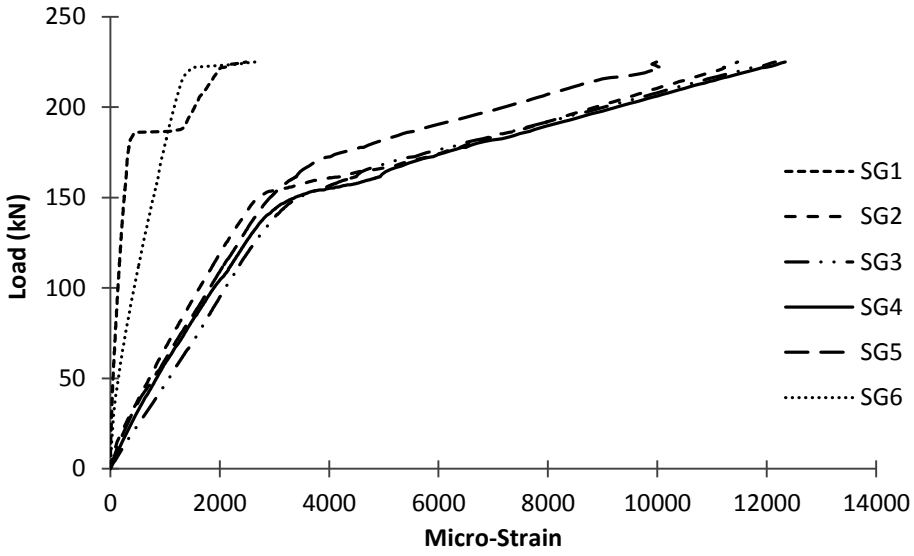

Figure 4.39: EBA2 load-strain curves

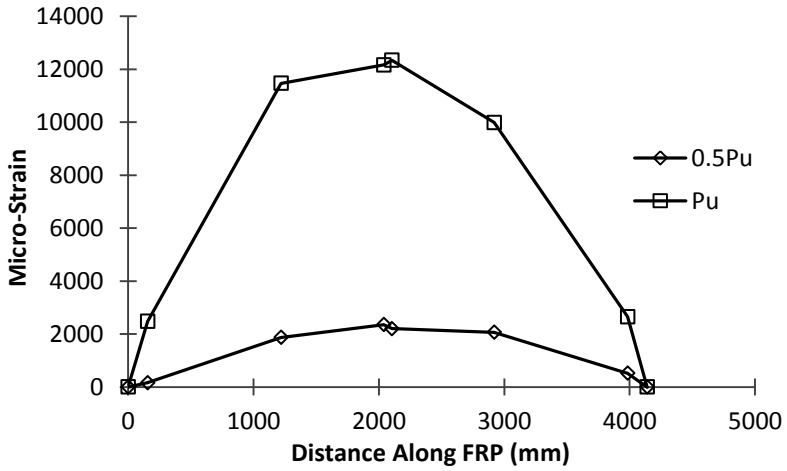

Figure 4.40: Strain profile in FRP of EBA2

EBA3

The final beam tested in Phase Two was EBA3. The beam was tested with Sikadur 30 epoxy to bond the anchors to the FRP and the concrete and with a total of 30

anchors. Four anchors were spaced at 100 mm at the ends while 22 anchors were spaced at 150 mm in the central region of the beam. It was believed that the increase of anchors would increase the bond area, and thus the bond strength, and would allow the FRP to develop a greater tensile force before debonding. In addition, end anchors were placed with a smaller spacing in an attempt to absorb the dynamic shock caused by the initial debonding near midspan to create a more localized and controlled debonding.

Of the seven original strain gauges on the tensile steel reinforcement, only three were functional at the time of testing due to prolong storage outside. The working strain gauges were located at 540, 1500 and 2250 mm from the centre of the west support. The strain captured by the operational strain gauges was recorded during the test.

During loading of the specimen, it was determined that tensile steel yielded at a load of 136.7 kN, at a corresponding displacement of 17.4 mm. At a load of 197 kN the first loud cracking sound was heard, indicating damage somewhere within the specimen. The FRP debonded on the east side at a load of 231.8 kN with a deflection of 80.2 mm. The debonded portion of the FRP extended from the east end of the beam to approximately 840 mm from the west end of the FRP. Within a distance of 700 mm of the east end, the failure plane occurred at the FRP-adhesive interface, while in the middle portion, the failure plane was at

the adhesive-concrete interface or within the concrete. No anchors were damaged or pulled out by the debonding process as can be seen in Figure 4.41(a).

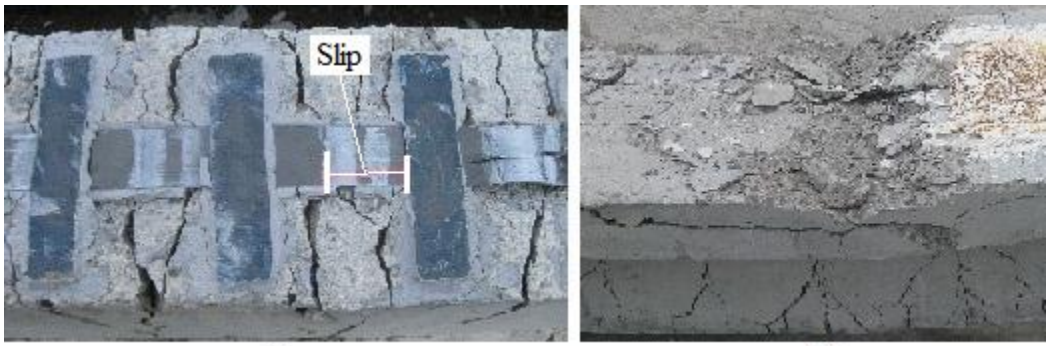

Figure 4.41: Failure of EBA3 (a) Slip of FRP and (b) Compression flange failure

Loading continued after the debonding, until failure of the beam at 196.1 kN and a corresponding midspan deflection of 223.8 mm. Failure was caused by concrete crushing in the compression flange near the west loading point following the yielding of the steel. The compression failure is shown in Figure 4.41(b), along with the FRP slip at failure. The load-deflection curve for EBA3 is shown in Figure 4.42 and appears to be trilinear prior to debonding and the beam reversion to a regular RC beam.

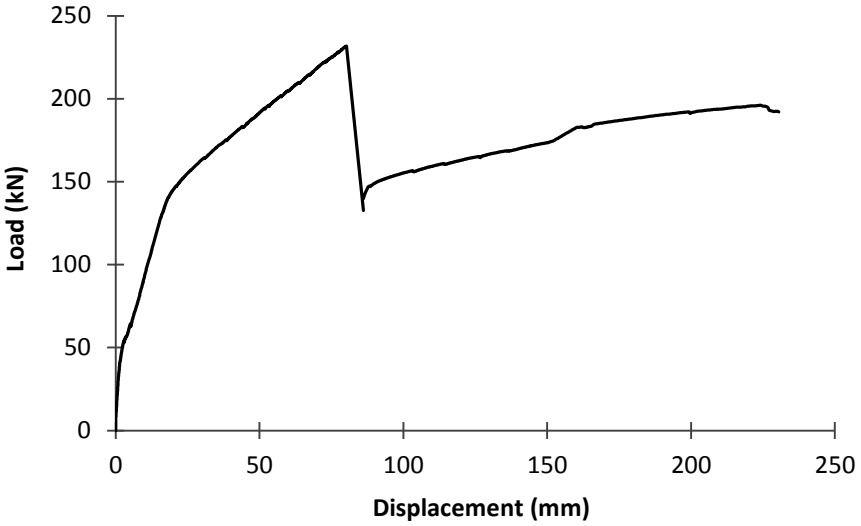

Figure 4.42: Load-displacement curve of EBA3

The maximum strain measured in the FRP at debonding was 13 675 με, or 80.4% of the ultimate strain of the FRP. The load-strain curves for EBA3 are shown in Figure 4.43. The strain profile along the FRP laminate at the debonding and half the debonding load is shown in Figure 4.44.

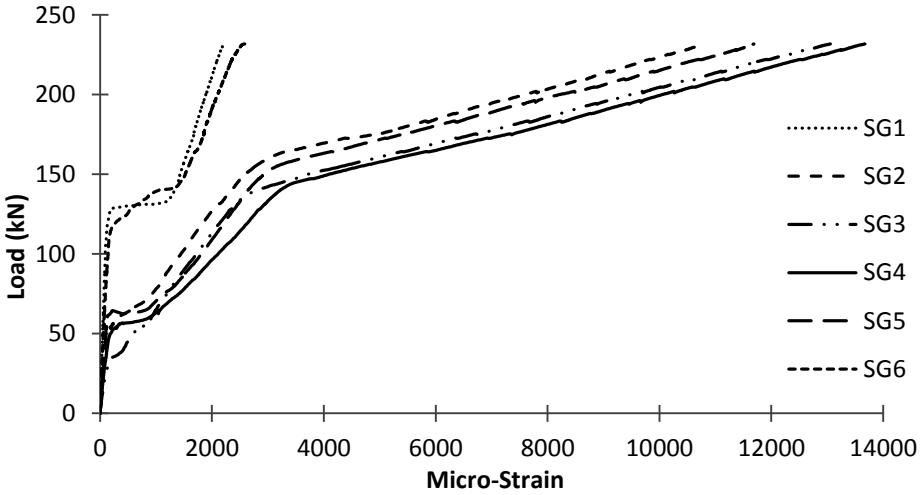

Figure 4.43: EBA3 load-strain curves

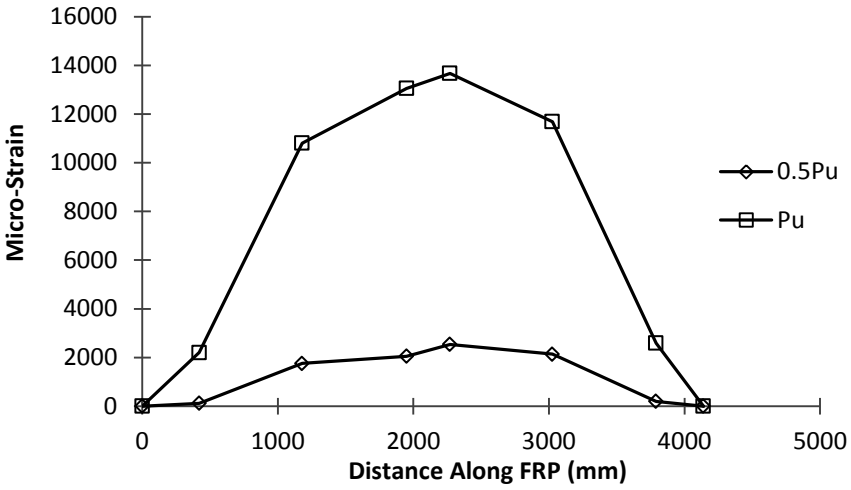

Figure 4.44: Strain profile within FRP at debonding of EBA3

4.2.4 SUMMARY OF PHASE TWO RESULTS

Six tests were performed in Phase Two, two control beams, one beam with FRP only epoxy bonded to the concrete and three beams with FRP epoxy bonded and anchored to the concrete. Two different types of epoxies were used to bond the anchors to the FRP and the concrete. In addition, two anchor configurations, consisting of 21 and 30 anchors, were used. Some of the key results are summarized in Table 4.2, which includes the yield load in each beam, the debonding load, the peak strain measured in the FRP laminate and the beam failure load after debonding.

Table 4.2: Summary of Phase Two results

Beam	CB1	CB2	EB1	EBA1	EBA2	EBA3
Number of Anchors	-	-	0	21	21	30
Yield Load (kN)	128.7	122.9	121	124	121*	136.7
Deflection at Yield (mm)	32.8	25.1	16.6	16.2	16.6*	17.4
Debonding Load (kN)	-	-	158.9	191.8	225.1	231.8
Deflection at Debonding (mm)	-	-	43.0	71.4	77.7	80.2
Peak Measured Strain in FRP (με)	-	-	7051	11 488	12 338	13 675
Peak Measured Strain in FRP (% of Ultimate)	-	-	41.5	67.6	72.6	80.4
Ultimate Load (kN)	192.7	180.2	-	150.8	204.1	196.1
Ultimate Deflection (mm)	220.5	179.9	-	102.6	195.3	223.8

*Steel had yielded prior to testing

Based on the above test results, one can see the benefits of using anchors to aid in the bonding of external FRP reinforcement to RC beams. The next chapter will further pursue these benefits with an analysis and discussion of the results.

CHAPTER 5 - ANALYSIS

5.1 GENERAL

The experimental results from Phase One and Phase Two will be analyzed separately. The analysis of Phase One will focus on the average ultimate shear stress, ultimate load, observed failure modes, load-elongation curves and the distribution of strain along the FRP at failure. The analysis of Phase Two will focus on the ultimate flexural load, observed failure mode, load-displacement curve and ductility of each beam. The analysis of both phases will, in particular, focus on the effectiveness of the anchoring system.

5.2 PHASE ONE

5.2.1 AVERAGE ULTIMATE SHEAR STRESS

The average ultimate shear stress, τ_{avg}, can be calculated from the results of Phase One using the area bonded to the concrete prism and the maximum load resisted by the FRP before debonding. For the tests without anchors, the bonded area is simply the area of the FRP laminate bonded to the concrete prism. For the tests with anchors, the bonded area is calculated as the bonded area of the FRP laminate together with the area of the anchor(s) on either side of the

laminate strip bonded to the concrete prism. The results are presented below in Table 5.1.

Table 5.1: Average shear stress of Phase One specimen

Name	Anchors per Face	Ultimate Load (kN)	Load per Side (kN)	Bonded Area (mm^2)	τ_{avg} (MPa)
DS1	0	73.4	36.7	11000	3.34
DS2	0	64.8	32.4	11000	2.95
DS3	1	65.5	32.8	18478	1.77
DS4	1	91.3	45.7	18478	2.47
DS5	1	96.5	48.3	18478	2.61
DS6	1	111.4	55.7	18478	3.01
DS7	1	117.8	58.9	18478	3.19
DS8	2	104.5	52.3	25956	2.01
DS9	2	127.0	63.5	25956	2.45

For the specimens without anchors, the bonded area was calculated as the product of the bonded length, 220 mm, and the width of the strip, 50 mm, for an area of 11 000 mm^2. For the other specimens, the area of the anchor head bonded to the concrete, calculated as 7478 mm^2 for each anchor, was added to the 11 000 mm^2 bonded area of the FRP strip.

The average shear stress of the specimens without anchors, DS1 and DS2, is 3.1 MPa. The specimens with one anchor and Sikadur 30 epoxy to bond the anchors performed similarly also with an average shear stress of 3.1 MPa for both specimen. Specimen DS9, which was believed to be tested successfully with two

anchors per face had an average shear stress 23% less than that of the unanchored specimens. It would appear that the addition of the second anchor does not increase the load carrying capacity of the anchored laminate as much as the first anchor. This could be due to the fact that shear stress distribution is not uniform along the bonded length and the anchor closer to the unloaded end of the strip contributes less to the resistance.

5.2.2 Ultimate Load

One can see from Table 5.2, the control specimens, DS1 and DS2, had the smallest average ultimate load out of all the specimens. The specimens with MBrace primer and epoxy adhesive performed the poorest among the specimens with one anchor per face. Specimen DS9 reached 127 kN and had the largest ultimate load, but since DS8 was low, the average for the specimens with two anchors per face was significantly reduced. It is important to note that due to random variability of concrete surface strength and workmanship, many replicate specimens must be tested to obtain a more reasonable assessment of the performance of the anchor.

Table 5.2: Average ultimate loads of Phase One specimen

Name	Anchors per Face	f'_c (MPa)	Epoxy	Ultimate Load (kN)	Average Load (kN)
DS1	0	39.1	-	73.4	69.1
DS2	0	39.1	-	64.8	
DS3	1	39.1	MBrace	65.5	78.4
DS4	1	35.4	MBrace	91.3	
DS5	1	35.4	Sikadur 300	103.1	103.1
DS6	1	39.1	Sikadur 30	111.4	114.6
DS7	1	35.4	Sikadur 30	117.8	
DS8	2	35.4	Sikadur 30	104.5	115.8*
DS9	2	35.4	Sikadur 30	127.0	

*Note: Specimen DS8 displayed unexpected results while testing that may have been the result of a manufacturing defect. However, the results of DS8 are still included in the average.

Based on the ultimate loads, it was concluded that the Sikadur 30 was the more suitable epoxy for bonding the laminate and the anchors to the concrete in the present tests.

The current ultimate loads can be compared with their corresponding values predicted by the model proposed by Chen and Teng (2001). They suggested Eq. 5.1 to calculate the effective bond length

$$L_e = \sqrt{\frac{E_f t_f}{\sqrt{f'_c}}} \tag{5.1}$$

where E_f and t_f are the modulus of elasticity and thickness of the FRP laminate.

Using Eq. 5.1 for the present test specimens, the effective bond length is 182.4 and 177.6 mm for the 35.4 and 39.1 MPa strength concrete prisms, respectively. The actual bonded length of the FRP laminate on the specimens was 220 mm, which is larger than the above calculated bond lengths. It should be noted that on two of the faces on specimens DS8 and DS9, the second anchor was 170 mm from the beginning of the initial FRP-concrete bond, meaning the end of the anchor was 195 mm along the bonded portion which is less than the computed 182.4 mm effective bond length.

Using the effective bond length, the ultimate load that can be resisted by the bonded laminate can be calculated using Eq. 5.2 as proposed by Chen and Teng (2001).

$$P_u = 0.427\beta_p\beta_L\sqrt{f'_c}b_f L_e \tag{5.2}$$

where β_p is a geometric factor related to the ratio of the FRP laminate width to the width of the concrete it is bonded to and β_L is equal to one for $L \geq L_e$ as in the current specimens.

The predicted ultimate loads are 56.8 and 58.3 kN for the two different concrete strengths used after the multiplication of the value obtained from Eq. 5.2 by two to account for the two laminate strips per specimen.

The predicted loads are conservative for specimens with no anchors as the specimens tested had an average ultimate load 18.5% higher than that predicted by the Chen and Teng (2001) model. Furthermore, they recommend a design equation similar to Eq. 5.2, except with a numerical coefficient of 0.315 instead of 0.427 and the equation is divided by a partial safety factor for the bond strength. Even with setting the safety factor to one, the average ultimate load of the specimens with one anchor was 60.7% higher than their predicted load.

The discrepancy between the predicted and experimental ultimate loads may be attributed to the fact that Chen and Teng used regression of test data which contained only 55 data points, of which only four involved CFRP laminate bonded to concrete. Regression of a larger data set with more specimens that have CFRP bonded to concrete may increase the accuracy of the predictions of the model.

5.2.3 Observed Failure Modes

All specimens within Phase One experienced debonding of the FRP laminate from the concrete prisms. In the case of the specimens without anchors, DS1 and DS2, the initiation of debonding rapidly led to the failure of the specimens. Specimen DS1 failed primarily within the concrete, while DS2 failed at the adhesive-concrete interface. The failure within the concrete of DS1 occurred at a 13.3% higher load than the debonding load of DS2. The surface treatment may

have been poor on specimen DS2, perhaps not sufficiently exposing the aggregate and pore structure possibly causing failure at the relatively weak interface.

For specimens with anchors, the FRP laminate debonded from the concrete and the anchors. The FRP laminate debonded from the underside of the anchors, without damaging or pulling out the anchors. Almost all specimens had a failure plane which occurred within the concrete. The exception was DS8 which failed at the adhesive-concrete interface. Similarly to DS2, the poor surface treatment may have caused the specimen to fail at the adhesive-concrete interface rather than within the concrete. In the companion test, DS9, the failure plane was within the concrete, which resulted in a 21.5% increase in the ultimate load over DS8.

Considering the lack of damage done to the anchors during testing, it may be advantageous to increase the number of anchors or to increase the anchor head area to increase the bonded area of the laminate to the anchor(s).

5.2.4 Load-Elongation Curves

In the Phase One tests, elongation of the specimens was measured as the movement of the head in the universal testing machine. Therefore, the elongation values include the slip at the FRP-concrete interface and elastic deformation of the unbonded portion of the FRP laminate. Because it is

impossible to extract the effect of each type of deformation from these measurements, only the global elongation will be discussed in a qualitative manner.

All the load-elongation curves begin with the specimens exhibiting linearly elastic behaviour as shown in Figure 5.1. Figure 5.1 displays all the load-elongation curves except for specimen DS5, in which elongation was measured with a different technique (see Section 4.1.2 for more details). With further increase in load, the control specimens DS1 and DS2 exhibit a reduction in stiffness resulting in larger increases in elongation per load increase. Since the unbonded portion of the FRP laminate is expected to be within its elastic limit, the reduction of stiffness is speculated to be caused by either microcracking within the concrete or slip at the FRP-concrete interface.

The specimens with anchors display linear-elastic behaviour for the duration of the test. It appears that the anchors maintain the bond between the FRP and concrete at the initiation of microcracking and the stiffness is not affected by this event. This would explain the absence of the loss of stiffness at the termination of the curves of the specimens with anchors. Companion specimens such as DS1 and DS2, DS6 and DS7, and DS8 and DS9 show similar initial stiffness and overall behaviour.

At the beginning of each curve, at a load of 1 to 3 kN, all curves appear to experience elongation with little to no increase in load. These elongations are inherent within the universal testing machine as the loading head moves relative to the screws which apply the load and are not indicative of the actual behaviour of the specimens.

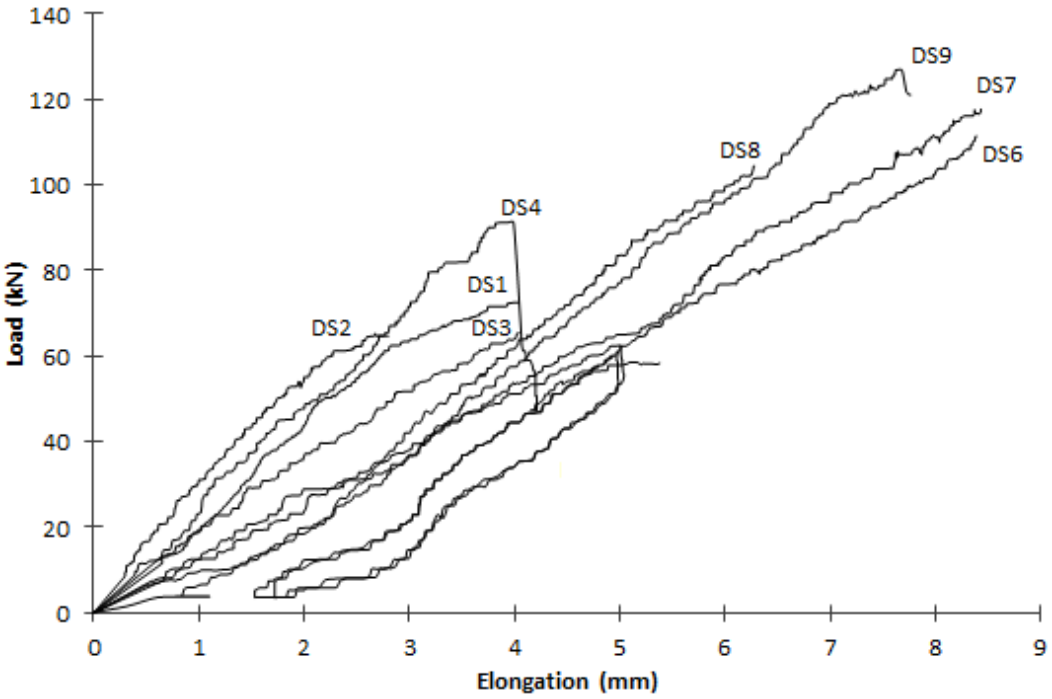

Figure 5.1: Load-elongation curves for Phase One

5.2.5 FRP Laminate Strain Distribution

The strain in the FRP at failure can be compared with the ultimate strain calculated using a closed-form analytical solution. Yuan et al. (2004) presented such a solution for FRP-concrete bonded joints. For simplification, the FRP-concrete bond is modeled considering three materials, with the FRP strip and

concrete, experiencing axial deformation while the adhesive undergoing only shear deformation. Any bending stresses within the FRP strip or the concrete are ignored while the shear is assumed to be constant over the thickness of the adhesive. Based on the assumptions of the model and first principles, the following relationships can be written

$$\sigma_p t_p b_p + \sigma_c t_c b_c = 0$$

$$\tau = f(\delta)$$

$$\sigma_p = E_p \frac{du_p}{dx} \tag{5.3}$$

$$\sigma_c = E_c \frac{du_c}{dx}$$

$$\delta = u_p - u_c$$

where σ_p, t_p and b_p are the axial stress, the thickness and width of the FRP strip, respectively, σ_c, t_c and b_c are the axial stress, the thickness and width of the concrete prism, τ is the shear stress in the adhesive, δ is the relative displacement between the FRP strip and concrete prism, E_p is the elastic modulus of the FRP strip, u_p is the displacement of the FRP strip and u_c is the displacement of the concrete prism. Considering the equilibrium of an infinitesimal element of the FRP strip, one can write

$$\frac{d\sigma_p}{dx} - \frac{\tau}{t_p} = 0 \tag{5.4}$$

When equations 5.3 are substituted into Eq. 5.4 and the interfacial fracture energy and local bond strength terms are included, one obtains the following governing differential equation

$$\frac{d^2\delta}{dx^2} - \frac{2G_f}{\tau_f^2}\,\lambda^2\, f(\delta) = 0 \tag{5.5}$$

Where G_f is the interfacial fracture energy, τ_f is the local bond strength and

$$\lambda^2 = \frac{\tau_f^2}{2G_f}\left(\frac{1}{E_p t_p} + \frac{b_p}{b_c E_c t_c}\right) \tag{5.6}$$

The differential equation can be solved if the local bond slip model is known. Yuan et al. (2004) used a bilinear model shown in Figure 5.2.

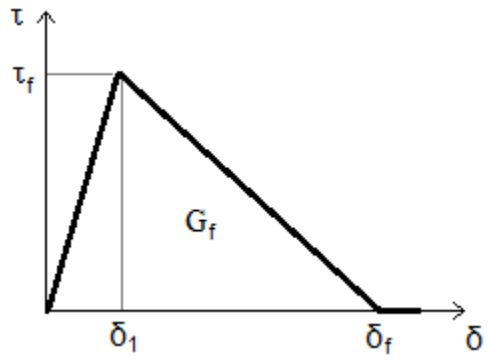

Figure 5.2: Local bond-slip model used by Yuan et al. (2004)

The solution to the differential equation can be obtained in four stages, the elastic stage, the elastic-softening stage, the elastic-softening-debonding stage and the softening-debonding stage. Of particular interest in this study is the elastic-softening stage in which the maximum load is achieved. In the latter stage, the solutions for τ and σ_p are

$$\tau = \tau_f \frac{cosh(\lambda_1 x)}{cosh[\lambda_1(L-a)]}, \quad for\ 0 \le \delta \le \delta_1$$

$$\sigma_p = \frac{\tau_f}{t_p \lambda_1} \cdot \frac{sinh(\lambda_1 x)}{cosh[\lambda_1(L-a)]}, \quad for\ 0 \le \delta \le \delta_1$$

$$\tau = -\tau_f \left\{ \frac{\lambda_2}{\lambda_1} tanh[\lambda_1(L-a)] * sin[\lambda_2(x-L+a)] - cos[\lambda_2(x-L+a)] \right\}, \quad for\ \delta_1 < \delta \le \delta_f \tag{5.7}$$

$$\sigma_p = \frac{\tau_f}{\lambda_2 t_p} \left\{ \frac{\lambda_2}{\lambda_1} tanh[\lambda_1(L-a)] * cos[\lambda_2(x-L+a)] + sin[\lambda_2(x-L+a)] \right\}, \quad for\ \delta_1 < \delta \le \delta_f$$

where x is the distance along the bond length from the free end of the FRP strip, L is the bond length, a is the length of the zone experiencing softening and

$$\lambda_1^2 = \lambda^2 \frac{2G_f}{\delta_1 \tau_f}$$

$$\lambda_2^2 = \lambda^2 \frac{2G_f}{(\delta_f - \delta_1)\tau_f} \tag{5.8}$$

The value of a can be determined by iteration using Eq. 5.9.

$$tanh[\lambda_1(L-a)] = \frac{\lambda_2}{\lambda_1} tan(\lambda_2 a) \tag{5.9}$$

In addition, the ultimate load can be calculated as

$$P_u = \frac{\tau_f b_p}{\lambda_2} \cdot \frac{\delta_f}{\delta_f - \delta_1} sin(\lambda_2 a) \tag{5.10}$$

To apply the above solution to the present investigation, one must first define the parameters G_f, τ_f, δ_1 and δ_f. Neubauer and Rostásy (1997) stated that for concrete fracture and FRP debonding in double shear tests involving CFRP-to-concrete bonds the fracture energy can be determined using

$$G_f = c_f f_{ct} \tag{5.11}$$

Where c_f is 0.204 mm as determined by an average of 51 specimens and f_{ct} is the surface tensile strength of concrete. The surface tensile strength of concrete can be estimated using MacGregor (1988)

$$f_{ct} = 0.53\sqrt{f'_c} \tag{5.12}$$

Therefore, the f_{ct} and G_f are calculated as 3.31 MPa and 0.676 N/mm, respectively. Knowing that G_f is the area under the local bond-slip curve in Figure 5.2, τ_f can be found to be a function of G_f and δ_f shown below

$$\tau_f = \frac{2G_f}{\delta_f} \tag{5.13}$$

Using a typical value of δ_f = 0.2 mm (Teng et al. 2002), τ_f is obtained as 6.76 MPa, which is close to the 7.2 MPa obtained by Yuan et al. (2004). Additionally, Wu and Niu (2007) give expressions for G_f and τ_f in terms of concrete strength as shown

$$G_f = 0.644\, f'^{0.19}_c$$

$$\tau_f = 3.50\, f'^{0.19}_c \tag{5.14}$$

These expressions yield G_f = 1.29 N/mm and τ_f = 7.02 MPa. The above local bond strength values are close to the value of 6.76 MPa used in the present investigation, however, the present fracture energy value is significantly larger than the values used by the above investigators. Regardless, the value of 0.676 N/mm will be used within the analytical solution.

For the control specimens, the axial stress in the laminate strip along its bonded length was calculated and is shown in Figure 5.3.

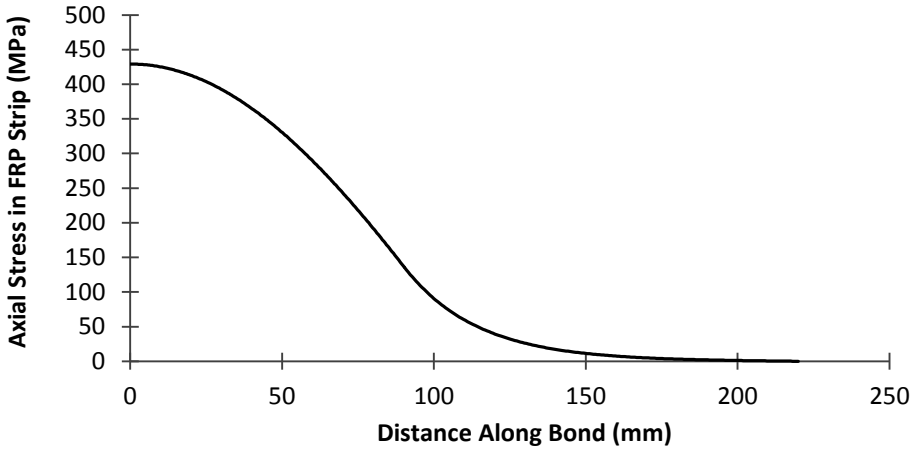

Figure 5.3: Axial stress in plate along FRP-concrete bond

By dividing the axial stress by the elastic modulus of the FRP strip, one can obtain the theoretical strain distribution along the bond length. The theoretical strain distribution thus determined along with the experimental strain distribution for the test specimens, DS1 and DS2, are presented in Figure 5.4.

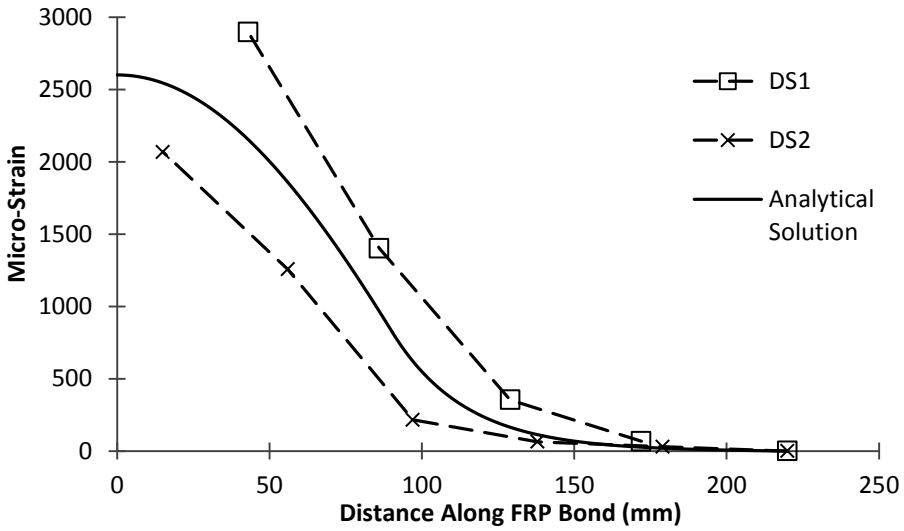

Figure 5.4: Strain in FRP strip at debonding in control specimens

The analytical solution falls in between the experimental curves and seems to be close to the average of the values of DS1 and DS2. However, at the beginning of the bond, the experimental specimens do not follow the decreasing trend like the analytical solution, but rather seem to follow a linear variation between the first three strain gauges. Notwithstanding this fact, the analytical solution seems reasonable.

The analytical solution can also be compared with the corresponding experimental data for the specimens with anchors and fitted with multiple strain gauges, as shown in Figure 5.5. One can see that the specimens with anchors achieve much higher strain than what is predicted. In addition, the shape of the curve is different for specimens DS7, DS8 and DS9. Instead of the strain being practically zero within approximately 70 mm from the end of the bond length, the strain in specimens DS7, DS8 and DS9 increases immediately near the end of the bond length, thus increasing the effective bond length. The shape of the curves of specimens DS8 and DS9 also seem to have an inverted parabola shape, while DS6 and DS7 follow a linear trend. This means that the anchors not only increase the effective bond length but can also change the shape of the strain profile. This change allows the specimens with anchors to resist a larger load.

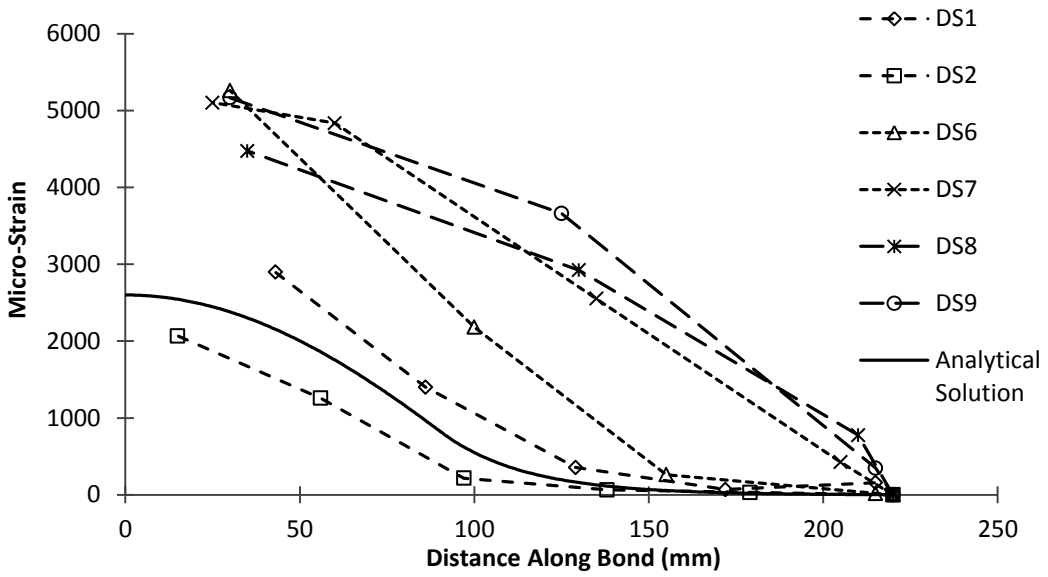

Figure 5.5: Strain along FRP-concrete bond at failure for specimens with multiple strain gauges

5.3 PHASE TWO

5.3.1 ULTIMATE FLEXURAL LOAD

To determine the effectiveness of the anchoring system, the experimental ultimate and debonding loads will be compared with the ultimate loads predicted using the CSA A23.3-04 concrete design code. Using the CSA A23.3-04 (CSA 2004), the ultimate flexural capacity of the beams are calculated and presented in Table 5.3. The ultimate capacity of the beams is calculated assuming full bond between the FRP strip and concrete at the failure of the beam. As a result, the calculated ultimate loads are based on full bond and rupture of the FRP laminate. Because of the poor correlation between the

experimental and calculated ultimate loads without considering strain hardening, it was decided to also calculate the ultimate loads taking strain hardening into account. From Table 5.3, it can be seen that the ultimate loads with strain hardening are in much better agreement with the corresponding experimental values, particularly in the case of the control beams.

Table 5.3: Debonding and failure loads compared with theoretical ultimate loads

Beam	Number of Anchors	Debonding Load (kN)	Failure Load (kN)	Ultimate Load Based on CSA A23.3-04 (kN)	
				Without Strain Hardening	With Strain Hardening
CB 1	-	-	192.7	116.5	182.4
CB 2	-	-	180.2		
EB1	0	158.9	-		
EBA1	22	191.8	150.8	199.3	225.5
EBA2	22	225.1	204.1		
EBA3	30	231.8	196.1		

The theoretical ultimate loads were calculated by assuming a strain in the FRP equal to its ultimate strain capacity, 17 000 με. Using strain compatibility, Figure 5.6(a), the strain values for the tensile steel, the compression steel (which was actually in tension) and the strain in the extreme compression fibre were found. The strain in the extreme compression fibre was calculated to be less than the ultimate strain of concrete, 0.0035 in the CSA design code, so typical stress block parameters which pertain to the failure of concrete could not be used. By

assuming a parabolic stress variation in the concrete, the stress block parameters, β_1 and α_1, applicable to the maximum strain within the concrete, can be found by using the recommendations of Collins and Mitchell (1999). When failure of concrete is not reached, the stress block parameters depend on the concrete compressive strength and the strain at which the maximum concrete stress is achieved. Using the recommendation from Collins and Mitchell (1999) and letting the concrete compressive strength of the Phase Two beams be 59.4 MPa, the concrete strain corresponding to the maximum stress was estimated as 0.00233. The ultimate moment could then be calculated using Figure 5.6(c) considering strain hardening of the tensile steel. Strain hardening was not considered for the compressive steel as the steel was within its elastic range.

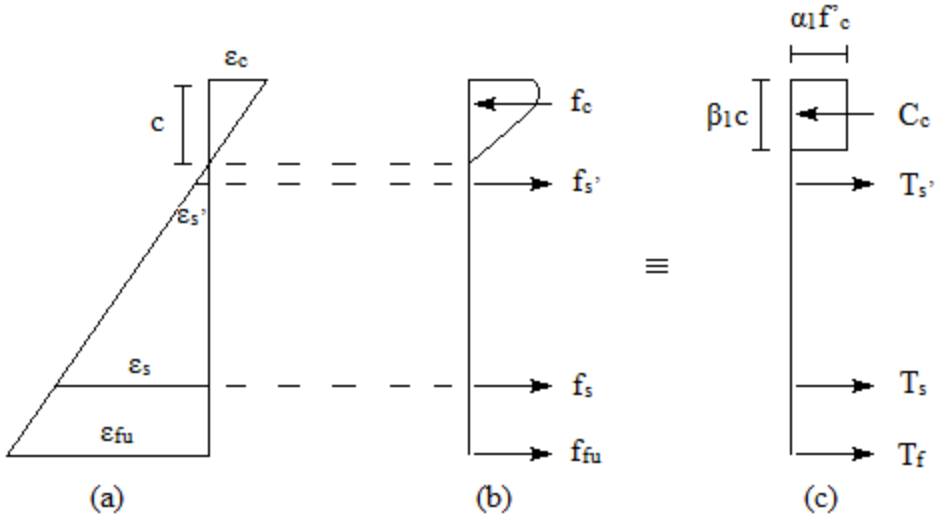

Figure 5.6: (a) Strain profile at ultimate, (b) Internal stresses and (c) Equivalent corresponding forces

The failure loads of the control beams are in good agreement with the predicted ultimate load values which include strain hardening. The control beams failed at 105.6 and 98.8% of the predicted value with strain hardening. Moreover, the failure loads of the beams with FRP reinforcement show closer agreement with the predicted values using strain hardening, albeit, less than in the case of the control beams. The small deviation from the predicted ultimate loads and the failure loads may be attributed to the variation in the stress-strain curves of the tensile reinforcement, in which the yield stress varied from 408 to 505 MPa.

When comparing the debonding loads to the predicted ultimate loads, the experimental loads were noticeably lower than the corresponding predicted values for beams EB1 and EBA1 as debonding occurred well before the full

theoretical capacity of the FRP was exhausted. The debonding load of EB1 and EBA1 was 70.5 and 85.1%, respectively, of the ultimate predicted capacity. Clearly, without the anchors, the beam achieved only 70.5% of its theoretical capacity based on full bond between the FRP and the concrete. The anchors in EBA1 increased the capacity by 20.7%

For beam EBA2 the debonding load was very close to its theoretical ultimate strength while for EBA3 was higher than its predicted capacity. The experimental debonding load for beams EBA2 and EBA3 was 99.8 and 102.8%, respectively, of the predicted ultimate load. With a failure mode of IC debonding for both beams, it is unexpected that the experimental debonding load would exceed the ultimate strength as rupture of the FRP strip was not observed in in either beam. The discrepancy may be attributed to the variation in the tensile steel yield strength, and the actual shape of the steel stress-strain curve. If the stress in the tensile reinforcement at the ultimate strain was larger than the stress calculated using a typical stress-strain curve for the steel, the ultimate load would be higher than expected. Additionally, the manufacturers' given properties for the FRP were used in the calculations. If the ultimate strain capacity or the elastic modulus was larger than the given value, the predicted ultimate load would fall short of the actual values.

Based on the experimental debonding loads, one can see that the anchoring system, regardless of the anchor spacing, allowed the beams to achieve higher debonding loads. The increase in debonding load of the beams with anchors over beam EB1, without anchors, is shown in Table 5.4. The anchoring system allowed beam EBA1, with MBrace epoxy, to achieve a 20.7% higher debonding load than that of the EB1. Using the Sikadur 30 epoxy, which performed best in the Phase One tests, beams EBA2 and EBA3 had a debonding load 41.7 and 45.9% higher than EB1. With an increase of 45.9% over beam EB1, the anchoring system proved its effectiveness in increasing the debonding load of epoxy bonded external FRP. Furthermore, the increase in the number of anchors allowed beam EBA3 to achieve a larger debonding load than beam EBA2.

Table 5.4: Debonding load increase over beam EB1

Beam	Number of Anchors	Debonding Load (kN)	Increase Over EB1 (%)
EB1	0	158.9	-
EBA1	22	191.8	20.7
EBA2	22	225.1	41.7
EBA3	30	231.8	45.9

In addition to investigating the increase of debonding loads of the beams with anchors over the beam with epoxy bonded FRP, it is important to examine the debonding load compared to the ultimate load of the control beams to

determine the strengthening effectiveness of the FRP anchoring system. A comparison between the debonding loads and the experimental and predicted ultimate loads of the control beams is shown in Table 5.5.

Table 5.5: Debonding load of beams with anchors compared to the experimental and predicted failure load of the control beams

Beam	Number of Anchors	Debonding Load (kN)	Increase Over Experimental CB Failure Load (%)	Increase Over Predicted CB Failure Load (%)
EBA1	22	191.8	2.9	64.6
EBA2	22	225.1	20.7	93.2
EBA3	30	231.8	24.3	99.0

The increase of debonding load over the experimental control beam failure load was greatest for beam EBA3 with an increase of 24.3%. This value, as the other similar values in the table, is relatively small due to the strain hardening within the tensile steel reinforcement. At the debonding, the stress and strain in the steel are slightly higher than the yield stress and strain. While at failure the tensile steel strain in the control beams is as much as 20 times the yield strain and thus much more strain hardening occurs. Because of the increase in the amount of strain hardening, the stress in the steel is much higher in the control beams at failure than in the beams EBA1, EBA2 and EBA3 at debonding.

Likewise, the debonding load can be compared with the predicted ultimate load of the control beams and are also shown in Table 5.5. The predicted values without strain hardening are shown for comparative purposes. The values without strain hardening were used, as these are the values that would be used in a design setting. In a design setting, the exact stress-strain relationship of the steel would not be known, and would be assumed as elasto-plastic. Therefore, all strengthening calculations would be based on the predicted ultimate load without strain hardening. When comparing the debonding loads with the expected ultimate loads of the beams without strain hardening, beams EBA2 and EB3 performed best with increases of 93.2 and 99.0%, respectively. This large increase over the expected ultimate load of the beams shows the effectiveness of the anchoring system in increasing the expected ultimate load of retrofitted beams.

To evaluate models of predicting intermediate crack (IC) debonding, Said and Wu (2008) compiled test data from specimens which were tested in flexure and failed due to IC debonding. The test specimens had no anchorage or wrapping at midspan and had a variety of specimen and loading geometry. Using the test data, the relationship between the axial stiffness of the FRP ($E_f t_f$) to the maximum debonding strain in the FRP ($\varepsilon_{deb.}$) was found and is shown in Figure 5.7. One can see from the figure that for an axial stiffness of 198 000 MPa·mm, the axial stiffness of the FRP in the present investigation, one would expect a

debonding strain of approximately 0.0075 if no anchors were present. This value is comparable to the strain value achieved by beam EB1, 0.00705, which had no anchors. However, beam EBA3, which achieved the highest debonding strain in the FRP failed at a strain of 0.0138, well above the expected value without anchors. The anchors allow the FRP to experience much higher debonding strain compared to debonding strain of specimens without anchors. It is important to note that like the specimens compiled in the study by Said and Wu (2008), the specimens in the present investigation all failed due to IC debonding.

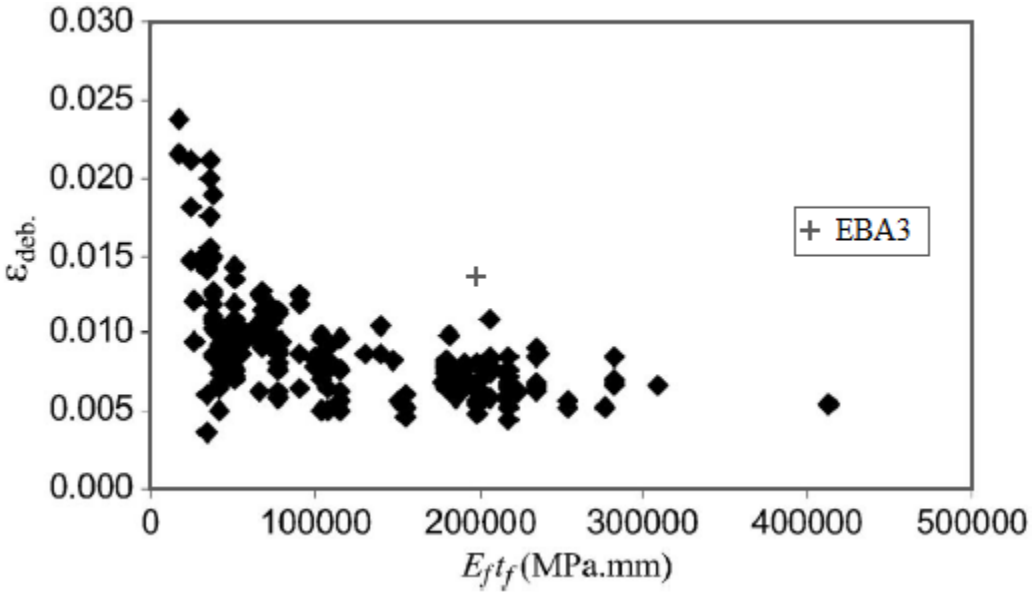

Figure 5.7: Maximum debonding FRP strain versus FRP axial stiffness (adapted from Said and Wu 2008)

It is difficult to determine the exact effect the preloading of beam EBA2 had on the test results, as no companion beam without preloading was tested due to

the already large scope of the investigation. However, the ultimate load can be compared with that of beam EBA3 which was similar, but with eight more anchors. One can see that beam EBA2 had a debonding load equal to 97.1% of that of beam EBA3. This is very high, as EBA3 is expected to have better performance due to the smaller anchor spacing in its midspan zone. This highlights the effectiveness of the anchoring system in repair situations and could be used advantageously in post-disaster situations where members may have experienced significant damage. This result is expected as Rahimi and Hutchinson (2001) tested retrofitted beams preloaded to 80% of their estimated failure load, and found they performed similarly to companion beams which did not undergo preloading.

In addition to comparing the ultimate loads, one can analyze the drop in load after debonding to determine the percentage of the load carried by the FRP just before debonding. After debonding of FRP, in each case the beam reverts to an ordinary RC beam and thus the drop in load is the load which was resisted solely by the FRP reinforcement. Table 5.6 shows the load at debonding, P_{deb}, the load immediately after debonding, P_{ad}, the difference between the two values, Δ_p, and the load carried by the FRP at debonding as a percentage of the debonding load.

Table 5.6: Load carried by FRP at debonding

Beam	P_{deb} (kN)	P_{ad} (kN)	Δ_p (kN)	Load Carried by FRP at Debonding (%)
EB1	156.2	123.7	32.5	20.8
EBA1	191.8	129.3	62.5	32.6
EBA2	225.1	161.4	63.7	28.3
EBA3	231.8	132.6	99.2	42.8

The load carried by the FRP in the beam without anchors was only 20.8% of the total load at debonding, while in beam EBA3, 42.8% of the load at debonding was carried by the FRP. As expected, all beams with anchors outperformed the beam without anchors. The results are similar to those of Mostafa (2011), in which similar percentages of load carried by the FRP were found in beams with and without anchors.

5.3.2 Observed Failure Modes

As expected, the control beams failed due to concrete crushing after the tensile steel reinforcement yielded. The failure mode for the beams with FRP reinforcement is believed to be IC debonding in all tests. Debonding of the FRP occurred very suddenly but through observations of the tests it was concluded that debonding initiated at large flexural cracks in the midspan zone of the beams.

Many patterns were observed in the beams with FRP reinforcement. All beams with FRP reinforcement failed due to IC debonding. Moreover, the failure plane occurred at the concrete-adhesive interface, mainly within a few millimeters into the concrete. The failure plane location is consistent with many FRP-concrete bonds tested in a variety of flexural and shear tests (Yuan et al. 2004, Chen and Teng 2001, Pan and Leung 2007 and Wu et al. 2011).

Another pattern which emerged for the beams with FRP reinforcement was that debonding of the FRP occurred over most of the length of the FRP-concrete bond, but not the full length. Debonding initiated at midspan and extended to one end of the bond, but not all the way to the other end. A length of FRP, less than the distance from the support to the adjacent load point, still remained fully bonded to the concrete. This phenomenon occurs because once one end of the FRP debonds, the shear stress within the strip significantly decreases and is not large enough to cause the remaining bond to fail. Because the partially debonded FRP is only bonded to a small length of the concrete outside the area of largest moment, it contributes little to the strength of the beam.

5.3.3 Load-Displacement Curves

The load-displacement curves of the control beams resembled typical RC beams, albeit with a significant strength increase after steel yielding due to strain

hardening of the tensile steel reinforcement. Therefore, the control beam curves will not be described further.

The load-displacement curves of the beams with FRP reinforcement are shown in Figure 5.8. Recall that the testing of EB1 was terminated at debonding, and thus the curve does not continue to the ultimate failure of the beam. Also, as beam EBA2 had already been tested as beam EB1, there may have been some inherent deflections in the beam at the beginning of the test which were not accounted for in the load-deflection curve. Nevertheless, the curve of beam EBA2 seems to closely follow the shape of the other curves.

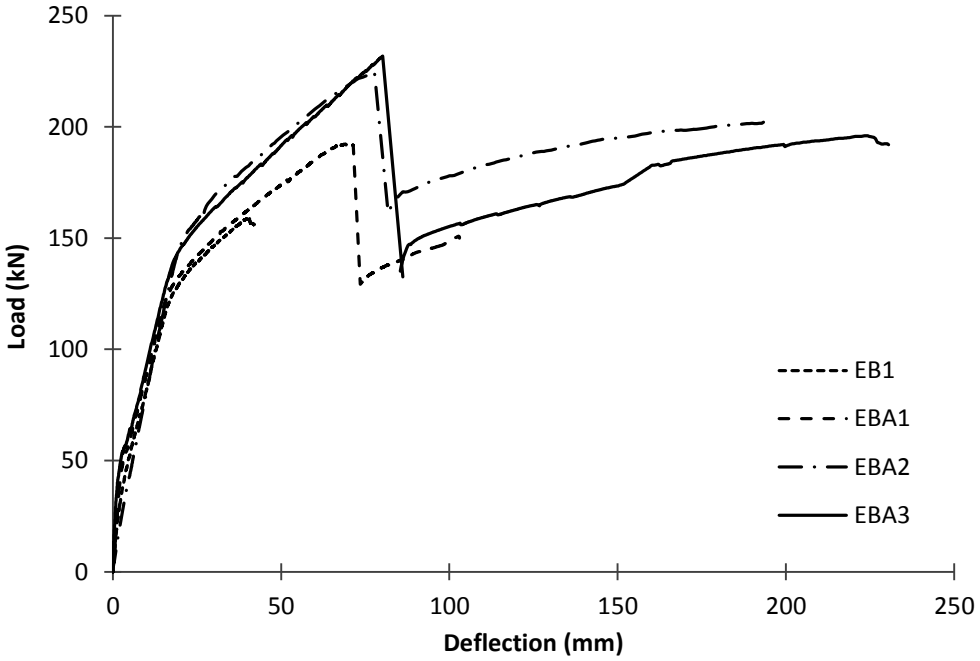

Figure 5.8: Load-deflection curves of beams with FRP reinforcement

The three beams which were tested to failure seem to follow the trilinear shape, as expected, of RC beams with FRP reinforcement (Chahrour and Soudki 2005, Said and Wu 2008, Smith et al. 2011, Wu et al. 2010 and Wu et al. 2011), before reverting to a typical RC beam at debonding. The change in stiffness within the trilinear portion of the curve is due to cracking of the concrete and yielding of the reinforcement.

A loss of strength greater than 20% in a load-deflection curve is considered detrimental to a beam. As a result, the deflection beyond debonding of FRP cannot be relied on in practical design. The ductility of the beams, ignoring the final portion of the curve, will be investigated in the next section.

5.3.4 DUCTILITY

For the case of RC beams, ductility is a measure of the deformation of the beam under load. For an elasto-plastic response, such as that of a RC beam, there is no single definition of ductility. However, it is commonly determined as a ratio of the deflection at failure to the deflection at yielding of the tensile steel reinforcement. In this investigation the ductility ratio at failure is expressed as ϕ_f. The ductility ratio can be extended to describe RC beams and slabs with external FRP reinforcement by considering the deflection at debonding of the FRP. Similar to the deflection ratio at failure, the deflection ratio at debonding can be expressed as the deflection at debonding to the deflection at yielding of

the tensile steel reinforcement. In this investigation this is expressed as ϕ_{db}. The ductility ratios for the specimens are shown in Table 5.7. Beams which achieve a large ductility ratio have the advantage of absorbing a significant amount of energy prior to failure/debonding and can act as warning of impending failure of the beam.

Table 5.7: Deflection and ductility ratios

Specimen	Deflection at Yield (mm)	Deflection at Debonding (mm)	Deflection at Failure (mm)	ϕ_{db}	ϕ_f
CB1	32.8	-	204.8	-	6.24
CB2	25.1	-	272.5	-	10.86
EB1	16.6	43.0	-	2.59	-
EBA1	16.2	71.4	102.6	4.41	6.33
EBA2	16.6	77.7	195.3	4.68	11.77
EBA3	17.4	80.2	223.8	4.61	12.86

Note that, the deflection at yield of EBA2 is estimated to be the same as EB1, as it was the same beam tested as EB1.

From Table 5.7, one can see that the final ductility ratio of the control beams was similar to that of specimen EBA1. However, specimens EBA2 and EBA3, showed higher failure ductility ratios than the control beams. The final ductility ratio was not available for specimen EB1 as the test was ceased at debonding and thus the deflection at failure could not be recorded.

The debonding ductility ratios were smaller to the ultimate ductility ratios. The EB FRP beam, EB1, underwent the smallest deflection prior to debonding and consequently had the smallest debonding ductility ratio. The beams with anchors had ductility ratios higher than EB1, with EBA2 and EBA3 being the highest with an 80.7 and 78.0% increase over EB1, respectively. This result shows the anchoring system significantly increased the ductility of the beams strengthened with FRP. Despite the decrease in ductility of the beams with anchors compared to the control beams, the debonding ductility ratios were all over four, which is considered acceptable within seismic zones (Park and Paulay 1973).

5.3.5 FRP Strain at Debonding

The maximum strain in the FRP reached in a test is an important parameter in determining the efficiency with which the FRP can be utilized. Large strains, i.e. strains close to the ultimate strain capacity, are essential for efficient use of FRP as well as efficient design. The peak strain measured in the FRP, and that strain as a percentage of its ultimate strain capacity are shown Table 5.8.

Table 5.8: Peak strain measured within FRP

Specimen	Max FRP Strain (με)	% of Ultimate Strain (%)
EB1	7051	41.5
EBA1	11 488	67.6
EBA2	12 338	72.6
EBA3	13 675	80.4

From the table one can see the beam without anchors, EB1, only reached a strain of 7051 με, which is only 41.5% of the ultimate strain capacity. For the beams with anchors, EBA3 experienced the highest strain within the FRP, which was 80.4% of the ultimate strain capacity. Thus, the anchor system increased the peak strain 94.0% over the beam without anchors. It is obvious the anchors allow the FRP to be subjected to larger strains. This is evident in the strain profiles measured at debonding as shown in Figure 5.9.

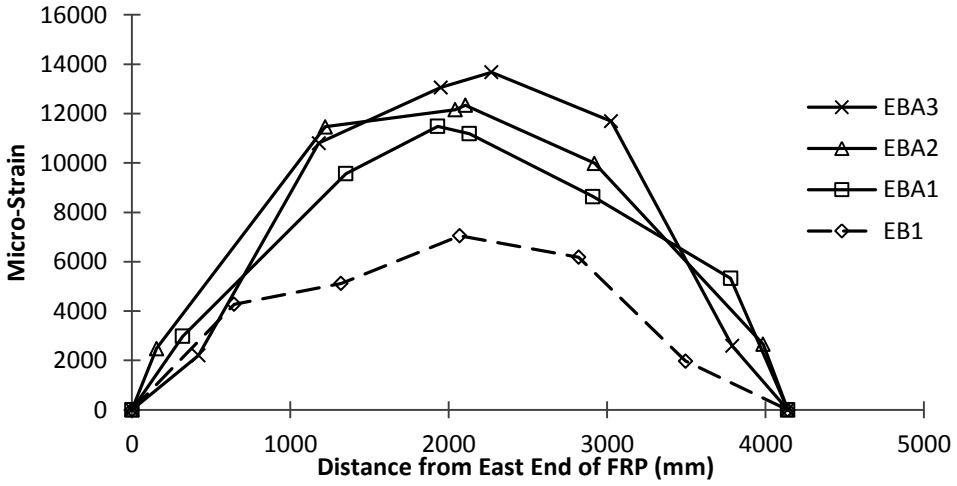

Figure 5.9: Strain profiles in FRP measured at debonding

The strain profiles show that the beams with anchors showed much higher strains at debonding than the beam without anchors. This emphasizes the importance of the anchoring system in improving the efficiency of the FRP reinforcement. It is also worthwhile to observe that the FRP strains do not follow their theoretical profile; theoretically, the strain within the constant moment

zone should be constant, while here the maximum generally occurs at midspan. Therefore, it is not possible to use conventional beam theory to predict the strain in the FRP laminate.

5.3.6 Anchor Efficiency Factor

An anchor efficiency or effectiveness factor was developed by Kalfat et al. (2011) to quantitatively compare the efficiency of anchoring systems. The anchorage effectiveness factor, a_e, is calculated by

$$a_e = \frac{\varepsilon_{f,max}}{0.41\sqrt{\frac{f'_c}{nE_f t_f}}} \tag{5.15}$$

where $\varepsilon_{f,max}$ is the maximum strain achieved in the FRP, n is the number of layers of FRP, E_f is the elastic modulus of the FRP and t_f is the thickness of one layer of FRP.

Using the expression, the effectiveness factors for the beams in the present investigation can be calculated. The factors for the beams with FRP reinforcement are given in Table 5.9.

Table 5.9: Anchorage effectiveness factors

Specimen	Maximum FRP Strain (με)	a_e
EB1	7050.8	0.99
EBA1	11 488.3	1.62
EBA2	12 337.9	1.74
EBA3	13 675.1	1.92

Kalfat et al. (2011) gave the effectiveness factors for specimens with, and without, different types of FRP anchorage systems applied to flexurally strengthened members. The average effectiveness factor for specimens without an anchorage system was found to be 0.58. The value of 0.99, achieved by beam EB1 without any anchors, is much higher than the average value found by Kalfat et al. (2011). In fact, of all the specimens without anchors within the study, the highest value was 0.87. The discrepancy may be due to the small sample size and/or due to the large amount of specimens which failed due to end debonding, which produced smaller effectiveness factors and was not present in the current investigation.

The most successful beam in terms of the effectiveness factor, EBA3, outperformed the averages of all the anchoring systems presented in the study. The highest preforming type of anchor in the study was the mechanically-fastened (MF) anchoring system which achieved an average factor of 1.87. Therefore, the anchoring system used on beam EBA3 was very successful

compared to the other anchoring systems included within that study. It is worth noting that a limited number of studies were assembled to create the average values, nonetheless, the effectiveness of the anchoring system in EBA3 is still apparent.

5.3.7 Predicted Laminate Debonding

Many models and guidelines are available in the literature to predict the onset of FRP IC debonding. One key criterion is the maximum strain in the FRP at which debonding will occur. Several guidelines and investigators specify this value. The peak measured strain from the beams in this investigation are compared in Table 5.10 with the specified strain by a few of these models.

Table 5.10: Predicted debonding strain in FRP and peak measured strain

Beam	Peak Measured Strain (με)	Predicted Debonding Strain (με)					
		Chen and Teng (2001)	Teng et al. (2003)	ACI (2008)	Said and Wu (2008)	Rosenboom and Rizkalla (2008)	CNR-DT 200/2004 (2004)
EB1	7051	3263	3669	7101	7289	8343	10 066
EBA1	11 488						
EBA2	12 338						
EBA3	13 675						

The predicted debonding strain by the various models does not include the effects of anchoring and thus should have comparable values to the strain measured in beam EB1 only. From the table one can see the ACI (2008) model

predicts the failure strain of beam EB1 with the greatest accuracy. The model by Said and Wu (2008) also gives an accurate prediction, albeit slightly higher than the ACI model. The models by Chen and Teng (2001) and Teng et al. (2003) greatly underestimate the failure strain while Rosenboom and Rizkalla (2008) and to a greater degree, the Italian CNR-DT 200/2004 guideline overestimate the failure strain. It should be pointed out that the Canadian CSA standard (CSA 2012) for FRP has adopted the ACI approach.

The focus of this study is not to determine the accuracy of these models, but rather to determine the effectiveness of the anchoring system. One can see from the table that the models all underestimate the debonding strain in the beams with anchors. As mentioned previously one can see the effect the anchors have on increasing the strain within the FRP strip at failure. This increase in strain and material efficiency needs to be reflected in the models that predict debonding strain.

5.3.8 SUMMARY

Large-scale testing of the six Phase Two beams proved successful as the anchoring system greatly improved many properties of the control beams and of the beam with FRP only epoxy bonded. The beam EBA3 with 30 anchors proved to be the most successful beam with the greatest strength increase over the control and epoxy bonded beam. Additionally, EBA3 had the largest measured

peak strain in the FRP which was 80.4% of the ultimate capacity of the FRP. The next chapter will provide a detailed summary and conclusions of this study.

CHAPTER 6 - SUMMARY AND CONCLUSIONS

6.1 SUMMARY

The high strength and elastic modulus of FRP has led to their increased use in the strengthening of RC structures. However, at major cracks within members local debonding of the FRP laminate can lead to the debonding of the entire laminate. This failure mode is called intermediate crack-induced (IC) debonding and is the failure mode studied and observed within this study. IC debonding causes premature debonding of FRP laminates, leading to inefficient FRP usage and limiting strengthening potential of the FRP. Carbon FRP anchors were used within this study to delay the onset of IC debonding and to increase the strengthening potential of the FRP laminate.

This study was undertaken to determine the effectiveness of strengthening RC members with externally bonded and anchored FPR laminate. A commercially available carbon FRP laminate of thickness 1.2 mm and width 50 mm was used in conjunction with carbon FRP anchors. The anchors were π-shaped and made of carbon FRP fabric and carbon fibre tow. Each anchor had a head plate with dimensions 200 x 50 mm and legs of length 90 mm with a diameter of 10 mm. The anchors straddled the FRP laminate and were bonded to the laminate and

the adjacent concrete. The laminate was bonded on one face along its entire length with an epoxy adhesive to the concrete.

6.1.1 PHASE ONE

Two phases of experimental work were completed within the study. In Phase One, nine specimens were tested in a double shear test, including two control specimens without anchors. To delay debonding, five specimens were tested with one anchor at each end of the laminate strips bonded to concrete prism faces. Additionally, within the latter specimens, three types of epoxy were used to determine the epoxy most suitable for use with the current FRP laminate and anchor combinations. The last two specimens were tested with the epoxy that was found the most promising and with two anchors per laminate end. Load, elongation and strain in the FRP were measured in all the specimens. Additionally, multiple strain gauges were placed along the bonded portion of the FRP in some specimens to capture the strain profile within the FRP laminate.

From the test results, the average ultimate shear stress, ultimate load, failure modes, load-elongation curves and the FRP laminate strain distribution were examined and compared. The laminate strain distribution at debonding was also compared with an analytical solution with reasonable agreement between them, particularly in the case of the control specimens. The results also showed that

the addition of two anchors at each end could substantially (84%) increase the load that can be resisted by the laminate before debonding.

6.1.2 PHASE TWO

Phase Two was the second phase completed and consisted of testing six large-scale T-beams. The beams had a span length of 4500 mm, 500 mm flange width, 400 mm height and 600 mm^2 of steel tensile reinforcement and were tested in four-point bending. Two beams without FRP reinforcement were tested as control beams for comparative purposes. The remaining four beams were tested with FRP laminate of 4140 mm in length epoxy bonded to the soffit of the beams. One beam was tested with the FRP laminate only surface bonded, with no anchors. The last three beams were retrofitted with bonded and anchored laminate and were tested with different anchor configurations. Two beams were tested with 21 anchors spaced at 200 mm. The beams had two different types of epoxy to bond the anchors to the FRP and the concrete. The remaining beam had 30 anchors spaced at 100 mm at the ends and 150 mm throughout the middle of the beam. Load, deflection and strain within the FRP were measured during the tests.

From the test results, the ultimate loads, failure modes, load-displacement curves, ductility and the peak FRP strain at debonding were examined and compared. Additionally, an anchor effectiveness factor was calculated for the

beams and compared with the efficiency factors reported in the literature for other anchor systems. The maximum debonding strain within the FRP was also compared with the corresponding values predicted by several well-known models and guidelines in the literature. The results showed that proper distribution and spacing of the anchor could increase the load bearing capacity of anchored and bonded laminate by 46% compared to only bonded laminate.

6.2 Conclusions

Based on the experimental results and analysis the following conclusions can be drawn.

6.2.1 Phase One

1. Specimens with two anchors per concrete prism face achieved the highest ultimate load. However, adding a second anchor did not increase the load carrying capacity of the specimen as much as the first anchor. This may be due to the fact the shear stress distribution along the bonded length of the FRP is not uniform, and the shear stress at the position of the second anchor is less than the shear stress at the position first anchor.
2. The maximum load resisted by the laminate with one anchor per end was 70% higher than the corresponding load resisted by the control specimens without any anchors. The maximum load resisted by the

laminate with two anchors at each end was 98% higher than that resisted by the control specimen.

3. Sikadur 30 epoxy was most suitable for bonding the anchors to the concrete and the FRP laminate as it led to the highest ultimate load compared to the other epoxies.
4. Specimens failed primarily within the concrete adjacent to the adhesive, with the exception of two specimens which failed at the adhesive-concrete interface. It is speculated that the surface treatment of these two specimens was not adequate, causing failure to occur at the relatively weak interface.
5. Control specimens, without anchors, exhibited nonlinearity and reduction of stiffness at the end of their load-elongation curves, while the anchored specimens responded in a linear elastic manner until debonding.
6. In the control specimens, the strain profile within the FRP closely resembled the profile predicted by the closed form analytical solution. The anchors seem to change the strain profile within the FRP at failure by increasing the effective bond length, and increasing the interfacial shear strength, thus allowing the FRP to resist higher load.
7. The maximum FRP laminate strain measured in the control specimens was 3549 με which is 21% of its rupture strain. The corresponding maximum strain in the specimen with one and two end anchors were

5520 and 5691 με, which are 32 and 33% of the laminate rupture strain. Thus the anchor increased the efficiency of the laminate by 60%.

6.2.2 PHASE TWO

1. A beam with 30 anchors, spaced at 100 mm at its ends and 150 mm within its midspan, had the largest debonding load and the highest increase (99%) in strength over the theoretical capacity of the control beams. The debonding load increased 46% compared to the beam without anchors.
2. The beam which was preloaded performed similar to the other beams, highlighting the effectiveness of the repair technique for restoring the strength of damaged beams.
3. At debonding the largest percentage of load carried by the FRP was 43% of the applied load and this occurred in the beam with 30 anchors.
4. IC debonding was the observed failure mode in these tests, with the failure plane occurring a few millimeters under the concrete surface.
5. The load-displacement curves of the beams with FRP exhibited a trilinear response prior to debonding and they reverted to an ordinary RC beam after debonding. The turning points of the trilinear response are initial cracking of the beams and yielding of the tensile steel reinforcement.

6. Although ductility was reduced in the beams with FRP reinforcement, the debonding ductility ratio of the beam with 30 anchors was increased 80.7% over the beam without anchors.
7. The beam with 30 anchors experienced the largest peak strain (13 675 με) within the FRP, which represents 80.4% of the ultimate strain capacity of the FRP laminate. The preceding peak strain also represents a 94.0% increase over the maximum strain measured in the FRP of the beam without anchors.
8. The π-shaped anchor tested in this investigation can delay IC debonding effectively, but the proper number and distribution of anchors must be carefully selected. The proper procedures for the selection needs to be developed in future investigations.

6.3 Recommendations for Future Work

1. Alter and optimize the dimensions of the anchors based on principles of mechanics. Test the effectiveness of anchors with different leg lengths, without legs and with a different sized head.
2. Test beams with different anchor configurations, i.e., change the anchor spacing and use different spacing in regions of low and high moment and shear.

3. Test the effectiveness of the anchors in slabs reinforced with several parallel strips and in beams strengthened against shear by FRP U-jackets.
4. Use more strain gauges to better map the strain profile within the FRP. Also, use more strain gauges at the midspan of beams to ensure the peak strain in the FRP is captured accurately.
5. Develop a systematic design method based on design and capacity for using the anchors in real applications.

REFERENCES

ACI (2008). "Guide for the Design and Construction of Externally Bonded FRP Systems for Strengthening Concrete Structures." American Concrete Institute, Farmington Hills, MI.

Aram, M. R., Czaderski, C., and Motavalli, M. (2008). "Debonding failure modes of flexural FRP-strengthened RC beams." *Composites Part B: Engineering,* 39(5), 826-841.

Bank, L. C., and Arora, D. (2007). "Analysis of RC beams strengthened with mechanically fastened FRP (MF-FRP) strips." *Composite Structures,* 79(2), 180-191.

Ceroni, F., and Peece, M. (2010). "Evaluation of Bond Strength in Concrete Elements Externally Reinforced with CFRP Sheets and Anchoring Devices." *Journal of Composites for Construction,* 14(5), 521-530.

Chahrour, A., and Soudki, K. (2005). "Flexural Response of Reinforced Concrete Beams Strengthened with End-Anchored Partially Bonded Carbon Fiber-Reinforced Polymer Strips." *Journal of Composites for Construction,* 9(2), 170-177.

Chen, J. F., and Pan, W. K. (2006). "Three dimensional stress distribution in FRP-to-concrete bond specimens." *Construction and Building Materials,* 20(1-2), 46-58.

Chen, J. F., and Teng, J. G. (2001). "Anchorage Strength Models for FRP and Steel Plates Bonded to Concrete." *Journal of Structural Engineering,* 127(7), 784-791.

CNR-DT 200/2004. (2004). "Guide for the Design and Construction of Externally Bonded FRP Systems for Strengthening Existing Structures." Rome.

Collins, M. P., and Mitchell, D. (1999). *Reinforced and Prestressed Concrete Structures.* Canadian Prestressed Concrete Institute.

CSA (2004). CSA Standard A23.3-04. "A23.3-04 Design of concrete structures standard." Canadian Standards Association, Mississauga, Ontario, Canada.

CSA (2012). CSA Standard S806-12. “Design and construction of building structures with fibre-reinforced polymers.” Canadian Standards Association, Mississauga, Ontario, Canada.

Elsayed, W.,E., Ebead, U. A., and Neale, K. W. (2009). "Studies on Mechanically Fastened Fiber-Reinforced Polymer Strengthening Systems." *ACI Structural Journal,* 106(1), 49-59.

fib. (2001). "Externally bonded FRP reinforcement for RC structures." Technical Report, Bulletin No. 14.

Galal, K., and Mofidi, A. (2009). "Strengthening RC Beams in Flexure Using New Hybrid FRP Sheet/Ductile Anchor System." *Journal of Composites for Construction,* 13(3), 217-225.

ISIS. (2001). "Strengthening Reinforced Concrete Structures with Externally-Bonded Fibre Reinforced Polymers." The Canadian network of centres of excellence on intelligent sensing for innovative structures.

Kalfat, R., Al-Mahaidi, R., and Smith, S. T. (2011). "Anchorage Devices used to improve the Performance of Reinforced Concrete Beams Retrofitted with FRP Composites: A-State-of-the-Art-Review." *Journal of Composites for Construction,* doi: http://dx.doi.org/10.1061/(ASCE)CC.1943-5614.0000276.

Kim, S. J., and Smith, S. T. (2009). "Behaviour of Handmade FRP Anchors under Tensile Load in Cracked Concrete." *Advances in Structural Engineering,* 12(6), 845-865.

Lee, J. H., Lopez, M. M., and Bakis, C. E. (2009). "Slip effects in reinforced concrete beams with mechanically fastened FRP strip." *Cement & Concrete Composites,* 31(7), 496-504.

Liu, I. S. T., Oehlers, D. J., and Seracino, R. (2007). "Study of Intermediate Crack Debonding in Adhesively Plated Beams." *Journal of Composites for Construction,* 11(2), 175-183.

MacGregor, J. G. (1988). *Reinforced Concrete: Mechanics and Design.* Prentice Hall, Englewood Cliff, New Jersey, USA.

Martin, J. A., and Lamanna, A. J. (2008). "Performance of Mechanically Fastened FRP Strengthened Concrete Beams in Flexure." *Journal of Composites for Construction,* 12(3), 257-265.

Mostafa, A. (2011). "A novel FRP anchor for preventing delamination in FRP strengthened concrete beams." PhD thesis, McMaster University, Hamilton.

Neubauer, U., and Rostasy, F. S. (1997). "Design aspects of concrete structures strengthened with externally bonded CFRP plates." *Proceedings of the Seventh International Conference on Structural Faults and Repairs,* 109-118.

Niemitz, C. W., James, R., and Brena, S. F. (2010). "Experimental Behavior of Carbon Fiber-Reinforced Polymer (CFRP) Sheets Attached to Concrete Surfaces Using CFRP Anchors." *Journal of Composites for Construction,* 14(2), 185-194.

Pan, J., and Leung, C. K. Y. (2007). "Effect of Concrete Composition on FRP/Concrete Bond Capacity." *Journal of Composites for Construction,* 11(6), 611-618.

Park, R., and Paulay, T. (1975). *Reinforced concrete structures.* Wiley, New York.

Rahimi, H., and Hutchinson, A. (2001). "Concrete Beams Strengthened with Externally Bonded FRP Plates." *Journal of Composites for Construction,* 5(1), 44-56.

Rosenboom, O., and Rizkalla, S. (2008). "Modeling of IC Debonding of FRP-Strengthened Concrete Flexural Members." *Journal of Composites for Construction,* 12(2), 168-179.

Said, H., and Wu, Z. (2008). "Evaluating and Proposing Models of Predicting IC Debonding Failure." *Journal of Composites for Construction,* 12(3), 284-299.

Saxena, P., Toutanji, H., and Noumowe, A. (2008). "Failure Analysis of FRP-Strengthened RC Beams." *Journal of Composites for Construction,* 12(1), 2-14.

Smith, S. T., Hu, S., Kim, S. J., and Seracino, R. (2011). "FRP-strengthened RC slabs anchored with FRP anchors." *Engineering Structures,* 33(4), 1075-1087.

Teng, J. G., Chen, J.,F., Smith, S. T., and Lam, L. (2002). *FRP-strengthened RC Structures.* John Wiley & Sons, Ltd, West Sussex, England.

Teng, J. G., Smith, S. T., Yao, J., and Chen, J. F. (2003). "Intermediate crack-induced debonding in RC beams and slabs." *Construction and Building Materials,* 17(6-7), 447-462.

Wu, Y. F., and Huang, Y. (2008). "Hybrid Bonding of FRP to Reinforced Concrete Structures." *Journal of Composites for Construction,* 12(3), 266-273.

Wu, Y. F., Yan, J. H., Zhou, Y. W., and Xiao, Y. (2010). "Ultimate Strength of Reinforced Concrete Beams Retrofitted with Hybrid Bonded Fiber-Reinforced Polymer." *ACI Structural Journal,* 107(4), 451-460.

Wu, Z. M., Hu, C. H., Wu, Y. F., and Zheng, J. J. (2011). "Application of improved hybrid bonded FRP technique to FRP debonding prevention." *Construction and Building Materials,* 25(6), 2898-2905.

Wu, Z., and Niu, H. (2007). "Prediction of Crack-Induced Debonding Failure in R/C Structures Flexurally Strengthened with Externally Bonded FRP Composites." *JSCE Journal of Materials, Concrete Structures and Pavements,* 63(4), 620-639.

Yuan, H., Teng, J. G., Seracino, R., Wu, Z. S., and Yao, J. (2004). "Full-range behavior of FRP-to-concrete bonded joints." *Engineering Structures,* 26(5), 553-565.

Yuan, H., and Wu, Z. (1999). "Interfacial fracture theory in structures strengthened with composite of continuous fiber." *Proc., Symp. of China and Japan: Sci. and Technol. of 21st Century,* 142-155.